

The feasibility and accuracy of Modulated Electron Radiation Therapy delivery and the design of novel scattering foils

Tanner Connell

Doctor of Philosophy

Department of Physics

McGill University

Montreal, Quebec

2014-09-14

A thesis submitted to McGill University in partial fulfillment of the requirements
of the degree of Doctor of Philosophy.

Copyright Tanner Connell

DEDICATION

I would like to dedicate this work to all those individuals who inspired and guided me throughout my education. I would not be where I am today without your help. In particular, I would like to dedicate this thesis to Dr. Ervin Podgorsak who was a great mentor and teacher, and who offered much support through a difficult time.

ACKNOWLEDGEMENTS

First and foremost, I would like to thank my supervisor Professor Jan Seuntjens for his support, guidance and encouragement over the past four years. Without his hard work and commitment to the development of a strong MERT research program, this project would not have been possible

I would also like to thank the staff at the McGill Medical Physics Unit. A great deal of effort was made on their part to provide assistance over the course of the project. I would like to recognize Margery Knewstubb and Tatjana Nisc for their administrative support. Also, thanks to Pierre Leger for much assistance with the FLEC device. Thanks to Joe Larkin, Bhavan Siva for assistance with technical questions and for helping with modifications to the accelerator. Thanks to Michael Evans and Stephen Davis for assistance with many measurements.

Thanks to my friends and fellow students for their help and support over the past few years. Many thanks to Andrew Alexander who has dedicated a great amount of time to supporting my use of MMCTP. Thanks to Pavlos Papaconstadopoulos who spent many hours helping me with measurements. I would also like to acknowledge Marc-Andre Renaud for contributing to many discussions on research issues.

Finally I would like to thank all my family and friends in and outside Montreal for supporting me throughout my degree. You've all made the past few years an amazing experience.

ABSTRACT

Modulated electron radiation therapy (MERT) represents as an active area of interest that offers the potential to improve healthy tissue sparing in treatment of certain cancer cases. Challenges remain, however, in accurate beamlet dose calculation, plan optimization, collimation method and delivery accuracy. In this work, we investigate the accuracy and efficiency of an end-to-end MERT plan and automated delivery method, as well as the possible advantages of the removal, or modification of the scattering foil from the beamline for MERT-specific applications. Treatment planning was initiated on a previously treated, whole breast irradiation case. The plan was delivered to radiochromic film placed in a water equivalent phantom for verification, using an automated motorized tertiary collimator. Separately, a treatment planning comparison was conducted on a simplified phantom geometry between a standard beamline and a beamline with the scattering foil removed for the purpose of investigating the reduction in bremsstrahlung dose to healthy tissue. The feasibility of custom, MERT-specific foils was investigated through simulation and measurements with optimized foils in the beamline. The results of the MERT delivery and verification showed good agreement between plan and film, with 3%/3 mm Gamma values of 62.1, 99.8, 97.8, 98.3, and 98.7 percent for the 9, 12, 16, 20 MeV, and combined energy deliveries respectively. A DVH comparison of the clinical beamline and the scattering-foil-free beamline with the idealized phantom revealed that for quasi-identical target coverage, the volume of each OAR receiving

a given dose was reduced, thus reducing the dose deposited in healthy tissue. The investigation of the optimal foil design for MERT applications showed that disk shaped aluminum foils for 12, 16 and 20 MeV were able to satisfy the design criteria and measurements with the manufactured prototype foils producing good agreement with simulated results. The results of our study showed that an accurate delivery utilizing an add-on tertiary electron collimator is possible using Monte Carlo calculated plans and inverse optimization. This brings MERT closer to becoming a viable option for physicians in treating superficial malignancies. Future MERT implementations could benefit from scattering-foil-free beamlines due the observed reduction in bremsstrahlung dose to healthy tissues and faster treatment times.

ABRÉGÉ

La radiothérapie à modulation d'électrons (MERT) est un domaine actif qui offre le potentiel d'améliorer la préservation de tissu en santé durant le traitement de certains cancers. Il reste certains défis, par contre, dans la précision des calculs de dose des petits faisceaux, l'optimisation du plan, les méthodes de collimation, et la précision du traitement. Nous examinons la précision et l'efficacité d'un plan MERT complet avec une méthode de traitement automatique, et examinons les avantages possibles du retrait ou de la modification du filtre métallique de diffusion du faisceau pour les applications MERT. Un sein qui avait précédemment subi un traitement d'irradiation total a été utilisé pour la planification du traitement. Le plan a été délivré à un film radiochromique placé dans un fantôme à équivalence d'eau pour une vérification, en utilisant un collimateur avec moteur tertiaire automatique. Afin de déterminer la réduction de la dose *Bremsstrahlung* au tissu en santé, une comparaison du plan de traitement a été faite sur un fantôme simplifié, avec un faisceau standard et un faisceau sans filtre métallique de diffusion. Une étude de faisabilité de filtres sur mesure pour MERT a été faite en utilisant des simulations et des mesures avec filtres optimisés dans les lignes de faisceaux. Les résultats de l'administration et de la vérification du MERT ont montré un bon accord entre le plan et le film, avec des valeurs Γ 3%/3 mm de 62.1, 99.8, 97.8, 98.3, et 98.7 pourcent pour 9, 12, 16, 20 MeV, et des énergies livrées combinées, respectivement. Une comparaison de l'histogramme dose-volume du faisceau clinique et du faisceau sans filtre métallique de diffusion avec fantôme

idéal démontre que pour une couverture quasi-identique de la cible, le volume de chaque organe à risque qui reçoit une dose est réduite, réduisant la dose déposée dans les tissus en santé. L'étude du filtre optimal pour les applications de MERT a démontrée que des filtres d'aluminium en forme de disque pour 12, 16 et 20 MeV satisfaisaient les critères de conception et les mesures avec les prototypes de filtres manufacturés étaient en accord avec les résultats simulés. Les résultats de notre étude ont démontré qu'une livraison exacte en ajoutant un collimateur tertiaire d'électron est possible avec des plans Monte Carlo calculés et l'optimisation inversé. Le MERT est donc maintenant plus près de devenir une option viable pour les médecins qui traitent des cancers superficiels. Une implementation future du MERT pourrait bénéficier d'un faisceau sans filtre métallique de diffusion, comme l'a démontré la réduction de la dose Bremsstrahlung aux tissus en santé, et le temps de traitement réduit.

TABLE OF CONTENTS

DEDICATION	ii
ACKNOWLEDGEMENTS	iii
ABSTRACT	iv
ABRÉGÉ	vi
LIST OF TABLES	xii
LIST OF FIGURES	xiv
CONTRIBUTIONS OF AUTHORS	xviii
1 Introduction	1
1.1 Radiotherapy in Oncology	1
1.2 Introduction to Modulated Electron Radiation Therapy	7
1.3 Hypothesis and Objectives	9
1.4 Thesis Outline	10
REFERENCES	11
2 Introduction to electron beam radiation therapy	14
2.1 Generation of electron beams	15
2.1.1 Microtrons	15
2.1.2 Linear accelerators	16
2.1.3 Treatment head components and final beam shaping	18
2.2 Electron interactions and general concepts	21
2.2.1 Particle and energy fluence	21
2.2.2 Stopping power	21
2.2.3 Bremsstrahlung radiation	22
2.2.4 Mass attenuation, mass energy transfer and mass energy absorption coefficients	23

2.2.5	Kerma	24
2.2.6	Absorbed dose	24
2.2.7	Central axis depth dose	25
2.2.8	Accelerator output and output factor	27
2.3	Dosimetry of radiation beams	29
2.3.1	Measurement phantoms	29
2.3.2	Dose measurement detectors	29
2.4	Monte Carlo dose calculation methods	34
2.4.1	EGSnrc codes	34
REFERENCES		39
3	Review of Modulated Electron Radiation Therapy	42
3.1	Bolus Conformal Therapy	43
3.2	MERT collimation devices	45
3.2.1	MLC	45
3.2.2	eMLC	49
3.2.3	FLEC	53
3.3	Treatment planning	55
3.3.1	McGill Monte Carlo Treatment Planning System	58
3.4	Summary of the current state of MERT and its direction	58
REFERENCES		61
4	Delivery validation of an automated modulated electron radiotherapy plan	66
4.1	Introduction	69
4.2	Materials and Methods	71
4.2.1	Validation of Monte Carlo model against measurements	71
4.2.2	Creation of MERT plan within the treatment planning system	73
4.2.3	Delivery of modulated electron plan	75
4.2.4	2D Verification of the plan delivery using EBT3 film	76
4.2.5	2D Verification of the plan delivery using MapCHECK	78
4.3	Results and discussion	78
4.3.1	Validation of Monte Carlo model against measurements	78
4.3.2	Device hardware and output factor QA	81
4.3.3	Creation of MERT plan	82
4.3.4	Delivery of the MERT plan	83

4.3.5	2D Verification of the plan delivery using EBT3 film	93
4.3.6	2D Verification of the plan delivery using MapCHECK . . .	96
4.4	Conclusions	97
4.5	Acknowledgments	99
REFERENCES		100
5	An experimental feasibility study on the use of scattering foil free beams for modulated electron radiotherapy	105
5.1	Introduction	107
5.2	Materials and Methods	109
5.2.1	Beamline Modification and Experimental Measurements . .	109
5.2.2	Monte Carlo Model Commissioning	111
5.2.3	Inverse Treatment Planning Study	114
5.3	Results and Discussion	116
5.3.1	Characterization of Scattering Foil-Free Beams	116
5.3.2	Monte Carlo Beam Matching	119
5.3.3	Inverse Treatment Planning Study	128
5.3.4	Dosimetric considerations from scattering foil removal . . .	129
5.4	Conclusion	130
REFERENCES		132
6	Design and validation of novel scattering foils for Modulated Electron Radiation Therapy	137
6.1	Introduction	139
6.2	Materials and methods	141
6.2.1	Design of custom foils	141
6.2.2	Experimental validation of custom foils	141
6.3	Results and discussion	143
6.3.1	General design goals	143
6.3.2	Experimental validation of custom foils	148
6.4	Conclusion	151
6.5	Acknowledgments	154
REFERENCES		155

7	Conclusions	157
7.1	Delivery of a modulated electron radiotherapy plan	158
7.2	Design of custom scattering foils	159
7.3	Future Work	159
	List of Abbreviations	161

LIST OF TABLES

<u>Table</u>	<u>page</u>
4-1 Comparison of measured and simulated output factors. Field sizes are for the width of the square field as defined by the FLEC with the secondary collimator setting defined in brackets.	80
4-2 A summary of the time required for each phase of the delivery in the current implementation and with possible optimizations to leaf sequence and FLEC leaf speed.	86
4-3 MU statistics for each beam quality tested. Also shown are the MU values weighted by the respective output factor giving an indication of the relative total dose contribution of each energy compared to the others.	86
4-4 Film gamma analysis values for all delivered energies for both 3%/3mm and 5%/5mm gamma criteria.	95
4-5 A summary of the x and y shifts needed to produce the optimal dose subtraction image of panel (d) of Figs. 2-6. All shifts were determined visually.	95
4-6 Pass percentages from the MapCHECK gamma analysis	97
5-1 Accelerator head parameters determined through comparison to measured data.	122
6-1 The aluminum foil thicknesses required to achieve the desired amount of beam broadening given as a percentage of the CSDA range in that material and the thickness. Beam energies are stated, with the nominal accelerating potential shown in brackets.	146
6-2 A comparison of different parameters between the clinical, no scattering foil and custom foil beamlines.	149

6-3 A summary of the simulated and manufactured (as determined by
measurements) foil thickness for 12, 16 and 20 MeV. 151

LIST OF FIGURES

<u>Figure</u>		<u>page</u>
1-1	The tumor control probability (TCP) and the normal tissue complication probability (NTCP) curves, which describe the tumor response probability as a function of tumor dose and complication probability as a function of normal tissue dose, respectively.	3
1-2	A Varian TrueBeam linear accelerator (courtesy of Varian®).	5
2-1	A schematic diagram of the different components in the head of a high-energy Varian accelerator.	19
2-2	Percent depth dose curves for electrons (solid lines) and photons (dashed lines)	25
2-3	Different range quantities	26
2-4	Relative output factor of a 12 MeV electron beam defined by the secondary collimator jaws without the electron applicator present. . .	28
3-1	The Few Leaf Electron Collimator (FLEC) used as a tertiary electron collimation device.	55
4-1	(a) The MERT plan	83
4-2	The MU distribution broken down by energy. MU bin width is 5 MU.	87
4-3	The 9 MeV film (a) and planned (b) dose distributions at a depth of 2 cm along with the 5%/5mm gamma map (c) and the plan minus film image subtraction as a percentage of the local planned dose (d).	88
4-4	The 12 MeV film (a) and planned (b) dose distributions at a depth of 2 cm along with the 5%/5mm gamma map (c) and the plan minus film image subtraction as a percentage of the local planned dose (d).	89

4-5	The 16 MeV film (a) and planned (b) dose distributions at a depth of 2 cm along with the 5%/5mm gamma map (c) and the plan minus film image subtraction as a percentage of the local planned dose (d).	90
4-6	The 20 MeV film (a) and planned (b) dose distributions at a depth of 2 cm along with the 5%/5mm gamma map (c) and the plan minus film image subtraction as a percentage of the local planned dose (d).	91
4-7	The combined-energy film (a) and planned (b) dose distributions at a depth of 2 cm along with the 5%/5mm gamma map (c) and the plan minus film image subtraction as a percentage of the local planned dose (d).	92
4-8	The (a) 9 MeV and (b) 12 MeV MapCHECK dose distributions shown on the left and the crossplane profile on the right.	96
4-9	The (a) 16 MeV and (b) 20 MeV MapCHECK dose distributions shown on the left and the crossplane profile on the right.	98
5-1	A schematic diagram of the Few Leaf Electron Collimator (FLEC) used in this study.	111
5-2	PDDs (a) and profiles (b) for 6, 9, 12, 16 and 20 MeV with (solid) and without (dashed) the scattering foil. In the profiles of (b), the secondary dose peak in the 4 to 7 cm region due to scatter of electrons over the back edge of the collimator jaw can be seen.	116
5-3	PDDs without the scattering foil, applicator or FLEC showing agreement between simulated and measured data for electron energies of 6, 9, 12, 16 and 20 MeV. (b) 9x9 cm ² profiles in the crossplane direction for 16 MeV again without the scattering foil, applicator or FLEC. Simulated results are plotted against measured data (solid line) for different thickness of the beryllium exit window and ionization chamber.	119
5-4	(a) PDDs of an 8x8 cm ² FLEC defined field for 6, 9, 12, 16 and 20 MeV showing measured and simulated results for both the clinical beamline and the experimental beamline. (b) Profiles under the same conditions are shown for 6, 12 and 20 MeV.	123

5–5	(a) PDDs of a 2x2 cm ² on-axis FLEC defined field for 6, 9, 12, 16 and 20 MeV showing measured and simulated results for both the clinical beamline and the experimental beamline. (b) Profiles under the same conditions are shown for 6, 12 and 20 MeV.	124
5–6	(a) PDDs of a 2x2 cm ² off-axis FLEC defined field for 6, 9, 12, 16 and 20 MeV showing measured and simulated results for both the clinical beamline and the experimental beamline. (b) Profiles under the same conditions are shown for 6, 12 and 20 MeV.	125
5–7	(a) Isodose lines from planned treatments using the clinical beamline (solid) and the experimental beamline (dashed). Also visible is the target (red) and the two organs at risk (orange and blue). (b) A DVH comparison of the same plan as in (a).	128
6–1	Electron fluence profiles taken at a SCD of 92 cm for 6, 9, 12, 16 and 20 MeV. Included in the figure are fluence profiles from the clinical scattering foils as well as profiles from a beamline with the foils removed (all shown as lines). The profiles simulated using custom designed foils for 12, 16 and 20 MeV are shown as lines marked with an asterisk. The grey shaded area represents the leaf edge of a hypothetical eMLC defining a 20x20 cm ² field.	149
6–2	PDD curves for the all energies are shown with the clinical foils and without foils (plain lines). The custom foils are labeled as lines marked with an asterisk. The insert shows a zoomed in portion of the bremsstrahlung tail.	150
6–3	12 MeV measured and simulated PDDs and profiles. On the left, the measured diode (black line) and PPC-40 (blue line) PDDs compared to the simulated values (asterisk). Shown right is the diode profile measurement (black line) compared to the simulated values (asterisk).	152
6–4	16 MeV measured and simulated PDDs and profiles. On the left, the measured diode (black line) and PPC-40 (blue line) PDDs compared to the simulated values (asterisk). Shown right is the diode profile measurement (black line) compared to the simulated values (asterisk).	152

6-5 20 MeV measured and simulated PDDs and profiles. On the left, the measured diode (black line) and PPC-40 (blue line) PDDs compared to the simulated values (asterisk). Shown right is the diode profile measurement (black line) compared to the simulated values (asterisk). 153

CONTRIBUTIONS OF AUTHORS

This thesis consists of three manuscripts, one published and two submitted. All manuscripts have been authored by me, however, each was made possible through assistance and collaboration by various co-authors.

The first manuscript, entitled "*Delivery validation of an automated modulated electron radiotherapy plan*", was based on work primarily completed by myself. Dr. Andrew Alexander provided much support on the treatment planning system. Pavlos Papaconstadopoulos provided assistance with some of the plan deliveries and film procedures. Monica Serban provided us with a suitable patient in which to conduct the study as well as providing advice on standard clinical practice. Dr. Slobodan Devic provided assistance in the implementation of the triple channel film method used as well as assistance with issues surrounding the film scanner. Dr. Jan Seuntjens provided guidance and advice through out all aspects of this work. The manuscripts was written by myself and reviewed by all other authors.

The second manuscript, entitled "*An experimental feasibility study on the use of scattering foil free beams for modulated electron radiotherapy*" was also based on work primarily completed by myself. Dr. Andrew Alexander gave support in the planning phase by providing a suitable test phantom scan and by providing assistance in MERT planning within the MMCTP treatment planing system. Michael Evans provided support while operating the water tank on multiple occasions. Dr. Jan Seuntjens provided support and over the course of the investigation and is also credited with developing the initial idea of scattering foil

modifications for MERT. The manuscripts was written by myself and reviewed by all other authors.

The work behind the third manuscript, entitled "*Design and validation of novel scattering foils for modulated electron radiation therapy*", was primarily completed by myself. Dr. Jan Seuntjens provided guidance throughout all aspects of this work. The manuscripts was written by myself and reviewed by all other authors.

CHAPTER 1

Introduction

Contents

1.1	Radiotherapy in Oncology	1
1.2	Introduction to Modulated Electron Radiation Ther- apy	7
1.3	Hypothesis and Objectives	9
1.4	Thesis Outline	10

1.1 Radiotherapy in Oncology

The main role of radiation therapy or radiotherapy (RT) is in the treatment of cancer through the delivery of a lethal dose of ionizing radiation to malignant cells. According to the Canadian Cancer Society [1], within Canada there were approximately 187 600 new cases of cancer, with 75 500 deaths in 2013. In the field of radiation oncology, radiation is prescribed to a tumor volume that covers the clinical extent of the disease as defined by imaging modalities such as Computed Tomography (CT), Positron Emission Tomography (PET) or Magnetic Resonance Imaging (MRI), plus a margin that accounts for sub-clinical disease and errors that occur in patient setup and delivery. The delivery of ionizing radiation to the tumor volume is done through the deposition of energy to tissue leading to DNA damage and consequently, cell death. The amount of dose deposited in

the medium (absorbed dose) is defined to be the amount of energy absorbed per unit mass of medium (J/kg) and is represented by the unit Gray (Gy). Damage to DNA can occur through energy deposition directly to the DNA or indirectly through interactions creating free radicals and reactive oxygen species. The probability of cell death is correlated with the absorbed dose deposited to the medium. The main objective in radiation oncology is to deliver dose to the tumor volume while simultaneously sparing healthy tissue from the harmful effects of ionizing radiation. This dose response is summarized by two parameters, the tumor control probability (TCP), which describes the probability of achieving tumor control as a function of target dose, and normal tissue complication probability (NTCP), which describes the risk of normal tissue complications as a function of dose to normal tissue [2]. These two curves are shown in Figure 1–1 and show that by horizontally separating the TCP and NTCP curves through appropriate planning techniques such as beam modulation, beam arrangement geometry or through the use of pharmaceuticals such as radio sensitizers, a high probability of tumor control can be achieved while minimizing acute and late toxicities. The ratio of the TCP and NTCP curves as a function of dose is known as the therapeutic ratio, and maximizing this quantity is the main goal of radiotherapy treatment planning.

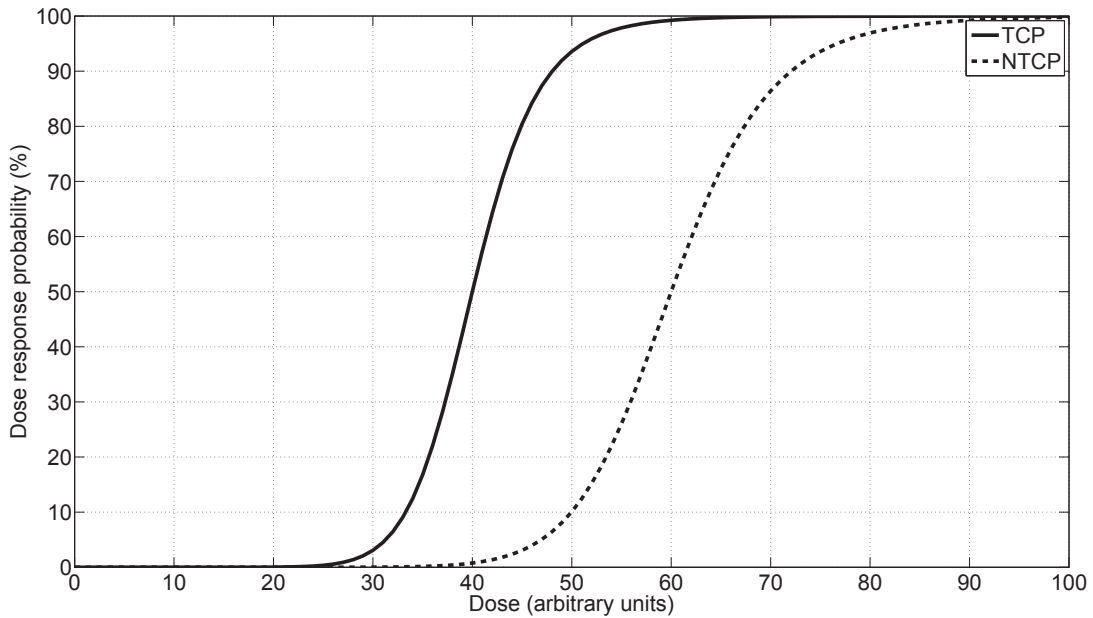


Figure 1–1: The tumor control probability (TCP) and the normal tissue complication probability (NTCP) curves, which describe the tumor response probability as a function of tumor dose and complication probability as a function of normal tissue dose, respectively.

The three main treatment modalities used in cancer therapy are surgery, chemotherapy and radiotherapy. Surgical resection involves the removal of the malignant mass or the entire organ. Chemotherapy refers to the use of one or more types of cytotoxic drugs to control the spread of malignant cells, or to eliminate them from the body. Radiotherapy involves the use of ionizing radiation to treat a variety of diseases including cancer and less commonly, some types of non-malignant disease. About half of all cancer patients will undergo some form of radiotherapy over the course of their treatment and is either delivered alone or in combination with surgery or chemotherapy [3]. In addition to these methods,

hormonal therapy, which involves manipulation of the endocrine system, is also used in the treatment of certain cancers such as breast and prostate.

Radiotherapy has been used since the discovery of the X ray by Roentgen in 1895 and has gone through much evolution over the years. Early RT was limited in the maximum photon energy available therefore limiting its uses. With the invention of the ^{60}Co teletherapy machine in the early 1950s higher energy photons became available and the role of RT was greatly expanded. Further advances in RT were made with the induction of medical linear accelerators (linacs) into clinical practice, bringing even higher beam energies as well as the capability to deliver electron beams. Typical energy ranges for both photon and electron therapies lie between 4 and 20 MeV and the choice of energy is dependent on tumor location and depth. An example of a modern linear accelerator is shown in Figure 1–2, where the patient would lie on the couch while the gantry would rotate around the patient to deliver radiation from one or more angles.

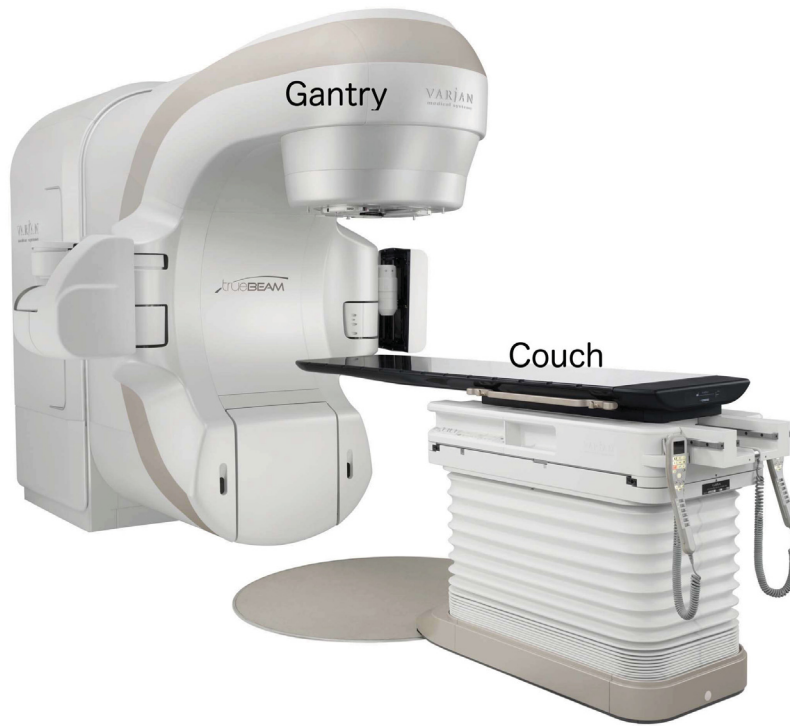


Figure 1–2: A Varian TrueBeam linear accelerator (courtesy of Varian®).

Modern radiotherapy can be classified as either external beam radiotherapy (EBRT) or brachytherapy. Brachytherapy involves placement of a sealed radioactive source into a body cavity, lumen, or surgically into other areas. EBRT entails directing externally produced photons or charged particles towards the target volume from outside the patient. Modern techniques in external beam radiotherapy, such as three dimensional conformal radiotherapy (3D CRT) and intensity modulated radiotherapy (IMRT), have allowed the transition from simple rectangular fields to more conformal techniques where the integrated dose to surrounding healthy tissues is minimized while maintaining equivalent or even higher target

dose [4]. The more recent of these two advances, IMRT, uses a combination of many small photon beams (beamlets) at multiple entry angles that sum together to produce highly conformal dose volumes that can even be concave in shape [5]. This modality was conceptualized by Brahme *et al.* in 1982 [6]. The first approach to inverse optimization of fluence modulated beams was published again by Brahme in 1988 [7]. Automated delivery systems followed in the early 1990s [8, 9, 10]. Commercial interest in this technique soon followed by all major vendors and rapid clinical implementation began throughout the mid to late 1990s.

The main advantage behind IMRT is its ability to create a recess or concavity within a particular dose distribution, typically with that cavity or cavities covering radiation sensitive organs at risk to reduce future complications. In traditional non-IMRT deliveries, when multiple beams converge on a common isocenter from various angles, the resulting dose distribution is convex in shape, meaning that the dose distribution will contain no concavities and will decrease as a function of distance away from the isocenter. However, as the fluence of these beams is allowed to be modulated by suitable beam shaping devices, very complex distributions containing concavities can be created. The physical basis behind this phenomenon can be described in a non-mathematical way by stating that a particular voxel (volumetric element or 3D pixel) in a high dose region is subject to a higher total photon fluence. This higher total fluence comes from the summed fluence from the multiple modulated beams that have high beamlet weights (one modulated field can be broken down into many smaller fields called beamlets) for those beamlets that are directed at that particular voxel. Conversely, when

the summed beamlet weights are relatively low for all beamlets that intersect a particular voxel, the dose at that point will also be relatively low. The task of the inverse optimization algorithm in the treatment planning phase is then to determine the optimal selection of beam weights that satisfies the minimum and maximum dose requirements of the target volume, while simultaneously satisfying the maximum dose requirements of the organs at risk. This is achieved through the use of a cost function that is constructed based on the organ and target dose constraints set by the planner. The inverse optimization algorithm will search the solution space of the cost function to find the global minima which represents the best dose distribution for the current planning constraints. Other types of constraints can also be used such as setting biological endpoints that can be derived based on dose response models for the tumor and healthy tissue.

1.2 Introduction to Modulated Electron Radiation Therapy

Electron therapy is used in cases that can benefit from the shape of the electron dose distribution as a function of depth, which includes a high entrance dose, relatively flat high dose section and then a rapid dose fall off whose depth of typically between 2-10 cm depends on the initial energy of the incident electrons (with higher energies penetrating to greater depths). The shape of this dose distribution as a function of depth is visualized in Figure 2-2. This leaves electron therapy as a particularly suitable modality, when compared to photon beams, for treating superficial malignancies confined to within a few cm of the patient surface. However, for the case where the target exhibits a variable depth of the distal edge, in conventional electron therapy the chosen electron energy must be the one

that is high enough to sufficiently cover the deepest part of the target. In regions where the distal edge of the target is at shallower depths, the same energy is also used leading to unnecessary dose exposure to healthy tissues beyond the target. Modulated electron radiation therapy (MERT) seeks to minimize this by matching the energy of each beamlet (energy modulation) to the depth of the distal edge of the target. Intensity modulation (adjustment of beamlet weights) is also used to ensure homogeneous dose coverage of the target.

Due to air scatter in both the unmodulated and modulated versions of electron therapy, the lateral sharpness of the electron beam is reduced as a function of distance from the collimator, requiring final collimation to be done within a few cm of the patient surface. This differs from photon collimation where an automated and motorized collimator is built into the treatment head at a position approximately 30 cm from the patient surface. The construction of the final electron collimation device shape, which consists of a molded aperture made of low melting point metal, is labor intensive and currently no commercial automated electron collimators exist. For this reason, as well as the fact that analytical dose calculation algorithms used to calculate dose in electron beams suffer from large inaccuracies under certain conditions [11, 12], modulated electron radiation therapy (MERT) has lagged behind its photon counterpart and is still exclusively in the research domain. However, the same principles behind photon IMRT planning and delivery can be applied to electron therapy should these two major issues be addressed. The topic of automated electron collimation has been investigated by various groups [13, 14, 15, 16, 17, 18], however each group has not

fully integrated each respective hardware solution into a fully automated delivery of an inversely optimized MERT plan based on accurate dose calculation methods. To address the issue of accurate dose calculation of electron beams under complex collimation geometry and tissue heterogeneity, Monte Carlo methods remain as the most accurate method. The main drawback of Monte Carlo dose calculation methods is the high computational cost, resulting in unacceptably long calculation times that preclude its adaptation in a clinical setting. However, increased access to cheap computing power and more efficient algorithms provide two options for overcoming this characteristic.

1.3 Hypothesis and Objectives

This work focuses on the accuracy and efficiency of an automated modulated electron radiation therapy (MERT) delivery as well as the potential benefits of incorporating modified scattering foils for this technique. We hypothesize that it is possible to accurately and efficiently deliver an automated MERT plan using a motorized tertiary collimator from a plan created using inverse optimization techniques and Monte Carlo dose calculation. It is also hypothesized that this type of plan could benefit from modification or removal of the scattering foil due to lower bremsstrahlung dose and higher dose rates.

To test the hypothesis, this work has the following objectives:

1. Develop an accurate Monte Carlo beam model for each clinically available electron beam energy.
2. To investigate the accuracy and efficiency of a MERT delivery using a tertiary electron collimator.

3. Investigate the potential benefits of custom scattering foils in MERT through simulations and measurements.

1.4 Thesis Outline

This thesis consists of three manuscripts. One manuscript has been published, while the other two have been submitted for review. Chapter 2 introduces the basic concepts related to the physics, generation and dosimetry of clinical electron beams. Chapter 3 focuses on the evolution and methods used in performing modulated electron radiotherapy deliveries, including collimator designs and treatment planning systems. Chapter 4 introduces submitted work done on the delivery and validation of an inverse optimized modulated electron radiotherapy plan.

Chapter 5 introduces published work in the area of bremsstrahlung reduction through removal of the scattering foil used to flatten electron beams in a clinical accelerator. Chapter 6 builds on the work of the previous chapter and discusses submitted work on the design of new optimized scattering foils specifically designed for MERT applications. Chapter 7 provides a summary and conclusion of the results and discusses potential future work on the topic of MERT.

REFERENCES

- [1] Canadian cancer statistics. Report, Canadian Cancer Society and Statistics Canada, 2013.
- [2] M Baumann and Cordula Petersen. Tcp and ntcp: a basic introduction. *Rays*, 30(2):99–104, 2004.
- [3] Radiation therapy for cancer. Report, National Cancer Institute, 2010.
- [4] S. A. Bhide and C. M. Nutting. Recent advances in radiotherapy. *BMC Med*, 8:25, 2010. Bhide, S A Nutting, C M eng Review England 2010/04/30 06:00 BMC Med. 2010 Apr 28;8:25. doi: 10.1186/1741-7015-8-25.
- [5] Thomas Bortfeld. Imrt: a review and preview. *Physics in medicine and biology*, 51(13):R363, 2006.
- [6] Anders Brahme, J-E Roos, and Ingemar Lax. Solution of an integral equation encountered in rotation therapy. *Physics in medicine and biology*, 27(10):1221, 1982.
- [7] A. Brahme. Optimization of stationary and moving beam radiation therapy techniques. *Radiother Oncol*, 12(2):129–40, 1988. Brahme, A eng Research Support, Non-U.S. Gov't NETHERLANDS 1988/06/01 Radiother Oncol. 1988 Jun;12(2):129-40.
- [8] MP Carol, H Targovnik, C Campbell, A Bleier, J Strait, B Rosen, P Miller, D Scherch, R Huber, and B Thibadeau. An automatic 3d treatment planning and implementation system for optimized conformal therapy. *Three-Dimensional Treatment Planning*, pages 173–87, 1993.
- [9] Thomas Bortfeld, Arthur L Boyer, Wolfgang Schlegel, Darren L Kahler, and Timothy J Waldron. Realization and verification of three-dimensional conformal radiotherapy with modulated fields. *International Journal of Radiation Oncology* Biology* Physics*, 30(4):899–908, 1994.

- [10] Spiridon V Spirou and Chen S Chui. Generation of arbitrary intensity profiles by dynamic jaws or multileaf collimators. *Medical physics*, 21:1031, 1994.
- [11] Joanna Cygler, Jerry J Battista, John W Scrimger, Ernest Mah, and John Antolak. Electron dose distributions in experimental phantoms: a comparison with 2d pencil beam calculations. *Physics in medicine and biology*, 32(9):1073, 1987.
- [12] George X Ding, Joanna E Cygler, Christine W Yu, Nina I Kalach, and G Daskalov. A comparison of electron beam dose calculation accuracy between treatment planning systems using either a pencil beam or a monte carlo algorithm. *International Journal of Radiation Oncology* Biology* Physics*, 63(2):622–633, 2005.
- [13] M. G. Karlsson, M. Karlsson, and C. M. Ma. Treatment head design for multileaf collimated high-energy electrons. *Medical physics*, 26(10):2161–7, 1999. Karlsson, M G Karlsson, M Ma, C M Med Phys. 1999 Oct;26(10):2161-7.
- [14] C. M. Ma, T. Pawlicki, M. C. Lee, S. B. Jiang, J. S. Li, J. Deng, B. Yi, E. Mok, and A. L. Boyer. Energy- and intensity-modulated electron beams for radiotherapy. *Phys Med Biol*, 45(8):2293–311, 2000. Ma, C M Pawlicki, T Lee, M C Jiang, S B Li, J S Deng, J Yi, B Mok, E Boyer, A L CA78331/CA/NCI NIH HHS/United States Comparative Study Research Support, Non-U.S. Gov't Research Support, U.S. Gov't, Non-P.H.S. Research Support, U.S. Gov't, P.H.S. England *Physics in medicine and biology Phys Med Biol*. 2000 Aug;45(8):2293-311.
- [15] M. C. Lee, S. B. Jiang, and C. M. Ma. Monte carlo and experimental investigations of multileaf collimated electron beams for modulated electron radiation therapy. *Med Phys*, 27(12):2708–18, 2000. Lee, M C Jiang, S B Ma, C M 5T32GM08294-11/GM/NIGMS NIH HHS/United States CA 78331/CA/NCI NIH HHS/United States Research Support, U.S. Gov't, Non-P.H.S. Research Support, U.S. Gov't, P.H.S. United States *Medical physics Med Phys*. 2000 Dec;27(12):2708-18.
- [16] K. R. Hogstrom, R. A. Boyd, J. A. Antolak, M. M. Svatos, B. A. Faddegon, and J. G. Rosenman. Dosimetry of a prototype retractable emlc for fixed-beam electron therapy. *Medical physics*, 31(3):443–62, 2004. Hogstrom,

Kenneth R Boyd, Robert A Antolak, John A Svatos, Michelle M Faddegon, Bruce A Rosenman, Julian G Med Phys. 2004 Mar;31(3):443-62.

- [17] T. Gauer, D. Albers, F. Cremers, R. Harmansa, R. Pellegrini, and R. Schmidt. Design of a computer-controlled multileaf collimator for advanced electron radiotherapy. *Physics in medicine and biology*, 51(23):5987–6003, 2006. Gauer, T Albers, D Cremers, F Harmansa, R Pellegrini, R Schmidt, R England Phys Med Biol. 2006 Dec 7;51(23):5987-6003. Epub 2006 Oct 30.
- [18] K. Al-Yahya, F. Verhaegen, and J. Seuntjens. Design and dosimetry of a few leaf electron collimator for energy modulated electron therapy. *Med Phys*, 34(12):4782–91, 2007. Al-Yahya, Khalid Verhaegen, Frank Seuntjens, Jan Research Support, Non-U.S. Gov't United States Medical physics Med Phys. 2007 Dec;34(12):4782-91.

CHAPTER 2
Introduction to electron beam radiation therapy

Contents

2.1	Generation of electron beams	15
2.1.1	Microtrons	15
2.1.2	Linear accelerators	16
2.1.3	Treatment head components and final beam shaping	18
2.2	Electron interactions and general concepts	21
2.2.1	Particle and energy fluence	21
2.2.2	Stopping power	21
2.2.3	Bremsstrahlung radiation	22
2.2.4	Mass attenuation, mass energy transfer and mass energy absorption coefficients	23
2.2.5	Kerma	24
2.2.6	Absorbed dose	24
2.2.7	Central axis depth dose	25
2.2.8	Accelerator output and output factor	27
2.3	Dosimetry of radiation beams	29
2.3.1	Measurement phantoms	29

2.3.2	Dose measurement detectors	29
2.4	Monte Carlo dose calculation methods	34
2.4.1	EGSnrc codes	34

Electron beam radiotherapy fills an important niche in the treatment of superficial disease in the clinic today. This chapter presents an overview of the many aspects involving the production, delivery and dosimetry of these beams.

2.1 Generation of electron beams

Beam production in radiotherapy typically consists of the acceleration of charged particles using either an electrostatic or cyclic electric field. The generation of electron beams involves taking the beam directly from the accelerating section and directing it at the patient using beam transport systems. The production of photon beams involves the extra step of inserting a bremsstrahlung target of sufficient thickness as to stop all primary electrons into the beamline. One of the earlier types of electron therapy was performed using a Van de Graaff generator as reported by Trump *et al.* in 1953 [1]. However, these static accelerators were limited to energies of around 2 MeV due to the need for very large voltage differentials in the acceleration process and were therefore only useful in treating superficial malignancies. Also, due to the very large size of the high-energy generators, the ability to rotate the unit to deliver beams from multiple angles was severely limited.

2.1.1 Microtrons

In 1945 Veksler introduced the circular orbit microtron [2]. This device employed a single accelerating section position between the gaps of two 180 degree

bending magnets. At each subsequent pass through the accelerating structure, the electron bunch gains a small amount of energy, leading to successively larger orbits. The size of the orbit is increased each time such that the electron bunch arrives back at the accelerating section when the electric field is in the proper phase to further accelerate the electron bunch. With this type of accelerating device, beam energies of 50 MeV were easily achieved with a relatively compact design when compared to linacs. The first Microtron designed for medical purposes was the MM50 microtron designed by Brahme *et al.* in cooperation with the company Scanditronix in the 1970s and early 1980s [3]. This type of microtron was put into clinical use in 1988 as was capable of producing both photon and electron beams. Due to its ability to easily switch beam energies and the broad range of electron energies available, it was well suited for MERT applications and was used in feasibility studies by two different groups in 1996 [4, 5]. Despite also having a narrow energy spread (allowing easy beam transport), ease of energy switching and the need for only a low power accelerating section, the microtron remains much less common than the linac.

2.1.2 Linear accelerators

The first linear accelerator used in radiotherapy was installed in 1953 at the Hammersmith hospital in the UK and was capable of producing an 8 MV photon beam [6]. Over the years, linacs became more efficient and compact, leading to higher beam energies and 360 degree isocentric rotation of the gantry around the patient. Modern accelerators are capable of producing either electron or photon

beams in the energy range of 4-25 MeV. The production of these beams is achieved through the integration of several major systems including:

1. radiofrequency (RF) power generation
2. electron injection system
3. accelerating waveguide
4. beam transport system
5. beam monitoring system

The main component in the RF power generation system is the microwave power source. This component is either a klystron or magnetron typically operating around the 3 GHz range. The RF generator is coupled to the accelerating waveguide to allow the propagation of RF into the waveguide. In its simplest form, the accelerating waveguide consists of a long cylinder divided up into cavities by many disks with small holes along the beamline to allow the passage of the electron beam and to allow the RF wave to fill the length of the waveguide. Before entering into the accelerating waveguide, the electron beam is formed within the electron injection system. Initially the electrons are boiled off a cathode through thermionic emission and are accelerated through a small hole in an anode with the help of a focusing electrode. Once in the accelerating waveguide, the electrons are accelerated along the length of the waveguide due to their interaction with the electric field as governed by the Lorentz force shown in equation 2.1,

$$\vec{F} = e(\vec{E} + \vec{v} \times \vec{B}) \quad (2.1)$$

where \vec{F} is the force acting on the particle, e is the electron charge, \vec{E} is the electric field, \vec{v} is the particle velocity, and \vec{B} is the magnetic field. As the electron bunch propagates down the length of the waveguide, the timing of the position of the electron bunch and the phase of the electric field is timed such that the electron always experiences a positive potential ahead of the bunch and a negative potential behind. Within the waveguide section, sets of coils are used for beam focusing and steering of the electron beam. Due to the length of modern high-energy waveguides (1.5 meters for 25 MeV), it is not practical to mount the waveguide pointing directly at the patient. The role of the beam transport system is to steer the electron beam from the waveguide exit and onto the target or scattering foil in photon or electron mode respectively. This is typically accomplished with a 270° doubly achromatic bending magnet in Varian accelerators that directs the beam down into the treatment head of the accelerator. Within the bending magnet, two scrapers act as an energy slit that confines the beam energy to within a limited range of the nominal value. This is accomplished due to the fact that higher-energy charged particles will take a path that consists of a greater radius of curvature compared to lower energy charged particles. By providing some physical limits in the deviation from the desired trajectory of the particles in the magnetic field, a fairly sharp peak in the energy distribution can be achieved.

2.1.3 Treatment head components and final beam shaping

A schematic diagram of the different components found typically found in the head of an accelerator operating in electron mode is seen in Figure 2–1.

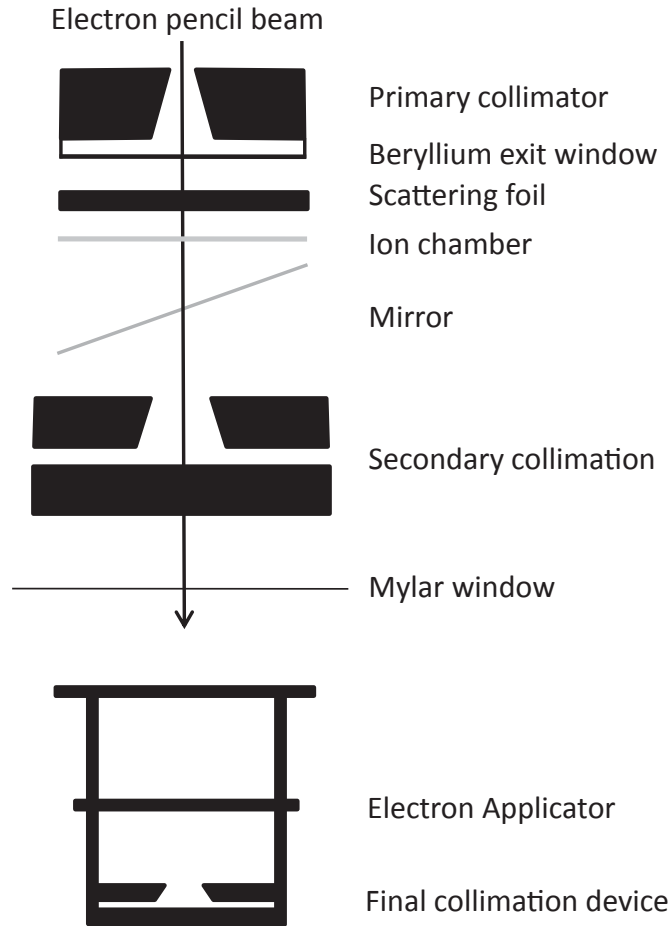


Figure 2-1: A schematic diagram of the different components in the head of a high-energy Varian accelerator.

Before reaching the scattering foil, the electron beam passes from vacuum and into normal atmosphere through a thin exit window. Although the major contributor to the scatter of the electron beam is the scattering foil, there is still a reasonable contribution from the remaining head components and the air gap between the exit window and the patient surface. Modern scattering foils consist of

a primary and a secondary foil as was first introduced by Kozlov and Shishov [7]. As the initial FWHM of the electron beam from microtrons and linear accelerators is quite narrow (on the order of 2-3 mm), the primary foil is in place to provide initial broadening to the beam before it reaches the secondary foil. The primary foil consists of a thin plate a high-Z material to minimize energy degradation of the beam. The secondary foil, also called a compensating foil, consists of multiple low-Z disks of varying diameters stacked on top of each other to form a pyramid shape. Its purpose is to transform the unflattened multiple scattering distribution into a relatively flat lateral profile at the level of the patient. This is achieved by preferentially scattering the central axis electrons (where fluence is highest) laterally outwards to where the fluence normally drops off as a function of distance off axis.

Close behind the scattering foil is the transmission ionization chamber. This component serves the dual purpose of monitoring the integrated dose and dose rate in addition to providing active feedback to the beam steering system on the beams current, lateral position and angle relative to the central axis. The secondary collimator jaws provide initial collimation of the electron beam and are set depending on the size of the interchangeable electron applicator that is in place. Both the secondary collimator and two electron scrapers built into the applicator provide progressively smaller square beam collimation down to the level of the electron applicator insert, which consists of an irregularly shaped aperture used to define the final lateral shape of the electron beam. The aperture

is made using a low melting-point metal that can be formed and reformed into any aperture shape within its square frame.

2.2 Electron interactions and general concepts

2.2.1 Particle and energy fluence

The particle fluence (Φ) is defined by the ICRU 60 report [8] to be the quotient of dN by da , where dN is the number of particles incident on the surface of a sphere of cross sectional area da and has the units of m^2 .

$$\Phi = \frac{dN}{da}. \quad (2.2)$$

The energy fluence (Ψ), mainly used to describe uncharged particle beams, is defined to be the quotient of dR by da , where dR is the radiant energy incident on the surface of a sphere of cross sectional area da and has the units of J/m^2 .

$$\Psi = \frac{dR}{da}. \quad (2.3)$$

2.2.2 Stopping power

The stopping power (S) is defined as the rate of energy loss (dE) per unit length (dl) traveled in the medium and has the units of MeV/cm .

$$S = \frac{dE}{dl}. \quad (2.4)$$

The stopping power is often normalized by the density of the medium (ρ) and that quantity is named the mass stopping power with units of $MeVcm^2/g$. The mass stopping power can be broken up into two separate quantities, the mass collisional stopping power (S_{col}) which describes the energy loss due to

collisions with orbital electrons and the mass radiative stopping power (S_{rad}) which describes the energy loss due to emission of bremsstrahlung by the electron through interactions with the electric fields of the nucleus and orbital electrons.

$$\frac{S}{\rho} = \frac{1}{\rho} \frac{dE}{dl} = \frac{S_{col}}{\rho} + \frac{S_{rad}}{\rho}. \quad (2.5)$$

The dose deposited by electrons in a medium can then be written in terms of the following quantities.

$$D_{med} = \Phi \frac{S_{col}}{\rho}. \quad (2.6)$$

2.2.3 Bremsstrahlung radiation

The quantity (S_{rad}) that was introduced in section 2.2.2 is an important quantity in describing the production of photon beams. In the case of photon radiotherapy, the electron beam is directed at a target designed with a thickness approximately 10% greater than the range of the electrons. This thickness is a best compromise between ensuring that all electrons are stopped in the target as well as minimizing the attenuation of the bremsstrahlung photons that will continue through the target to form the treatment beam. However, in the production of electron beams, the bremsstrahlung interactions with head components will result in undesirable contamination photons that are mixed in with the electrons. (S_{rad}) can be written as follows:

$$S_{rad} = N_a \sigma_{rad} E_i, \quad (2.7)$$

where N_a is the number of atoms per unit mass, σ_{rad} is the total cross section for bremsstrahlung production for a given energy and E_i is the initial total energy of the electron. The mass radiative stopping power is proportional to Z and E_i for energies above 2 MeV.

2.2.4 Mass attenuation, mass energy transfer and mass energy absorption coefficients

The mass attenuation coefficient (μ/ρ) represents the probability that an uncharged particle (photon) will undergo an interaction within a specific medium. It is defined by the following:

$$\frac{\mu}{\rho} = \frac{1}{\rho dl} \frac{dN}{N}, \quad (2.8)$$

where ρ is the density of the medium, dl is the distance the photon has traveled and dN/N is the fraction of particles that will experience an interaction.

The mass energy transfer coefficient (μ_{tr}/ρ) is related to the mass attenuation coefficient in the following way:

$$\frac{\mu_{tr}}{\rho} = \frac{\bar{E}_{tr}}{h\nu} \frac{\mu}{\rho}, \quad (2.9)$$

where $\bar{E}_{tr}/h\nu$ is the mean fraction of energy transferred to charged particles by photons.

The mass energy absorption coefficient (μ_{ab}/ρ) is related to the mass energy transfer coefficient by:

$$\frac{\mu_{ab}}{\rho} = \frac{\mu_{tr}}{\rho} (1 - \bar{g}), \quad (2.10)$$

where \bar{g} is the radiation yield which represents the fraction of energy transferred to the medium that is lost through radiative processes.

2.2.5 Kerma

The Kinetic Energy Relaxed per unit MAss (Kerma or K) is defined as the mean energy transferred to a medium (\bar{E}_{tr}) per unit mass. (\bar{E}_{tr}) represents the sum of the initial kinetic energies of charged particles liberated by uncharged particles. Kerma has the units of J/kg and is defined as:

$$K = \frac{d\bar{E}_{tr}}{dm}, \quad (2.11)$$

where dm is a small mass of medium.

Kerma can be related to the previous quantities in the following ways:

$$K = K_{col} + K_{rad} = \Psi \frac{\mu_{tr}}{\rho}, \quad (2.12)$$

$$K_{col} = K(1 - \bar{g}) = \Psi \frac{\mu_{ab}}{\rho}, \text{ and} \quad (2.13)$$

$$K_{rad} = K\bar{g} = \Psi \frac{\mu_{tr}}{\rho} \bar{g}, \quad (2.14)$$

where Ψ represents the energy fluence.

2.2.6 Absorbed dose

The absorbed dose is defined as the mean energy imparted ($d\bar{E}_{abs}$) by ionizing radiation to a finite volume of medium with small mass dm . It has units of J/kg which is defined in SI units as the gray (Gy). Absorbed dose is defined by the following equation:

$$D = \frac{d\bar{E}_{ab}}{dm}. \quad (2.15)$$

2.2.7 Central axis depth dose

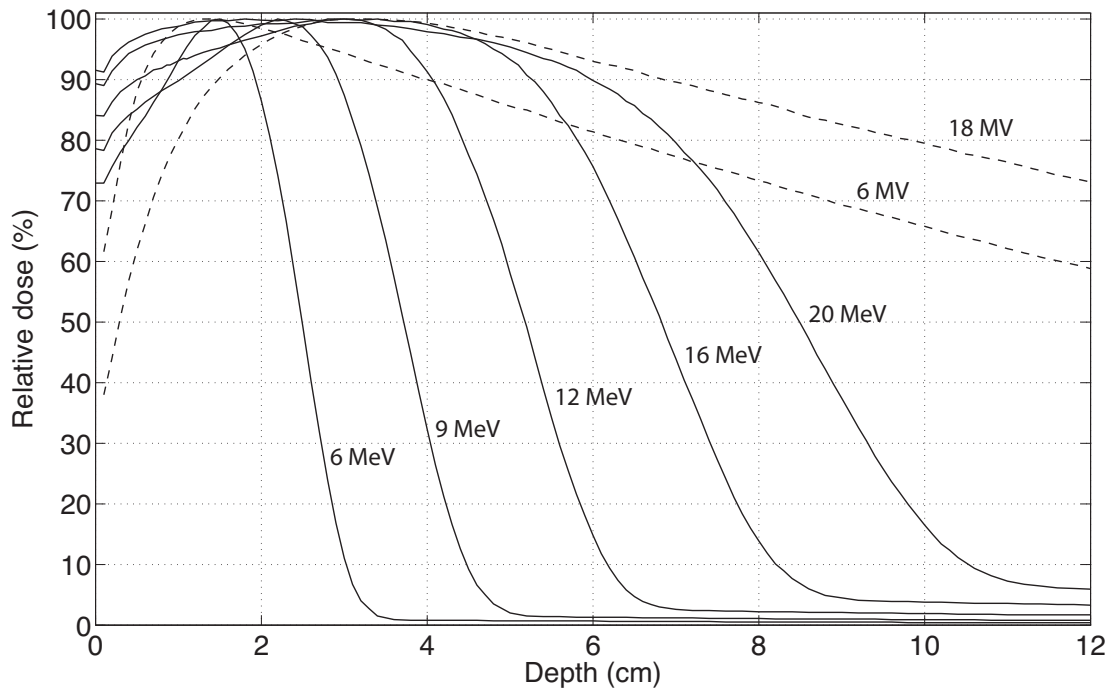


Figure 2–2: Percent depth dose curves for electrons (solid lines) and photons (dashed lines)

The central axis depth dose, or percent depth dose (PDD) is a representation of the absorbed dose as a function of depth along the central axis. An example figure showing the dose deposition characteristics of photons (dashed lines) and electrons (solid lines) for some common clinical energies in water is shown in Figure 2–2. It can be seen that there are very distinct differences between the photon and electron curves. In the case of the electron PDDs, the dose rapidly falls off as a function of depth due to the energy degradation of the electrons that typically represents approximately 2 MeV/cm in water. The sharp reduction in dose beyond a certain depth, and therefore sparing of distal healthy tissue, is one

of the main advantages of electron therapy that makes it particularly suitable for superficial targets.

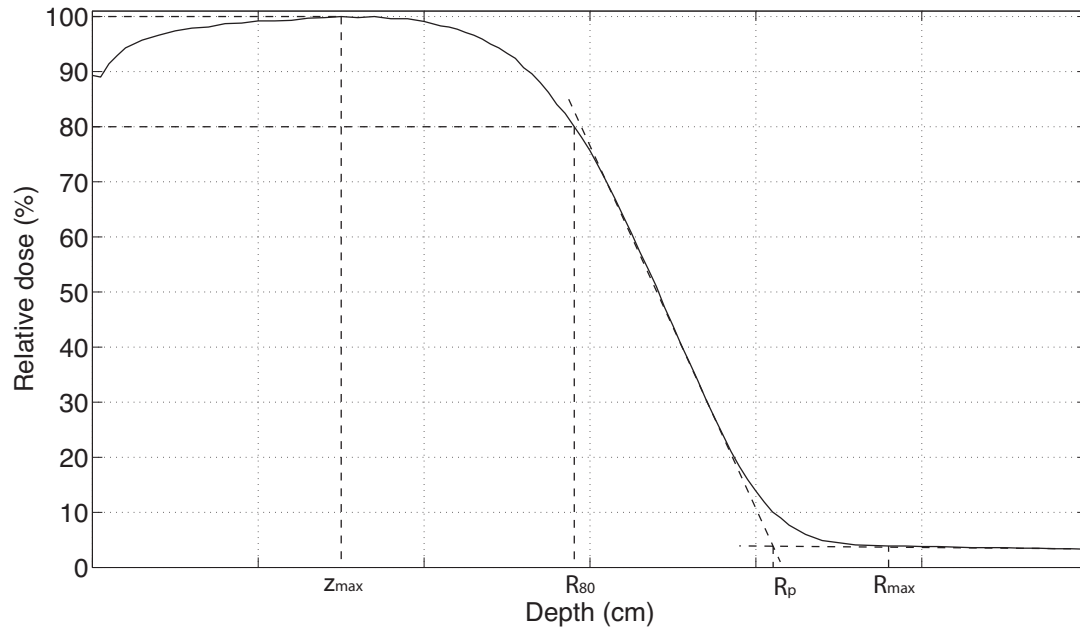


Figure 2–3: Different range quantities

Figure 2–3 illustrates some of the dosimetric parameters of the electron PDD including:

1. z_{max} : The depth at which the dose maximum occurs.
2. R_{80} : The depth at which the dose drops to 80 percent of its maximum dose.
3. R_p : The practical range which is defined as the depth at the intersection of a line tangential to the R_{50} : value and a line tangential to the bremsstrahlung tail
4. R_{max} : The maximum range of electrons of a particular energy in a given medium.

Beyond the R_{max} value, there still exists a slowly decreasing dose known as the bremsstrahlung tail that is a result of contamination photons. These photons are a result of electron interactions with the head components (approximately 50% of the total contribution) as well as within the water phantom itself. The magnitude of this dose as a function on the dose at d_{max} increases as a function of energy and is typically less than 4% for 20 MeV clinical electron beams [9].

2.2.8 Accelerator output and output factor

According to the ICRU, the overall accuracy in tumor dose delivery should be within $\pm 5\%$ [9]. To achieve the desired accuracy in dose delivery, the photon and electron beams must be calibrated to give a known dose under certain reference conditions. The machine conditions under which calibration takes place are typically defined by a 10×10 cm² field size projected to the phantom surface, and a nominal source to surface distance (SSD) of 100 cm. According to the AAPM task group report number 51 [10], the dose reference point in photon beams is defined at a depth of 10 cm in water, whereas the reference point in electron beams is defined at a reference depth (d_{ref}) that is related to the R_{50} value. The calibration itself entails matching the dose measured under these reference conditions to a machine-specific quantity, the monitor unit (MU). The MU is an integer that represents the integrated signal recorded from the accelerators internal transmission ionization chamber. Under the aforementioned reference conditions, one MU is set to be equal to 1 cGy at the depth of dose maximum (d_{max}), which is related back to the reference point through the PDD.

The beam calibration is performed under these specific reference conditions as the cGy per MU value is dependent on field size. In photon therapy, this variation of dose output as a function of field size is referred to as the relative dose factor (RDF) and is subject to only minor variations of $\pm 5\%$ from the reference condition. However, in electron therapy, the dose output factor is highly sensitive to the secondary collimator setting, as shown in 2–4. Under normal clinical treatment conditions, the secondary collimator is therefore left at a relatively large field setting, even when small fields, as defined by the applicator insert, are in use. The change in dose output as a function of secondary collimator setting and final beam collimation (typically the applicator insert) must be modeled correctly in the treatment planning system in order to achieve accurate dose prediction.

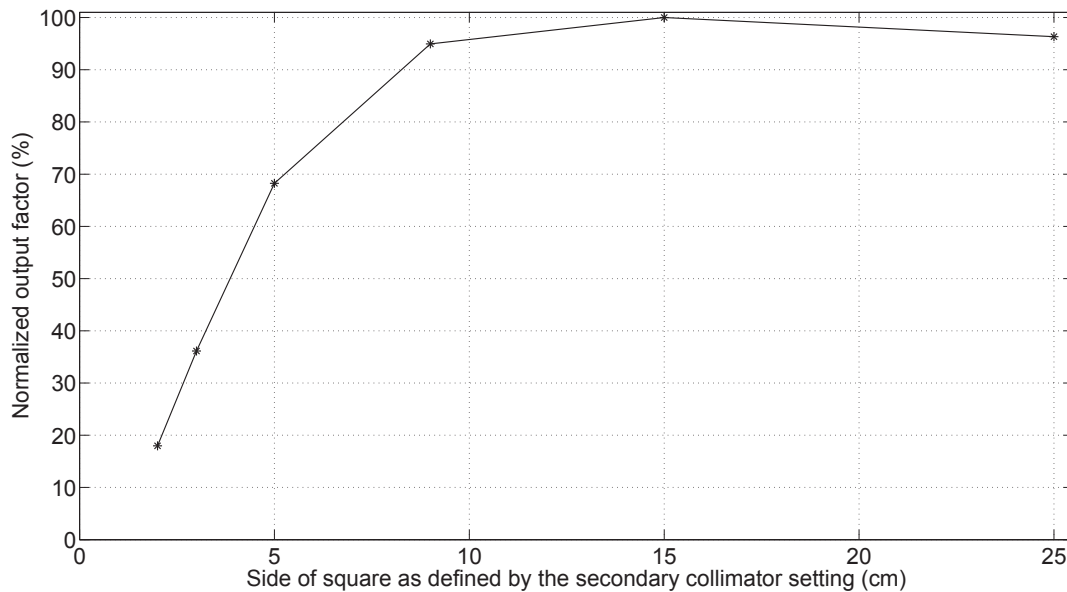


Figure 2–4: Relative output factor of a 12 MeV electron beam defined by the secondary collimator jaws without the electron applicator present.

2.3 Dosimetry of radiation beams

2.3.1 Measurement phantoms

In order to achieve accurate and reproducible dose measurements, different measurement media known as phantoms are used with well-defined compositions and geometries. Since the end goal in radiation therapy is to deliver dose to tissue, these phantom materials are often made of tissue-like materials. Since tissue is mainly composed of water, scanning water tanks are commonly used where it is desirable to move the detector within the phantom. These water tanks are typically $(60\text{ cm})^3$ and have a motorized translation mechanism that can move an attached detector in all three axes. Although these water tanks are ideal for 3D relative dosimetry, they are difficult and time consuming to setup. For other applications, water equivalent slabs of solid epoxy resins mixed with powders are often used. One common type of these is Solid Water[®], which features a density close to water of 1.04 g/cm^3 . Solid Water[®] is very easy to setup and use when performing film dosimetry or chamber dosimetry using slabs machined with a hole or recess to fit the chamber. Other phantoms exist that provide many different shapes and chemical compositions that vary depending on the application.

2.3.2 Dose measurement detectors

Ionization chambers

Ionization chambers remain a very common and accurate way to measure dose. They are often used to determine relative dose measurements, and when calibrated against a primary standard, they can also be used as secondary standard to determine absolute dose. Ionization chambers are typically a gas-filled

cavity that is enclosed by two electrodes of opposing polarity. As radiation passes through the detector, ion pairs of electrons and ionized molecules are created in the gas volume. The electric field present between the two electrodes causes the newly created ions to experience an attractive force in opposing directions with the electrons traveling towards the more positively charged electrode and the positively charged ions experiencing a force towards the more negatively charged electrode. This flow of charge can be measured using an attached electrometer and can then be converted to dose to air using:

$$D_{air} = \frac{Q}{m_{air}} \left(\frac{W_{air}}{e} \right), \quad (2.16)$$

where Q is the measured charge, m_{air} is the mass of air in the collecting volume, and (W_{air}/e) is the mean energy required to produce an ion pair in air per unit charge (33.97 J/C for dry air). The conversion of dose to air to dose to medium, which is the central quantity of interest in radiotherapy, is done using Bragg-Gray or Spencer-Attix cavity theory. The measurement of dose in electron beams using Bragg-Gray cavity theory is correct when the following two assumptions are true:

1. The size of the cavity is small relative to the range of charged particles incident on it so as to not perturb the fluence of the incoming particles.
2. No secondary (δ) electrons are created inside the cavity and all electrons have sufficient energy to cross the cavity without coming to a stop.

When these conditions are true, conversion of dose to medium (D_{med}) from the measured dose to air (in the case of an air filled ionization chamber) can be determined by the ratio of the average unrestricted mass collision stopping powers:

$$D_{med} = D_{cav} \left(\frac{\bar{S}}{\rho} \right)_{med,cav}, \quad (2.17)$$

where D_{cav} is the dose measured in the air cavity and $(\bar{S}/\rho)_{med,cav}$ is the average unrestricted mass collision stopping power for the medium of interest divided by the same quantity for air [11].

The most common type of ionization chamber is the cylindrical type. It consists of a cylindrical wall that is held at a certain potential and a central electrode that sits along the central axis of the chamber wall and is held a different potential. Measurement volumes can typically vary between 0.1 and 1 cm³ [9]. Farmer chambers are cylindrical chambers that typically have an air cavity volume of 0.6 cm³ and are commonly used in both photon and electron beam dosimetry.

Parallel plate chambers are another type of chamber that consists of two circular disks of 5-15 mm in diameter placed within 1-2 mm of one another. The small separation of electrodes offers high spatial resolution along one axis and is particularly useful in surface dose measurements and in the reference dosimetry of electron beams of 10 MeV and below due to the steep dose gradients encountered.

Silicon diodes

Silicon diodes can be used as dosimeters and are very desirable under certain conditions due to their high sensitivity and small size relative to air filled ionization chambers. Radiation interactions in and around the depletion layer

cause currents to form that can be read out by an electrometer. In measuring profiles and depth dose measurements in electron beams, diodes measure dose directly as opposed to the ionization that is measured by ionization chambers. However, diodes do suffer from multiple deficiencies which must be considered such as sensitivity drift caused by the accumulation of radiation damage, temperature dependence, dose rate dependence, angular dependence and energy spectrum dependence [9]. Over-response of the diode in the bremsstrahlung tail region due to the photon contamination has also been reported and is attributed to the higher effective Z of the diode relative to water [12, 13]. This over response is on the order of up to 1 percent of the dose at depth maximum for a 21 MeV beam. 2D arrays of diodes can provide instant planar dose information with relatively high spatial density and are routinely used for dosimetric verification of clinical plans.

Radiochromic film

Film offers an very high planar spatial resolution compared to chambers or diodes. It is particularly well suited for planar dose measurements as detector systems are either comparatively slow at acquiring 2D distributions (if one scanning detector is used) or expensive (if high resolution 2D arrays of many detectors are used).

Radiochromic film represents a new type of film dosimetry that has replaced radiographic film in most clinical applications. Radiographic film consists of a sheet of plastic that contains a radiation sensitive emulsion layer of silver bromide (AgBr) grains [9]. Exposure of the film to radiation causes a latent image to form that can be related to dose. Processing of the film using special chemicals

transforms the latent image into a visible image where the optical density can then be converted to dose using a calibration curve (referred to as a sensitometric curve). One main drawback of radiographic film is its sensitivity to visible light and great care must be taken in the handling and processing of the film to avoid accidental exposure to ambient light. Alternatively, radiochromic film contains an active ingredient that is polymerized upon exposure to radiation, directly changing the optical properties of the film. The film is considered to be self-developing, however, the film continues to polymerize to some extent as a function of time and care must be taken to maintain a consistent amount of time (such as 24 hours) between exposure and reading the dose. Radiochromic film is dose rate independent and has little dependence on temperature, humidity and beam energy in the therapeutic energy range (1-25 MeV).

The calibration and analysis of radiochromic film to high accuracy can be accomplished using the recently described method of triple channel film dosimetry [14]. The reading of radiochromic film is often performed using commercial flat bed document scanners. The measured quantity is again optical density which is stored as a pixel intensity value from a scanner operating in transmission mode. The pixel value can be converted to dose using a calibration curve constructed from film strips irradiated to known doses. During scanning, the pixel value is stored for red, green and blue colour channels. By analyzing the intensities of the three colour channels relative to one another, corrections for such things as active layer thickness variations and scanner artifacts can be generated and applied to the

final image, resulting in higher accuracy and elimination of other time consuming techniques used to correct for these effects.

2.4 Monte Carlo dose calculation methods

The Monte Carlo (MC) method is a way of solving the Boltzmann transport equation for photons and electrons that is otherwise too difficult to achieve analytically. The propagation of these particles through a medium is simulated by sampling probability distributions using random or pseudo random numbers to determine when an interaction will occur and the interaction type. This technique was first suggested by Ulam and Von Neuman in 1947 as a way to perform radiation shielding calculations relating to neutrons [15]. The use of MC methods in medical physics has grown very fast over the past few decades due to increasing computational power and the decreased cost in accessing these resources. According to a review paper published by Rogers, the number of papers containing the words 'Monte Carlo' in the title have doubled every 5 years between 1967 and 2000 [16]. Monte Carlo methods are considered to be the gold standard in accurate dose calculations due to their ability to accurately predict scatter doses and dose in heterogeneous media, in contrast to model-based algorithms [17].

2.4.1 EGSnrc codes

The EGS (Electron Gamma Shower) code was created out of code developed at the Stanford Linear Accelerator (SLAC) National Accelerator Laboratory in the 1960s and 70s. Many upgrades to the code have been made since its inception. One branch in the development of the code is named EGSnrc and is the main version in use for radiotherapy simulation. [18, 19, 20, 21, 22]. Other

versions of EGS exist however, with EGS5 still in active development and in use in applications outside radiotherapy. EGSnrc is maintained by a group located at the Institute for National Measurement Standards, Ionizing Radiation Standards, NRC (National Research Council), Ottawa, Ontario, Canada. EGSnrc is a general purpose code designed to simulate the coupled transport of both photons and electron through arbitrary geometry. This code system has been used and benchmarked extensively for radiotherapy and medical imaging applications in the energy range of 10 keV to 30 MeV. Modeled photon interactions in this energy range include coherent (Rayleigh) scattering, photo-electric effect, incoherent (Compton) scattering and pair production. The transport of electrons and positrons includes both elastic as well as inelastic scattering.

Generally, simulation of the particle transport first entails the creation of a particle with a particular position, angle and energy. The code then tracks the primary particle and in turn, all of the resulting secondary, tertiary, etc. particles (referred to as a particle shower) until they reach a certain minimum user-determined energy threshold or leave the geometric boundary. The process of transporting many primary particles, or histories as they are often referred, is typically done millions of times in order to achieve the desired statistical uncertainty which decreases as $N^{-1/2}$, where N is the number of histories. The transport of this many particles requires a great amount of computational power. Typical single core simulations can take between minutes and days depending on the chosen parameters and the desired uncertainty. However, due to the 'embarrassingly parallel' nature of MC simulations (each history is independent

of the rest), distribution of the work to multi-CPU clusters or even graphical processing units (GPUs) can greatly reduce the simulation time.

In the case of electrons in the therapeutic energy range of a few MeV, a great number of interactions per unit length will occur, resulting in a high computational burden. EGSnrc uses a condensed history technique [23] which entails condensing many interactions into a single step to improve the efficiency. The PEGS4 data preprocessing code can be used in conjunction with EGSnrc to create the data files containing cross sectional data for each media over a wide range of energies.

BEAMnrc

BEAMnrc [24] is an EGSnrc user code also developed and maintained at NRC in collaboration with the OMEGA (Ottawa Madison Electron Gamma Algorithm) project. It is used to model radiotherapy sources and contains the framework to create the geometries necessary to model typical components found in various radiation producing devices. Individual equipment components are defined using 'component modules' (CM) that are part of the BEAMnrc system. There are various types of component modules that are written to model specific types of components and each CM accepts geometrical parameters and inputs specific to that module. The inputs to each CM, and general parameters such as number of histories, energy cutoffs etc. are stored within an input file that is passed to the BEAMnrc executable. The output of the BEAMnrc simulation consists of a phasespace which is a record of each particle that crosses a certain plane and includes the particle type, weight, position, angle and energy as well as 'latch bits' that can be used to track the interaction history of that particle.

DOSXYZnrc

DOSXYZnrc is also an EGSnrc user code. It is primarily used to score dose within a rectilinear volume often defined as either a homogeneous medium such as water or as a heterogeneous medium derived from a patient CT scan or some geometry specified by the user.

In the case where the voxel geometry is created from a patient CT scan, the determination of tissue material and density relies on accurate calibration of the CT scanner and accurate, artifact-free reconstruction. As stated by du Plessis *et al.*, this conversion of CT numbers (defined as Hounsfield units or HU) into tissue properties is one of the main factors that determine the accuracy of patient dose calculations [25]. The relation of the HU value to tissue property is done through assigning media types to different ranges of HU value. The number of media is typically six or fewer, however, as discussed by Vanderstraeten *et al.*, the use of 14 materials was recommended over the conventional 5 materials due to local differences which were mostly smaller than 5% [26]. In this work, voxels were assigned one of four materials including air, lung, tissue and bone depending on the HU of the voxel. In addition to assigning material type, density is also scaled based upon the voxel HU value.

The typical input to the DOSXYZnrc user code is the phasespace output from BEAMnrc. This can often be simplified by compiling a specific BEAMnrc simulation as a shared library to the DOSXYZnrc executable. This allows the output particles from the BEAMnrc simulation to be passed directly to the DOSXYZnrc simulation, without the need to store them in an intermediate

phasespace. Simulation parameters and phantom geometry are again specified in an ASCII input file. During the simulation, photon and electron transport are performed in the same way as in the BEAMnrc simulation, with the exception of basic parameters set in the input file. The resulting output of the DOSXYZnrc simulation is the creation of a 3D dose matrix file that contains the dose and estimated statistical uncertainty in each voxel. This file can easily be read into custom analysis scripts written in MATLAB (Mathworks, Natick MA).

REFERENCES

- [1] J. G. Trump, K. A. Wright, W. W. Evans, J. H. Anson, H. F. Hare, J. L. Fromer, G. Jacque, and K. W. Horne. High energy electrons for the treatment of extensive superficial malignant lesions. *Am J Roentgenol Radium Ther Nucl Med*, 69(4):623–9, 1953. TRUMP, J G WRIGHT, K A EVANS, W W ANSON, J H HARE, H F FROMER, J L JACQUE, G HORNE, K W eng Not Available 1953/04/01 Am J Roentgenol Radium Ther Nucl Med. 1953 Apr;69(4):623-9.
- [2] V. I. Veksler. A new method of acceleration of relativistic particles. *J. Phys.*, 9:153–158, 1945.
- [3] A Brahme, T Kraepelien, and H Svensson. Electron and photon beams from a 50 mev racetrack microtron. *Acta Oncologica*, 19(4):305–319, 1980.
- [4] Simo Hydynmaa, Anders Gustafsson, and Anders Brahme. Optimization of conformal electron beam therapy using energy-and fluence-modulated beams. *Medical Physics*, 23:659, 1996.
- [5] Björn Zackrisson and Mikael Karlsson. Matching of electron beams for conformal therapy of target volumes at moderate depths. *Radiotherapy and oncology*, 39(3):261–270, 1996.
- [6] J. S. Laughlin. Development of the technology of radiation therapy. *Radiographics*, 9(6):1245–66, 1989. Laughlin, J S eng Biography Historical Article Portraits 1989/11/01 Radiographics. 1989 Nov;9(6):1245-66.
- [7] A. P. Kozlov and V. A. Shishov. Forming of electron beams from a betatron by foil scatterers. *Acta Radiol Ther Phys Biol*, 15(6):493–512, 1976. Kozlov, A P Shishov, V A eng SWEDEN 1976/12/01 Acta Radiol Ther Phys Biol. 1976 Dec;15(6):493-512.
- [8] ICRU. Fundamental quantities and units for ionizing radiation. Report, ICRU, 1998.

- [9] E. B. Podgorsak. *Radiation Oncology Physics: A Handbook for Teachers and Students*. IAEA, 2005.
- [10] Peter R Almond, Peter J Biggs, BM Coursey, WF Hanson, M Saiful Huq, Ravinder Nath, and DWO Rogers. Aapms tg-51 protocol for clinical reference dosimetry of high-energy photon and electron beams. *Medical physics*, 26:1847, 1999.
- [11] Faiz M Khan, Karen P Doppke, Kenneth R Hogstrom, Gerald J Kutcher, Ravinder Nath, Satish C Prasad, James A Purdy, Martin Rozenfeld, and Barry L Werner. Clinical electron-beam dosimetry: Report of aapm radiation therapy committee task group no. 25. *Medical physics*, 18:73, 1991.
- [12] L. L. Wang and D. W. Rogers. Monte carlo study of si diode response in electron beams. *Medical physics*, 34(5):1734–42, 2007. Wang, Lilie L W Rogers, David W O Med Phys. 2007 May;34(5):1734-42.
- [13] B. A. Faddegon, J. Perl, and M. Asai. Monte carlo simulation of large electron fields. *Physics in medicine and biology*, 53(5):1497–510, 2008. Faddegon, Bruce A Perl, Joseph Asai, Makoto R01 CA104777-01A2/CA/NCI NIH HHS/R01 CA104777-02/CA/NCI NIH HHS/ England Phys Med Biol. 2008 Mar 7;53(5):1497-510. Epub 2008 Feb 21.
- [14] A. Micke, D. F. Lewis, and X. Yu. Multichannel film dosimetry with nonuniformity correction. *Med Phys*, 38(5):2523–34, 2011. Micke, Andre Lewis, David F Yu, Xiang eng 2011/07/23 06:00 Med Phys. 2011 May;38(5):2523-34.
- [15] J. Ulam, S.M. von Neumann. On combination of stochastic and deterministic processes. *Bull. Amer. Math Soc.*, 53:1120, 1947.
- [16] D. W. Rogers. Fifty years of monte carlo simulations for medical physics. *Phys Med Biol*, 51(13):R287–301, 2006. Rogers, D W O eng Review England 2006/06/23 09:00 Phys Med Biol. 2006 Jul 7;51(13):R287-301. Epub 2006 Jun 20.
- [17] Indrin J Chetty, Bruce Curran, Joanna E Cygler, John J DeMarco, Gary Ezzell, Bruce A Faddegon, Iwan Kawrakow, Paul J Keall, Helen Liu, and C-M Charlie Ma. Report of the aapm task group no. 105: Issues associated with clinical implementation of monte carlo-based photon and electron external beam treatment planning. *Medical physics*, 34(12):4818–4853, 2007.

- [18] Richard L Ford and Walter Ralph Nelson. Egs code system: computer programs for the monte carlo simulation of electromagnetic cascade showers. version 3.[egs, pegs, testsr, in mortran]. Report, Stanford Linear Accelerator Center, CA (USA), 1978.
- [19] W Ralph Nelson, H Hirayama, and David WO Rogers. The egs4 code system slac-265 stanford linear accelerator center, 1985.
- [20] Alex F Bielajew and DWO Rogers. Presta: the parameter reduced electron-step transport algorithm for electron monte carlo transport. *Nuclear Instruments and Methods in Physics Research Section B: Beam Interactions with Materials and Atoms*, 18(1):165–181, 1986.
- [21] I. Kawrakow. Accurate condensed history monte carlo simulation of electron transport. i. egsnrc, the new egs4 version. *Med Phys*, 27(3):485–98, 2000. Kawrakow, I eng Research Support, Non-U.S. Gov't 2000/04/11 09:00 Med Phys. 2000 Mar;27(3):485-98.
- [22] I Kawrakow and DWO Rogers. The egsnrc code system. *NRC Report PIRS-701, NRC, Ottawa*, 2000.
- [23] Martin J Berger. Monte carlo calculation of the penetration and diffusion of fast charged particles. *Methods in computational physics*, 1:135–215, 1963.
- [24] D W O Rogers, B A Faddegon, G X Ding, C M Ma, J We, and T R Mackie. Beam: a monte carlo code to simulate radiotherapy treatment units. *Med. Phys.*, 22:503–24, 1995.
- [25] FCP Du Plessis, CA Willemse, MG Ltter, and L Goedhals. The indirect use of ct numbers to establish material properties needed for monte carlo calculation of dose distributions in patients. *Medical physics*, 25:1195, 1998.
- [26] Barbara Vanderstraeten, Pik Wai Chin, Michael Fix, Antonio Leal, Grisel Mora, Nick Reynaert, Joao Seco, Martin Soukup, Emiliano Spezi, and Wilfried De Neve. Conversion of ct numbers into tissue parameters for monte carlo dose calculations: a multi-centre study. *Physics in medicine and biology*, 52(3):539, 2007.

CHAPTER 3
Review of Modulated Electron Radiation Therapy

Contents

3.1	Bolus Conformal Therapy	43
3.2	MERT collimation devices	45
3.2.1	MLC	45
3.2.2	eMLC	49
3.2.3	FLEC	53
3.3	Treatment planning	55
3.3.1	McGill Monte Carlo Treatment Planning System . . .	58
3.4	Summary of the current state of MERT and its di- rection	58

Intensity modulated radiation therapy (IMRT) has evolved in the last two decades to be capable of delivering highly conformal plans through the use of many small photon fields arranged in a complex geometry that is determined through inverse optimization. Due to issues surrounding the lack of both fast and accurate electron dose calculations, as well as lack of commercial hardware optimized for small field electron collimation, the adoption of modulated electron radiation therapy (MERT) has been lagging behind its photon equivalent and has only been confined to research interests and feasibility studies involving phantoms

up to this point. However, in the past two decades there have been a few groups pursuing this technique as a viable clinical alternative to photon modalities as it is particularly suited to healthy tissue sparing under certain geometries should these challenges be addressed. An overview of this past work is the topic of this chapter.

3.1 Bolus Conformal Therapy

Bolus Conformal Therapy represents one possible way to modulate the depth of penetration of the incoming electron beam. The implementation of this technique involves the placement of tissue equivalent material on top of the patient surface and modulating the thickness as a function of position to account for such things as the depth of the distal edge of the tumor and for superficial anatomical contours such as the nose in nasopharynx cases. The presence of the bolus material effectively controls the depth of penetration of the incoming electrons by providing scattering material in which energy degradation occurs, effectively causing a local reduction in the mean energy of the electrons at the surface of the patient.

As early as 1984, Galbraith *et al.* were discussing the use of bolus in electron therapy [1]. They investigated partial bolussing as a means to increasing the skin dose of low energy electron beams to create a more uniform dose in the first few cm without changing the depth of penetration of the beam. This was accomplished by by the addition of a regular field with a bolused field that contained enough bolus to highly degrade the energy of the electrons so that their range was limited to the buildup region where additional dose was desired.

Low *et al.* reported on the creation of a set of computational tools to design acceptable bolus shapes [2]. The tools were tested on clinical cases including a simple wedge, nose, paraspinal muscle and parotid irradiation. This work was later extended to include 3D dose calculation inside a radiotherapy treatment planning system [3] and was implemented in the treatment of a patient presenting with chondrosarcoma. A bolus based on the bolus-design algorithms was fabricated through machining of resin-impregnated wax using a computer driven milling machine. The planning including bolus showed good sparing of distal critical structures whereas the comparison plan containing no bolus was deemed to be clinically unacceptable.

Perkins *et al.* also demonstrated a custom bolus technique using a computerized milling machine for fabrication [4]. The bolus shape was designed within a 3D treatment planning system containing the CT images of the patient. The results of two postmastectomy irradiations using the custom bolus were discussed, which showed improved dose conformality and homogeneity compared to standard techniques.

Kudchadker *et al.* investigated the use of MLC-based intensity modulation as a means to restore dose homogeneity that can be affected when an irregular proximal surface is present [5]. Three sample patients were chosen in a planning study where bolus plans including intensity modulation would be compared to non-modulated plans. In all three cases, they were able to show that intensity modulation was able to improve the dose homogeneity.

Although the utility of such techniques has been demonstrated, the use of bolus conformal therapy has not become widespread due to its limitations. The time and cost of milling patient specific bolus shapes, in addition to homogeneity issues that require intensity modulation have held this technique back from being viewed as clinically practical. More recent investigations have focused on energy modulation to control the electron depth of penetration and intensity modulation using either the photon MLC or tertiary electron collimators, both of which are discussed in the following section.

3.2 MERT collimation devices

Traditional electron therapy requires final electron collimation to within a few cm from the patient surface due to a moderate contribution from air scatter in broadening the beam and spreading out the width of the penumbra region. The static nature of these patient-specific collimation apertures, and the great amount of time spent in their construction, have necessitated more automated collimation solutions, such as those used in photon therapies, in any possible MERT application. There have been three main approaches to this problem:

1. Use of the photon MLC for electron beams.
2. Development of an electron-specific MLC (eMLC)
3. Development of a few-leaf electron collimator (FLEC)

3.2.1 MLC

The introduction of photon MLCs greatly increased the treatment planners ability to spare healthy tissue by providing greater conformity of the radiation field to the target. However, the use of the MLC to define conventional electron

fields was not practical under normal conditions due to the high degree of beam scattering between the MLC and the patient surface, resulting in unacceptable penumbra. However, utilizing the photon MLC to collimate electron beams through various means has been investigated thoroughly by many authors due to the obvious advantage of already having the hardware implemented on the accelerator. By finding ways to overcome the obstacles in electron collimation using the photon MLC, the clinical acceptance and implementation of MERT would be much easier due to the elimination of the need to develop, implement and maintain the additional electron collimation hardware and software needed for MERT delivery.

Klein *et al.* investigated the use of the pMLC collimated electron beams compared to applicator defined beams, however, despite using the minimum practical collimator to patient separation, the MLC defined beams were inferior to the applicator defined beams [6]. However, in the same study, segmented arcs for treatment of the chest wall proved promising due to the ease of matching adjacent electron fields with wide penumbra. To extend on this work, they later investigated the use of the MLC in defining multi-segment fields for a static gantry angles [7]. They were able to successfully deliver conformal, modulated plans to various phantom and target arrangements, however, they stopped short of commenting on the superiority of this technique compared to other methods due to remaining questions about the feasibility and practicality of this method.

At the same time, Zackrisson *et al.* investigated the implementation of a MM50 microtron using the attached photon MLC for energy and intensity

modulation [8]. The microtron featured a scanned electron beam and a treatment head filed with helium, both factors that contribute to less beam scatter and sharper penumbra. Example thyroid, nasal and thoracic plans consisting of few fields with energy modulation (and in two cases different gantry angles) were compared to conventional single field electron therapy with favorable results.

Karlsson *et al.* investigated different modifications that could be made to a linear accelerator that would allow it to deliver acceptable MLC collimated electron beams [9]. Within the BEAMnrc Monte Carlo system, they modified such accelerator parameters as the positions of the scattering foil and MLC, the thickness of the monitor chamber and adding a helium bag within the treatment head to displace the normal atmosphere. With appropriately chosen parameters, they were able to achieve acceptable penumbra widths for clinical use as well as shifting the position of the virtual electron source to a location that matched the photon source leading to easier matching of photon and electron fields. Based upon these findings, Bloomquist *et al.* investigated the application of these same modifications to three commonly available accelerator types [10]. These modified beams were also evaluated on criteria of virtual source position, penumbra and field matching suitability. It was again found that appropriate modifications to common accelerator types could improve upon traditional clinical beams and were suitable for field matching with photon beams.

A characterization of electron beams defined by a Siemens (Siemens, Munich, Germany) photon MLC was reported by du Plessis *et al.* [11]. They discussed output stability, beam penumbra, bremsstrahlung dose, MLC leakage and virtual

source position. They also performed a simplified energy modulated delivery involving multiple adjacent field segments of increasing energy to create a wedge-shaped dose distribution.

Jin *et al.* conducted a dosimetric evaluation of an intact breast phantom irradiation using photon MLC defined electron beams [12]. The investigation included inverse optimization of the 3D dose distribution using an in-house Monte Carlo based treatment planning system.

Klein *et al.* did an through evaluation of a Monte Carlo model of a Varian photon MLC used to define electron beams down to very small fields as low as $1 \times 1 \text{ cm}^2$ [13]. The models were evaluated on agreement of the profiles, PDDs and output to measured data. One result of this work was the discussion of some of the limitations of photon defined electron beams. They concluded that fields should be limited in minimum field size to no less than $2 \times 2 \text{ cm}^2$ at 70 cm SSD due to excessive photon contamination present at higher energies and poor penumbra and low output seen for lower energy beams of smaller size. Also concluded from their work was the sufficiency of the photon MLC in defining small segment electron beams for MERT purposes at an optimal SSD of 70 cm, eliminating the need to resort to additional tertiary electron collimation or the use to helium in the treatment head to minimize scatter. As a follow up to their work, Klein *et al.* later published work on the planning and delivery of MERT plans collimated by the photon MLC [14]. A simple forward-planned step function distribution was created in a phantom geometry to match a hypothetical target of variable distal depth. The plan was delivered in step and shoot fashion to film placed within the

phantom which confirmed the predicted dose distribution and showed adequate dose conformity of the 80% isodose line across the distal edge of the target. In addition to the phantom study, they also investigated two clinical cases consisting of a post-mastectomy chest wall and cutaneous lymphoma of the scalp. Forward planning was again performed on each patient CT using multiple energies and a few field segments. In both cases they were able to show good target conformity and OAR sparing. Deliveries of each case were performed on mock phantoms to ensure the delivery could be safely conducted without collisions. Delivery time of the single couch and gantry-angle chest wall case was reported to be well within clinically acceptable limits and took 3.5 minutes.

Mihaljevic *et al.* reported on a Monte Carlo study involving the commissioning of an accurate electron beam model collimated by an Elekta photon MLC. Various source parameters were varied including beam divergence angle and beam width as well as selecting a Gaussian energy distribution as opposed to the more common monoenergetic approach. Results showed that PDD agreement between simulations and measurement was within 1%/1 mm.

3.2.2 eMLC

In addition to investigating the use of commonly available photon MLC collimators to shape electron beams, several investigations into the development of MLCs specifically optimized for electron collimation (electron MLC or eMLC) have been reported due to limitations of photon MLCs for that purpose.

Lee *et al.* reported on the design and construction of a prototype eMLC to collimate modulated electron beams [15]. The motivation for the use of such

a device was due to the poor suitability of the photon MLC for such purposes, particularly for lower beam energies, despite the use of helium between the MLC and the patients surface to reduce scatter. In the design of the collimator, they considered leaf thickness, shape and material with the leaves located at the bottom of a 25x25 cm² applicator just a few cm from the patient surface. The optimal combination of parameters was determined to be an eMLC made with tungsten leaves 15 mm thick and 5 mm wide. Additionally, the use of Monte Carlo dose calculation methods were shown to be accurate in predicting the dose distribution from such a device. An experimental prototype was constructed consisting of 30 manually driven steel leaf pairs 2.54 cm thick.

Using the same eMLC, Ma *et al.* reported on the feasibility of optimizing a MERT plan using such a device and showed that an eMLC with 5 mm leaf widths could adequately define the complex field shapes required for MERT [16]. They also performed a comparison of Monte Carlo calculated dose distributions to that of an analytical 3D pencil beam algorithm within a commercial treatment planning system for a single 1x1 cm² field. The calculations were done for normal and oblique incident beams on a patient-phantom based on CT data. Results showed significant differences between Monte Carlo and the analytical algorithms, indicating that current analytical methods are inadequate for MERT dose calculations in heterogeneous media.

Also studying the feasibility of a manual eMLC, Ravindran *et al.* investigated beam characteristics such as PDD, profiles, penumbra, surface dose and effective source position using a different linear accelerator than the previous group [17].

A prototype device was constructed which consisted of 16 mm thick leaves made of Lipowitz alloy. This thickness resulted in an x-ray transmission of 5 at 14 MeV and is not considered adequate for modulated deliveries. Experimental measurements were taken showing similar PDD characteristics to the applicator, however, penumbra was sharper. Surface dose was greater for the eMLC defined beams compared to the applicator defined beams.

Hogstrom *et al.* also investigated the feasibility of a tertiary retractable eMLC [18]. As described in their work, the use of a retractable eMLC offers the possibility of isocentric treatment in the extended position (source to collimator distance, or SCD of 90 cm). In the retracted position (SCD of 63 cm), the gantry can be rotated safely around the patient and photon therapy with the eMLC still attached is possible. The first prototype device consisted of 21 pairs of brass leaves measuring 3 cm in thickness and 0.9 cm in width. Characterization through experimental measurements showed interleaf leakage to be less than 0.1% and for x-ray transmission to be less than 1.6% at 15 MeV. Other dosimetric characteristics such as PDD, profiles and dose output factors were consistent with the 20x20 cm² applicator. They concluded that certain improvements to the design could be made in future prototypes including switching the leaf material to 2 cm of tungsten to further reduce the x-ray transmission as well as reducing the leaf width to 5 mm to increase the resolution. They also concluded that a collimator based on these design criteria could replace the applicator for fixed beam deliveries and they hypothesized that it could also be used for dynamic conformal arc therapy as well as MERT which is a topic of future work.

Gauer *et al.* also reported on the design and feasibility of a tertiary eMLC consisting of 24 pairs of brass leaves 1.8 cm thick and 0.6 cm wide [19]. Beam penumbra was found to be noticeably worse for eMLC collimated fields than the standard applicator and was attributed to the shorter source to collimator distances. Total weight was a design consideration to avoid gantry sag and the authors were able to keep the total weight of the prototype device to approximately 20 kg through the use of brass as opposed to the dosimetrically superior tungsten. This choice resulted in approximately 3% x-ray transmission through the leaves at 17 MeV. In later work, the motorized version of their eMLC was characterized in terms of gantry stability and dosimetric characteristics [20]. The motorized version weighed 30 kg and could be safely mounted onto the gantry with a minimal gantry sag of less than 0.6 mm with the gantry at 90 degrees. Beam junctions of different fields were found to be adequate in terms of dose uniformity across the junction provided the two adjoining fields were of similar energy. Radiation leakage was reported to be 2.5% at 14 MeV. Minimum field sizes of 3x3 cm² were recommended due to reductions in the therapeutic range and dose output.

Vatanen *et al.* were the first to report on dosimetric characteristics of a prototype eMLC modeled by a beam model implemented in a commercial treatment planning system [21]. The eMLC consisted of 42 leaf pairs with a thickness of 2 cm of steel and a width of 5 mm. The collimator featured a very small gap of 8 mm between the leaf bottoms and the phantom surface. This geometry causes dose horns in the profiles near the field edges due to scatter from the leaf edges.

The application of the beam model for eMLC defined fields showed good agreement for the various energies, field sizes and source to surface distances that were investigated.

Eldib *et al.* [22] studied the dosimetric characteristics of another eMLC designed specifically for MERT [22]. The design of the MLC consisted of 25 tungsten leaf pairs, each 2 cm thick and 0.6 cm wide. The main focus of their study was finding the optimal field gap in the junction region between different fields which varied between 0.4 and 0.7 cm for the junctions between low and high-energy fields respectively.

3.2.3 FLEC

One form of electron collimation that has been suggested is the use of just four jaws configured in similar fashion to the secondary photon collimator in most accelerators. This type of collimator offers the possibility of defining any rectangular shaped field with much less mechanical and technical complexity than an eMLC. However, this design suffers from longer delivery times compared to an eMLC as the fields must be swept across the target in two dimensions and opposed to just one dimension with an eMLC. One such prototype was described by Al-Yahya *et al.* in 2007 and is the same prototype used in this work [23]. Termed the Few Leaf Electron Collimator (FLEC), this device consists of four copper bars of 1.2 cm thickness and a width of 3.0 cm and is shown in Figure 3–1. These four jaws are mechanically driven by computer controlled stepper motors and are capable of defining any rectangular field up to a maximum of 8x8 cm². The whole device rests in the bottom of a Varian 15x15 cm² electron applicator,

giving approximately 5 cm of clearance between the bottom of the collimator and the isocenter. The device itself interfaces with a National Instruments (National Instruments Corporation, Austin, TX) MID-7604 stepper motor controller. The controller interfaces with a PC running custom control software written in C++. The C++ code is able to import FLEC control files which contain a list of field positions as well as beam energy, MU setting and secondary collimator setting. The FLEC control computer is also able to interface with the accelerator at the time of delivery to automatically control the various machine settings.

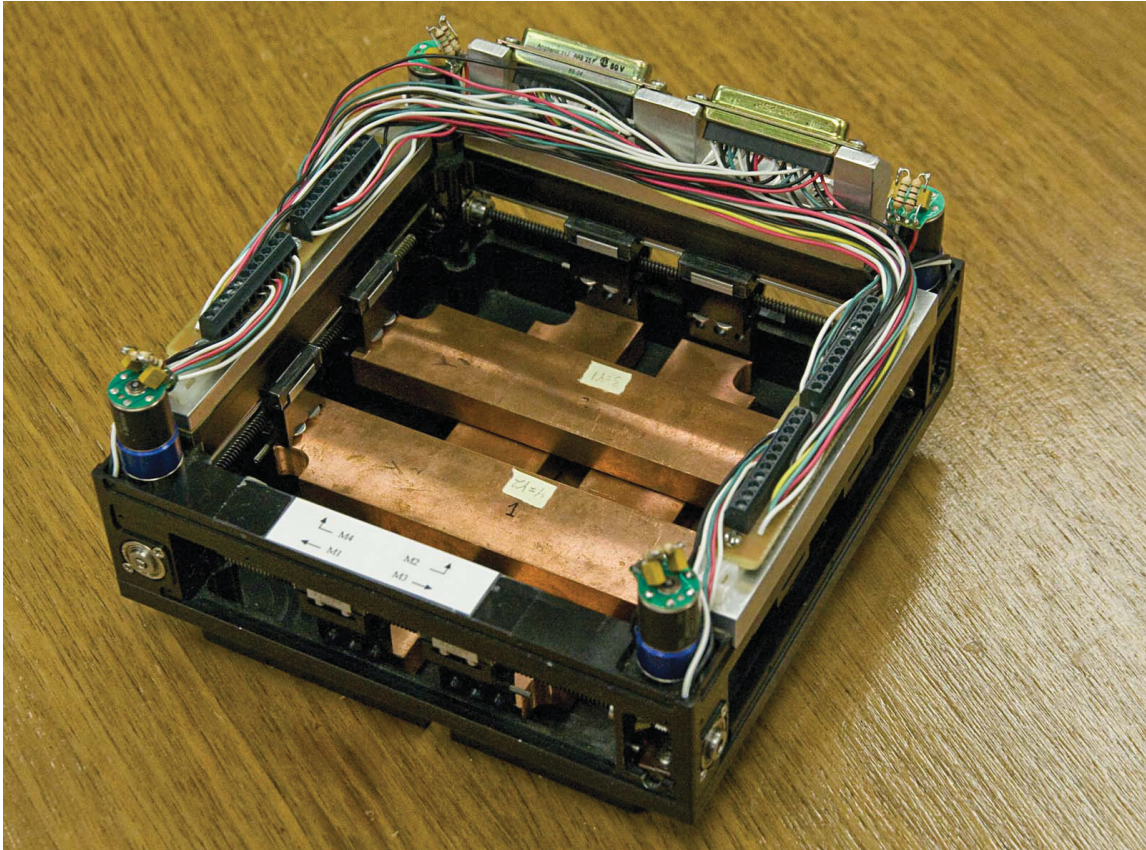


Figure 3–1: The Few Leaf Electron Collimator (FLEC) used as a tertiary electron collimation device.

3.3 Treatment planning

Treatment planning is a critical step in any MERT delivery process. Various groups have conducted comparisons of MERT plans to more conventional modalities. Their methods have included less accurate, but fast analytical dose calculation algorithms as well as very accurate Monte Carlo methods. Some simpler planning studies have used forward planning techniques, while others have developed inverse planning capabilities capable of determining optimal beam weights for many fields by using algorithms to minimize a cost function to find the optimal balance between target coverage and healthy tissue sparing. The general conclusion from these studies is that for certain target geometries, MERT, either on its own or in combination with photon IMRT, is superior to IMRT alone in sparing large volumes of healthy tissues from the low dose bath that is commonly found with intensity modulated photon therapies. However, generally speaking, many of these studies have also found that MERT target coverage is not as homogeneous as modulated photon modalities. The remainder of this section will present an overview of these MERT studies and their findings.

Hyodynmaa *et al.* investigated the utility of scanned pencil beams from a racetrack microtron [24]. Inverse optimization of the beam weights of multiple pencil-beam kernels including 5 energies and many spatial positions produced plans on two phantom geometries and three representative clinical cases. They

found that the local dose maximum was typically lower than conventional or bolus techniques. Although lacking the necessary hardware to deliver such a treatment, they hypothesized in their conclusion that using current fourth generation accelerators, clinical delivery of such plans would be possible.

Lee *et al.* discussed the creation of a Monte Carlo based treatment planning system to investigate the feasibility of MERT planning using a tertiary eMLC [25]. The system was used to generate plans in a homogeneous phantom as well as a CT phantom. Different dose calculation methods were compared: (i) a fast beamlet method which does not account for leaf scatter or transmission and (ii) the slower, but more accurate Monte Carlo method. They proposed a fast calculation method that included leaf transmission and leaf-end scatter.

Also conducting a MERT treatment planning study, Ma *et al.* compared a Monte Carlo calculated MERT plan to a 6 MV photon plan for treatment of an intact breast [16]. The MERT plan was able to provide superior dose homogeneity to the target and reduced the max dose to lung from 50 Gy to 35 Gy compared to the tangential photon plan, however, the MERT plan did exhibit a larger volume of lung exposed to low doses due to penetration of some electrons into the lung and bremsstrahlung contamination. They also showed that the MERT plan avoided the inclusion of a large volume of normal tissue in the high dose volume, with over 1000 cm³ receiving between 10 and 30 Gy less dose with the MERT technique. Building on this work, a follow-up study was conducted comparing the dosimetric results of IMRT, MERT and tangential photons in the treatment of the breast [26]. It was concluded that MERT was superior to either modality.

Jin *et al.* also conducted a dosimetric evaluation of an intact breast phantom irradiation planned using a Monte Carlo based treatment planning system capable of inverse optimization [12]. Dosimetric evaluation of the 22 segment delivery of differing energies and intensities was performed using radiographic film and an ionization chamber. The 2D planar dose film distribution agreed to the planned dose distribution to within 1%/1 mm while the ionization chamber measurements agreed to within 1.4%.

Al-Yahya *et al.* reported on a Monte Carlo based treatment planning study comparing conventional 3D-CRT, IMRT, IMRT in conjunction with MERT and 3D-CRT in conjunction with MERT [27]. The planning study was conducted on two parotid cases and one breast case. They found that for all three cases, conformity and homogeneity were preserved while improving normal tissue sparing for the combined MERT and photon plans. The reduction in the whole body dose calculated in the MERT plans was particularly great compared to the IMRT plan alone.

Gauer *et al.* conducted a treatment planning study comparing MERT to helical photon IMRT and conventional photon therapy for breast and chest wall irradiations [28]. They found that when comparing helical photon therapy to MERT, they achieved superior PTV coverage (homogeneity) at the expense of increased low doses to the heart contralateral breast and both lungs. MERT was superior to conventional therapy in all metrics used including PTV coverage. They conclude that MERT is a strong candidate for superficial malignancies in the chest

area, particularly for younger patients who are at a greater risk of developing a radiation induced secondary malignancy.

3.3.1 McGill Monte Carlo Treatment Planning System

The McGill Monte Carlo treatment planning (MMCTP) system was designed to provide a platform capable of Monte Carlo calculated photon and electron dose distributions and incorporates many common tools for analysis and comparison of these distributions [29]. As it is a Monte Carlo based system, it opens up the possibility of accurately calculating small field electron beams collimated by tertiary collimators with commercial analytical algorithms which suffer from poor dose accuracy under these conditions. In addition to having many features expected in a treatment planning system such as, dose visualization superimposed over CT images, contouring of structures, DVH analysis etc., the treatment planning system also contained a module for the calculation and optimization of a MERT plan using the FLEC tertiary collimator developed by Al-Yahya *et al.* [23]. Within this environment, MERT plans could be created for comparison against other plans, or exported to the FLEC control computer for delivery to a phantom as a way to validate the accuracy of the planning and delivery stages.

3.4 Summary of the current state of MERT and its direction

A brief summary of the historical developments in modulated electron therapy has been presented, from early attempts to modulate electron range through bolus techniques, to the use of multiple energy deliveries with MLC-type beam collimation, and to the development of planning methods and tools. The early methods involving bolus have been largely abandoned due to the time

consuming process of manufacturing patient specific boluses. Other issues have been reported in accurate and reproducible placement of the bolus, in addition, there are manufacturing challenges as access to computerized milling machines is a requirement in bolus fabrication. However, the latter limitation may be mitigated with the rapid growth and decreased cost of 3D printing.

Most recent efforts have focused on MERT delivery using conventional radiotherapy accelerators in conjunction with some form of MLC collimation. These methods remain very promising, however, the development of a full end-to-end planning and delivery workflow is a significant undertaking for research groups who lack the support and resources of commercial vendors. The creation of a capable MERT program entails research in the areas of general treatment planning, inverse optimization, as well as the development of a suitable collimator and its control and automation. Nonetheless, some of these groups continue to advance their work on these fronts with the likely intent of producing a sufficiently mature process and implementing it as part of a clinical trial.

The FLEC method of electron beam collimation has the limitation of longer treatment times due to inefficiencies in defining large numbers of fields when compared to MLC methods, however, from both a treatment planning and hardware perspective, the FLEC device has a reduced complexity that and has allowed it to advance to a mature endpoint. The current work presented in this thesis shows the integration of the treatment planning (including inverse optimization of Monte Carlo calculated beams) and hardware aspects of a MERT delivery. The

demonstration of plan creation, delivery and dose accuracy verification using these methods has been a first in this field.

REFERENCES

- [1] Duncan M Galbraith and J Alan Rawlinson. Partial bolussing to improve the depth doses in the surface region of low energy electron beams. *International Journal of Radiation Oncology* Biology* Physics*, 10(2):313–317, 1984.
- [2] DA Low, G Starkschall, SW Bujnowski, LL Wang, and KR Hogstrom. Electron bolus design for radiotherapy treatment planning: bolus design algorithms. *Medical physics*, 19:115, 1992.
- [3] Daniel A Low, George Starkschall, Neil E Sherman, Stanley W Bujnowski, James R Ewton, and Kenneth R Hogstrom. Computer-aided design and fabrication of an electron bolus for treatment of the paraspinal muscles. *International Journal of Radiation Oncology* Biology* Physics*, 33(5):1127–1138, 1995.
- [4] George H Perkins, Marsha D McNeese, John A Antolak, Thomas A Buchholz, Eric A Strom, and Kenneth R Hogstrom. A custom three-dimensional electron bolus technique for optimization of postmastectomy irradiation. *International Journal of Radiation Oncology* Biology* Physics*, 51(4):1142–1151, 2001.
- [5] Rajat J Kudchadker, Kenneth R Hogstrom, Adam S Garden, Marsha D McNeese, Robert A Boyd, and John A Antolak. Electron conformal radiotherapy using bolus and intensity modulation. *International Journal of Radiation Oncology* Biology* Physics*, 53(4):1023–1037, 2002.
- [6] Eric E Klein, Zuofeng Li, and Daniel A Low. Feasibility study of multileaf collimated electrons with a scattering foil based accelerator. *Radiotherapy and oncology*, 41(2):189–196, 1996.
- [7] Eric E Klein. Modulated electron beams using multi-segmented multileaf collimation. *Radiotherapy and oncology*, 48(3):307–311, 1998.
- [8] Björn Zackrisson and Mikael Karlsson. Matching of electron beams for conformal therapy of target volumes at moderate depths. *Radiotherapy and oncology*, 39(3):261–270, 1996.

- [9] M. G. Karlsson, M. Karlsson, and C. M. Ma. Treatment head design for multileaf collimated high-energy electrons. *Medical physics*, 26(10):2161–7, 1999. Karlsson, M G Karlsson, M Ma, C M Med Phys. 1999 Oct;26(10):2161-7.
- [10] Michael Blomquist, Magnus G Karlsson, Björn Zackrisson, and Mikael Karlsson. Multileaf collimation of electrons: clinical effects on electron energy modulation and mixed beam therapy depending on treatment head design. *Physics in medicine and biology*, 47(7):1013, 2002.
- [11] F. C. du Plessis, A. Leal, S. Stathakis, W. Xiong, and C. M. Ma. Characterization of megavoltage electron beams delivered through a photon multi-leaf collimator (pmlc). *Physics in medicine and biology*, 51(8):2113–29, 2006. du Plessis, F C P Leal, A Stathakis, S Xiong, W Ma, C-M England Phys Med Biol. 2006 Apr 21;51(8):2113-29. Epub 2006 Apr 3.
- [12] L. Jin, C. M. Ma, J. Fan, A. Eldib, R. A. Price, L. Chen, L. Wang, Z. Chi, Q. Xu, M. Sherif, and J. S. Li. Dosimetric verification of modulated electron radiotherapy delivered using a photon multileaf collimator for intact breasts. *Physics in medicine and biology*, 53(21):6009–25, 2008. Jin, L Ma, C-M Fan, J Eldib, A Price, R A Chen, L Wang, L Chi, Z Xu, Q Sherif, M Li, J S England Phys Med Biol. 2008 Nov 7;53(21):6009-25. Epub 2008 Oct 3.
- [13] E. E. Klein, M. Vicic, C. M. Ma, D. A. Low, and R. E. Drzymala. Validation of calculations for electrons modulated with conventional photon multileaf collimators. *Physics in medicine and biology*, 53(5):1183–208, 2008. Klein, Eric E Vicic, Milos Ma, Chang-Ming Low, Daniel A Drzymala, Robert E England Phys Med Biol. 2008 Mar 7;53(5):1183-208. Epub 2008 Feb 11.
- [14] Eric E Klein, Joseph Hanley, John Bayouth, Fang-Fang Yin, William Simon, Sean Dresser, Christopher Serago, Francisco Aguirre, Lijun Ma, and Bijan Arjomandy. Task group 142 report: quality assurance of medical accelerators. *Medical physics*, 36:4197, 2009.
- [15] M. C. Lee, S. B. Jiang, and C. M. Ma. Monte carlo and experimental investigations of multileaf collimated electron beams for modulated electron radiation therapy. *Med Phys*, 27(12):2708–18, 2000. Lee, M C Jiang, S B Ma, C M 5T32GM08294-11/GM/NIGMS NIH HHS/United States CA

- 78331/CA/NCI NIH HHS/United States Research Support, U.S. Gov't, Non-P.H.S. Research Support, U.S. Gov't, P.H.S. United States Medical physics Med Phys. 2000 Dec;27(12):2708-18.
- [16] C. M. Ma, T. Pawlicki, M. C. Lee, S. B. Jiang, J. S. Li, J. Deng, B. Yi, E. Mok, and A. L. Boyer. Energy- and intensity-modulated electron beams for radiotherapy. *Phys Med Biol*, 45(8):2293–311, 2000. Ma, C M Pawlicki, T Lee, M C Jiang, S B Li, J S Deng, J Yi, B Mok, E Boyer, A L CA78331/CA/NCI NIH HHS/United States Comparative Study Research Support, Non-U.S. Gov't Research Support, U.S. Gov't, Non-P.H.S. Research Support, U.S. Gov't, P.H.S. England Physics in medicine and biology Phys Med Biol. 2000 Aug;45(8):2293-311.
- [17] B. P. Ravindran, I. R. Singh, S. Brindha, and S. Sathyan. Manual multi-leaf collimator for electron beam shaping—a feasibility study. *Physics in medicine and biology*, 47(24):4389–96, 2002. Ravindran, B Paul Singh, I Rabi Raja Brindha, S Sathyan, S England Phys Med Biol. 2002 Dec 21;47(24):4389-96.
- [18] K. R. Hogstrom, R. A. Boyd, J. A. Antolak, M. M. Svatos, B. A. Faddegon, and J. G. Rosenman. Dosimetry of a prototype retractable emlc for fixed-beam electron therapy. *Medical physics*, 31(3):443–62, 2004. Hogstrom, Kenneth R Boyd, Robert A Antolak, John A Svatos, Michelle M Faddegon, Bruce A Rosenman, Julian G Med Phys. 2004 Mar;31(3):443-62.
- [19] T. Gauer, D. Albers, F. Cremers, R. Harmansa, R. Pellegrini, and R. Schmidt. Design of a computer-controlled multileaf collimator for advanced electron radiotherapy. *Physics in medicine and biology*, 51(23):5987–6003, 2006. Gauer, T Albers, D Cremers, F Harmansa, R Pellegrini, R Schmidt, R England Phys Med Biol. 2006 Dec 7;51(23):5987-6003. Epub 2006 Oct 30.
- [20] T. Gauer, J. Sokoll, F. Cremers, R. Harmansa, M. Luzzara, and R. Schmidt. Characterization of an add-on multileaf collimator for electron beam therapy. *Phys Med Biol*, 53(4):1071–85, 2008. Gauer, T Sokoll, J Cremers, F Harmansa, R Luzzara, M Schmidt, R eng Research Support, Non-U.S. Gov't England 2008/02/12 09:00 Phys Med Biol. 2008 Feb 21;53(4):1071-85. doi: 10.1088/0031-9155/53/4/017. Epub 2008 Feb 1.
- [21] T Vatanen, E Traneus, and T Lahtinen. Dosimetric verification of a monte carlo electron beam model for an add-on emlc. *Physics in medicine and biology*, 53(2):391, 2008.

- [22] A. A. Eldib, M. I. ElGohary, J. Fan, L. Jin, J. Li, C. Ma, and N. A. Elsherbini. Dosimetric characteristics of an electron multileaf collimator for modulated electron radiation therapy. *Journal of applied clinical medical physics / American College of Medical Physics*, 11(2):2913, 2010. Eldib, Ahmed Abdel Rahman ElGohary, Mohamed I Fan, Jiajin Jin, Lihui Li, Jinsheng Ma, Charlie Elsherbini, Nader A J Appl Clin Med Phys. 2010 Apr 12;11(2):2913.
- [23] K. Al-Yahya, F. Verhaegen, and J. Seuntjens. Design and dosimetry of a few leaf electron collimator for energy modulated electron therapy. *Med Phys*, 34(12):4782–91, 2007. Al-Yahya, Khalid Verhaegen, Frank Seuntjens, Jan Research Support, Non-U.S. Gov't United States Medical physics Med Phys. 2007 Dec;34(12):4782-91.
- [24] Simo Hydynmaa, Anders Gustafsson, and Anders Brahme. Optimization of conformal electron beam therapy using energy-and fluence-modulated beams. *Medical Physics*, 23:659, 1996.
- [25] M. C. Lee, J. Deng, J. Li, S. B. Jiang, and C. M. Ma. Monte carlo based treatment planning for modulated electron beam radiation therapy. *Phys Med Biol*, 46(8):2177–99, 2001. Lee, M C Deng, J Li, J Jiang, S B Ma, C M 5T32GM08294-11/GM/NIGMS NIH HHS/United States CA78331/CA/NCI NIH HHS/United States Research Support, U.S. Gov't, Non-P.H.S. Research Support, U.S. Gov't, P.H.S. England Physics in medicine and biology Phys Med Biol. 2001 Aug;46(8):2177-99.
- [26] C. M. Ma, M. Ding, J. S. Li, M. C. Lee, T. Pawlicki, and J. Deng. A comparative dosimetric study on tangential photon beams, intensity-modulated radiation therapy (imrt) and modulated electron radiotherapy (mert) for breast cancer treatment. *Phys Med Biol*, 48(7):909–24, 2003. Ma, C M Ding, M Li, J S Lee, M C Pawlicki, T Deng, J CA78331/CA/NCI NIH HHS/United States Comparative Study Evaluation Studies Research Support, U.S. Gov't, Non-P.H.S. Research Support, U.S. Gov't, P.H.S. Validation Studies England Physics in medicine and biology Phys Med Biol. 2003 Apr 7;48(7):909-24.
- [27] K. Al-Yahya, M. Schwartz, G. Shenouda, F. Verhaegen, C. Freeman, and J. Seuntjens. Energy modulated electron therapy using a few leaf electron collimator in combination with imrt and 3d-crt: Monte carlo-based planning and dosimetric evaluation. *Med Phys*, 32(9):2976–86, 2005. Al-Yahya, Khalid Schwartz, Matthew Shenouda, George Verhaegen, Frank Freeman, Carolyn

Seuntjens, Jan Research Support, Non-U.S. Gov't United States Medical physics Med Phys. 2005 Sep;32(9):2976-86.

- [28] T. Gauer, K. Engel, A. Kiesel, D. Albers, and D. Rades. Comparison of electron imrt to helical photon imrt and conventional photon irradiation for treatment of breast and chest wall tumours. *Radiotherapy and oncology : journal of the European Society for Therapeutic Radiology and Oncology*, 94(3):313–8, 2010. Gauer, Tobias Engel, Konrad Kiesel, Antje Albers, Dirk Rades, Dirk Ireland Radiother Oncol. 2010 Mar;94(3):313-8. Epub 2010 Jan 28.
- [29] A. Alexander, F. Deblois, G. Stroian, K. Al-Yahya, E. Heath, and J. Seuntjens. Mmctp: a radiotherapy research environment for monte carlo and patient-specific treatment planning. *Phys Med Biol*, 52(13):N297–308, 2007. Alexander, A Deblois, F Stroian, G Al-Yahya, K Heath, E Seuntjens, J Research Support, Non-U.S. Gov't England Physics in medicine and biology Phys Med Biol. 2007 Jul 7;52(13):N297-308. Epub 2007 Jun 6.

CHAPTER 4
Delivery validation of an automated modulated electron radiotherapy plan

Tanner Connell, Andrew Alexander, Pavlos Papaconstadopoulos, Monica Serban,
Slobodan Devic and Jan Seuntjens

Med. Phys., Under review, 2014

Contents

4.1	Introduction	69
4.2	Materials and Methods	71
4.2.1	Validation of Monte Carlo model against measurements	71
4.2.2	Creation of MERT plan within the treatment planning system	73
4.2.3	Delivery of modulated electron plan	75
4.2.4	2D Verification of the plan delivery using EBT3 film	76
4.2.5	2D Verification of the plan delivery using MapCHECK	78
4.3	Results and discussion	78
4.3.1	Validation of Monte Carlo model against measurements	78
4.3.2	Device hardware and output factor QA	81
4.3.3	Creation of MERT plan	82
4.3.4	Delivery of the MERT plan	83

4.3.5	2D Verification of the plan delivery using EBT3 film	93
4.3.6	2D Verification of the plan delivery using MapCHECK	96
4.4	Conclusions	97
4.5	Acknowledgments	99

There has been substantial development of a MERT technique within the McGill Medical Physics Unit. Al-Yahya *et al.* have developed an automated and motorized Few Leaf Electron Collimator (FLEC) as a means to define small electron fields for MERT purposes [1]. The device was validated dosimetrically for individual fields with respect to agreement of percent depth dose distributions and lateral profiles as well as output prediction. Separately, on the treatment planning aspect of the project, Alexander *et al.* developed a novel Monte Carlo based treatment planning system (MMCTP) capable of inverse optimization of modulated electron beams using a FLEC device as the electron collimator [2].

This next chapter introduces a submitted paper that describes a full end-to-end MERT delivery from the planning stage to delivery and dosimetric validation. This work ties in the two past projects, the MMCTP planning system used to create the plans and the FLEC device as a suitable collimator for MERT applications, to test their feasibility and accuracy as part of one unified workflow.

Abstract.

Purpose: Modulated electron radiation therapy (MERT) represents as an active area of interest that offers the potential to improve healthy tissue sparing in treatment of certain cancer cases. Challenges remain however in accurate beamlet dose calculation, plan optimization, collimation method and delivery accuracy. In

this work, we investigate the accuracy and efficiency of an end-to-end MERT plan and automated delivery method.

Methods: Treatment planning was initiated on a previously treated whole breast irradiation case including an electron boost. All dose calculations were performed using Monte Carlo methods and beam weights were determined using a research-based treatment planning system capable of inverse optimization. The plan was delivered to radiochromic film placed in a water equivalent phantom for verification, using an automated motorized tertiary collimator.

Results: The automated delivery, which covered 4 electron energies, 196 subfields and 6183 total MU was completed in 25.8 minutes, including 6.2 minutes of beam-on time. The remainder of the delivery time was spent on collimator leaf motion and the automated interfacing with the accelerator in service mode. Comparison of the planned and delivered film dose gave 3%/3 mm gamma values of 62.1, 99.8, 97.8, 98.3, and 98.7 percent for the 9, 12, 16, 20 MeV, and combined energy deliveries respectively. Delivery was also performed with a MapCHECK 2 device and resulted in 5%/5 mm gamma pass rates of 88.8, 86.1, 89.4, and 94.8 percent for the 9, 12, 16, and 20 MeV energies respectively.

Conclusions: Results of our study showed that an accurate delivery utilizing an add-on tertiary electron collimator is possible using Monte Carlo calculated plans and inverse optimization, which brings MERT closer to becoming a viable option for physicians in treating superficial malignancies.

4.1 Introduction

Electron therapy is still used in many centers for the treatment of sites confined to superficial regions. Electrons offer superior distal tissue sparing due to their rapid dose fall off beyond z_{\max} , which is determined by the nominal beam energy. Modulated electron radiation therapy (MERT) continues to be an area of active research and offers the possibility of offering more conformal dose distributions than conventional electron therapy and a much-reduced low-dose bath when compared to photon modalities. MERT relies on energy modulation to conform the dose to the distal edge of the PTV and intensity modulation to provide a homogeneous dose to the PTV.

Various groups [3, 4, 5, 6, 7] have reported on the feasibility of using the photon MLC as a possible collimation device, while others [8, 9, 10, 11, 12, 13, 14] have manufactured add-on electron MLCs that are positioned closer to the patient in an effort to minimize the penumbra width due to air scatter. It was reported that acceptable penumbra can be obtained with photon MLCs by using SSDs in the 70 cm range [15]. Other groups have reported on the design and use of a computer-controlled few-leaf electron collimator (FLEC) that is positioned in the electron applicator tray within a few cm from the patient surface [1]. Beam collimation from this device is achieved with four copper leaves similar to the configuration of the secondary collimator jaws. An evaluation of dosimetric accuracy of the Monte Carlo dose model was evaluated for small fields with measurements and simulations agreeing between 1% and 3%.

There have been multiple dosimetric comparisons of MERT with other electron and photon modalities. MERT has been benchmarked against IMRT and conventional photon treatments for treatment of breast cancer with the MERT plans giving reduced maximum dose to the lung and heart compared to the photon modalities [16]. The efficacy of MERT in combination with 3D-CRT and IMRT was tested with results showing reduced whole body dose over the photon modalities alone [17]. Gauer *et al.* [18] have showed superior MERT plans of whole breast and chest wall irradiations when compared to helical photon IMRT, while Salguero *et al.* [19] showed MERT to be superior to conventional electrons for post-mastectomy chest wall irradiations.

The practicality and dosimetry of MERT deliveries has been the focus of some investigations. Klein *et al.* [15] validated Monte Carlo as an accurate dose calculation tool for small fields defined using the photon MLC with good results. This model was subsequently used, along with forward planning techniques, to deliver an idealized test plan to film in Solid Water (GAMMEX, WI, USA) [4]. In this study, they also reported on the parameters and efficiency of delivering an actual clinical plan to a chest wall case, however, no quantitative comparison of the plan and delivery were done. Jin *et al.* [5] have investigated the delivery accuracy of an inverse optimized MERT plan that was delivered to a heterogeneous breast phantom. The plan was delivered to both film and ion chamber using the photon MLC and showed very good agreement with the planned dose distribution.

These studies have shown the potential benefits of MERT as a new tool for Radiation Oncologists to treat certain malignancies, however, there have been

no dosimetric studies based on the delivery of an inverse optimized plan using a tertiary collimator. The aim of this work was to conduct a full end-to-end evaluation of the delivery and QA of an inverse optimized, Monte Carlo calculated MERT case. This test would demonstrate the integration of the many separate phases into one complete clinical workflow that would allow this technique to be compared to other clinical options on the grounds of efficiency, practicality and accuracy. A previously treated whole breast irradiation patient was selected as a good candidate for this study based on shallow and variable tumor depth that still fit within the maximum treatment area of $8 \times 8 \text{ cm}^2$ of the Few Leaf Electron collimator (FLEC) [1] used to shape the beam. Due to the addition of the FLEC as an external beam shaping device, careful evaluation of not only the relative spatial distribution of the dose, but the output as well is of importance due to large reductions in beam output for the smaller fields ($2 \times 2 \text{ cm}^2$) and lower beam energies. In addition to verifying accurate delivery, we recorded the time spent at each phase so that the practicality and efficiency of this MERT delivery method in its current form could be evaluated and compared to other available techniques. Device QA tests were also evaluated and discussed as a way to ensure safe delivery of future cases.

4.2 Materials and Methods

4.2.1 Validation of Monte Carlo model against measurements

In order to properly predict dose distributions from plans composed of many small $2 \times 2 \text{ cm}^2$ electron beams, a highly accurate Monte Carlo treatment head model is required that not only accurately predicts the shape of the dose

distributions, but the output as well. The model used was adapted from the one commissioned by Connell *et al.* [20] where beam tuning was done both with and without the scattering foils in the beamline of a Varian (Varian Medical, Inc., Palo Alto, CA) 2100 EX linear accelerator. This model was then tested and modified to ensure its accuracy in predicting change in dose output between reference conditions and the small FLEC defined fields used in the MERT delivery.

Measurements of dose per 100 MU were taken for all electron energies and field sizes of 10x10 cm² defined with the standard insert as well as 8x8, 4x4 and 2x2 cm² FLEC defined fields at a depth of z_{\max} using a Wellhofer WP700 water tank (IBA Dosimetry, Bartlett, TN). Measurements were taken with a model 6517A Keithley electrometer connected to a PTW micro liquid ion chamber, model 31018, operated at +800 Volts. Dose rate for all measurements was set to 200 MU/minute and dose was corrected for polarity and recombination effects according to Tolli *et al.* [21].

Monte Carlo simulations were conducted using the BEAMnrc user code [22] to model the treatment head and DOSXYZnrc to score dose to the water phantom. Voxel dimensions along the central axis were set to the equivalent square of the 2.5 mm diameter sensitive volume of the liquid ion detector to minimize volume averaging that starts to become significant for the smaller fields. The voxel boundaries were chosen such that the center of the voxels coincided with the center of the detector and simulations were run until the uncertainty at z_{\max} was under 0.3%. Dose per incident particle was extracted from Monte Carlo simulations at

z_{\max} for each energy and field size combination used in the measurements using MATLAB (Mathworks, Natick MA).

4.2.2 Creation of MERT plan within the treatment planning system

All treatment planning was performed within an in-house Monte Carlo based treatment planning system referred to as McGill Monte Carlo Treatment Planning (MMCTP) [2]. This software features full Monte Carlo simulation support using the BEAMnrc and DOSXYZnrc user codes and inverse optimization planning. The selected patient had undergone whole breast irradiation for invasive ductal carcinoma and was selected as a representative case where MERT could be beneficial. Replanning studies of this nature are covered under an institutional agreement approved by the research ethics board. The patient received radiotherapy to the left breast consisting of 42.56 Gy in 16 fractions delivered with tangential photon beams and included a 10 Gy in 4 fractions conventional electron boost. This patient was well suited to our study as the size of the PTV was just small enough to fit within the FLECs maximum aperture of 8x8 cm². In this study, the MERT delivery was planned with the goal of providing a replacement to the conventional electron boost, however, the choice of patient was selected solely as a clinically relevant example to test the automated delivery accuracy. The focus of this work was not to make a statement of the superiority of MERT over the conventional treatment for this patient and no comparisons were made.

Similarly to previous work by Connell *et al.* [20], once the patient was imported into MMCTP, 245 2x2 cm² feathered beamlets with a 1 cm overlap were generated onto the planning CT for all energies (6, 9, 12, 16 and 20 MeV) at the

same gantry angle of 70 degrees that was used in the actual plan. Monte Carlo pre-calculation of each of the beamlets was conducted with the original planning CT, and the statistical uncertainty of voxels with a dose greater than 50% of the maximum dose was kept to less than 1.5% per beam. Simulation took approximately 4 days on a 104 core cluster using a 3x3x3 mm³ dose grid, however, this method transported each particle from the initial source and through the treatment head. If this technique was to be used on multiple patients, much time could be saved by creating a library of phasespaces at the distal edge of the collimator for each of the 245 fields and using that as an input to the patient specific dose calculation as described by Alexander *et al.* [23], however as this study involved only one patient, it was not implemented. Through benchmarking, it was noted that for this particular application, greater than 95% of the simulation time was taken up by the BEAMnrc simulation of the head, indicating that use of a phasespace library would greatly reduce the simulation time. Beam weights were adjusted using inverse optimization of a cost function based on PTV, heart and lung dose as well as dose constraints to one planning structure located around the sides of the PTV as well as one distal to the PTV. A gap of approximately 1 cm was left between the PTV and the planning structures to account for the gradient region between the high and low dose areas. Dose normalization of the optimized plan was chosen to match the dose of the electron boost dose. The dose prescription of the electron boost was 2.5 Gy per fraction at the 90% point on the depth dose curve, which is equivalent to 2.78 Gy at z_{\max} . We chose to normalize

the MERT plan so that 95% of the PTV was covered by our prescription dose of 2.78 Gy, which is standard practice in inverse planning.

Comparing the planned and delivered dose distributions required recalculation onto a Solid Water slab phantom. A 30x30x12 cm³ arrangement of Solid Water slabs was scanned using a Phillips (Amsterdam, The Netherlands) Brilliance CT Big Bore scanner and imported into MMCTP. Beam weights from the patient CT were transferred to the QA plan and the doses were then resumed as both individual energies and as a composite delivery of all energies.

4.2.3 Delivery of modulated electron plan

The process of transferring the beam weights from the planning system to the automated FLEC control software is done through exporting a FLEC control file from MMCTP and importing it into the FLEC control software. This file consists of lines of plain text for each beam that contains the beam energy, FLEC leaf setting, secondary collimator setting and MU for each beam. The full details of the FLEC electronics, its control software and the interfacing of the device with the Varian 2100 EX linear accelerator are described in previous work by Al-Yahya *et al.* [1].

As the control software interacts with the accelerator operated in service mode through keystrokes delivered through an RS-232 port, all key commands needed to set the energy, secondary collimator setting and MU value are entered automatically. Currently the software pauses for user input at various control points before allowing the routine to advance to the next step. At this time, these pauses are necessary as it is not possible to receive feedback from the accelerator

on the status of interlocks. Therefore, one key press is required before turning the beam on in which the user must first verify that the accelerator has finished setting the energy, jaw position and MU setting. A second key press is required at the end of beam delivery before programming the next beam. In order for the accelerator to work in this unorthodox way, several interlocks must first be overridden including ACC, COLL, MOTN and KEY. Since the delivery is performed with the key in the on position, the MOTN and KEY override allows for movement of the secondary collimator without the need to turn off the key between each beam.

4.2.4 2D Verification of the plan delivery using EBT3 film

The recent multichannel film dosimetry method outlined by Micke *et al.* [24] was implemented in MATLAB (Mathworks, Natick MA). Pieces of EBT3 model GafChromicTM film (Ashland Specialty Ingredients, Wayne, NJ) were scanned using an Epson 11000 XL (Seiko Epson Corporation, Nagano, Japan) photo scanner at 150 dpi in transmission mode with all automatic corrections turned off. A sheet of glass from an old scanner bed was placed on top of each sheet of film before scanning to hold the film flat against the scanner top. This helps to prevent nonuniformities caused by the tendency of the film to curl after being cut. Calibration film strips were exposed at z_{\max} in Solid Water using a 20 MeV electron beam defined by a 10x10 cm² standard cutout. Exposures of 0, 25, 50, 100, 150, 200, 250 and 350 cGy were used in the generation of the three color-channel calibration curves.

The plan was delivered to EBT3 film placed at a depth of 2 cm in Solid Water. Other depths were not considered due to positioning uncertainty caused by the steep dose gradients and possible volume averaging errors associated with the relatively large dose calculation grid of $3 \times 3 \times 3 \text{ mm}^2$. The plan was broken up into its four distinct energies of 9, 12, 16 and 20 MeV and delivered individually to its own sheet of film as well as one composite delivery where all energies were delivered to the same sheet. Optical density was converted to dose using the triple channel method referenced above. All measurements were corrected for daily output variations of the accelerator.

The calculated 2D dose planes at a depth of 2 cm in the Solid Water phantom were extracted from the summed dose distributions for each of the energy combinations used above. The dose plane was imported into MATLAB for comparison against the film images. A planned vs. delivered dose comparison was performed through dose subtraction of the planned distribution and the film distribution resampled onto the same grid as the plan. Downsampling of the film image was done using exact-area sampling where each pixel value of the downsampled image will be the mean value of the dose surface within that pixels square. This method is preferred to interpolation as it more closely approximates the volume averaging encountered in the simulations which used a $3 \times 3 \times 3 \text{ mm}^3$ dose calculation grid. A gamma analyses was also conducted with distance to agreement, dose difference and threshold values of 3 mm, 3% and 10% respectively as well as 5 mm, 5% and 10%.

4.2.5 2D Verification of the plan delivery using MapCHECK

The plan was also delivered onto a MapCHECK 2 phantom (Sun Nuclear Corporation, Florida, USA). The effective depth of the 2D diode array is at 2 cm of water equivalent material, which provides a convenient comparison against the EBT3 measurements taken at the same depth (discussed in section 2D Verification of the plan delivery using EBT3 film). Since energy specific calibrations are used for the diode array, only one energy was recorded at a time. Analysis of the single energy deliveries was done within the MapCHECK SNC Patient Software (Sun Nuclear Corporation, Florida, USA) with gamma criterion set to 3 mm, 3% and 10% for distance to agreement, dose difference and threshold value respectively as well as 5 mm, 5% and 10%.

4.3 Results and discussion

4.3.1 Validation of Monte Carlo model against measurements

Results showing the measured and simulated output factors for all energies and different field size combinations are given in Table 4–1. The convention used to identify output factors, such as $2(3.0) \text{ cm}/8(9.0) \text{ cm}$, refers to the recombination corrected electrometer reading for a $2 \times 2 \text{ cm}^2$ FLEC defined field with the secondary collimator set to $3 \times 3 \text{ cm}^2$, divided by the corrected reading for an $8 \times 8 \text{ cm}^2$ FLEC defined field with a secondary collimator setting of $9 \times 9 \text{ cm}^2$.

Of note is the particularly large decrease in output for the smaller $2 \times 2 \text{ cm}^2$ fields and lower energies. This is due to the relatively small secondary collimator setting that blocks a significant fraction of the primary electron beam that would otherwise contribute to the dose at the detector. This differs from the clinical

configuration in which a Cerrobend cutout would be used to define the 2x2 cm² opening and the jaw setting would be between 11x11 cm² and 20x20 cm², depending on the energy, when using the 6x6 cm² applicator. This decrease in output is still present, but reduced when using other forms of collimation such as tertiary electron MLCs or the photon MLCs as such narrow jaw settings are not required. It is possible to compensate for these lower dose rates by redesigning or removing the scattering foils to reduce the amount of beam scattering, leading to much higher dose rates on the central axis. The unflattened beam could then be compensated for by automatically adjusting the beam weights during the optimization process in the treatment planning system. The same approach is currently used for the so-called Flattening Filter Free (FFF) photon IMRT beams on Varian TrueBeam linacs.

The standard convention for setting the secondary collimator for a FLEC defined field was to add a jaw margin of 5 mm beyond the FLEC leaf setting. As such, a 2x2 cm² (projected to the isocenter) FLEC field setting would mean the secondary collimator was set to 3.0x3.0 cm². Initial disagreement between simulated and measured output for 2x2 cm² FLEC defined fields was on the order of a few percent and could not be rectified by changing source parameters alone. MC simulations showed that the output factor was very sensitive to the secondary collimator setting, with the output changing by -5.6% and +6.8% for a 0.5 mm decrease and increase, respectively, in the individual jaw position (2.9 x 2.9 cm² and 3.1 x 3.1 cm² vs. the normal 3.0 x 3.0 cm²). Such adjustments to the simulated jaw positions are not unreasonable given the QA tolerances of 1

Table 4–1: Comparison of measured and simulated output factors. Field sizes are for the width of the square field as defined by the FLEC with the secondary collimator setting defined in brackets.

	Measurement Depth (cm)				
	z=2.0	z=2.0	z=2.0	z=2.0	z=1.3
Measured	20 MeV	16 MeV	12 MeV	9 MeV	6 MeV
4(5.0) cm/8(9.0) cm	0.928	0.861	0.757	0.596	0.436
2(3.0) cm/8(9.0) cm	0.678	0.544	0.408	0.244	0.152
Simulated	20 MeV	16 MeV	12 MeV	9 MeV	6 MeV
4(5.0) cm/8(9.0) cm	0.892	0.851	0.737	0.578	0.435
2(3.0) cm/8(9.0) cm	0.634	0.519	0.388	0.229	0.147
2(3.1) cm/8(9.1) cm	0.676	0.542	0.399	0.241	0.154
% Diff [100*(Sim-Meas)/Sim]	20 MeV	16 MeV	12 MeV	9 MeV	6 MeV
4(5.0) cm/8(9.0) cm	-4.0	-1.1	-2.7	-3.0	-0.1
2(3.0) cm/8(9.0) cm	-6.9	-4.9	-5.1	-6.5	-3.2
2(3.1) cm/8(9.1) cm	-0.3	-0.3	-2.1	-1.3	1.5

mm per jaw set out in the TG-142 Report [4]. The QA process and implications of the FLEC device are discussed later in section 4.3.2, Device hardware and output factor QA. Looking at the percentage difference between the measured and simulated 2(3.0) cm/8(9.0) cm output factors displayed in Table 4–1, the simulated output factors show a systematically lower value by -5.32% averaged across all energies. After applying the corrected jaw setting, with an increased margin of 0.5 mm, the mean discrepancy was reduced to -0.48%. All subsequent simulations were adjusted to include a jaw position that was 0.5 mm greater than the jaw position setting used on the accelerator.

4.3.2 Device hardware and output factor QA

Calibration of the FLEC leaves entails setting two parameters for each leaf, the steps per mm value of the stepper motor and the offset value which gives the number of steps between the position of the leaf at the home switch and the reference position which in this case is the position that defines the $8 \times 8 \text{ cm}^2$ field. To verify the correct settings, a simple QA test was produced that consisted of a printed pattern of two rectangles and a cross that was used to center the jig in the light field using the projected crosshairs. The two squares represent the projected light fields at 100 cm SSD for the $8 \times 8 \text{ cm}^2$ and $2 \times 2 \text{ cm}^2$ FLEC defined fields. The offset value can be determined independently of the steps per mm value as the jaw position at the home switch and the jaw position when defining the $8 \times 8 \text{ cm}^2$ reference field are less than 1 mm apart. The correct steps per mm parameter is verified by moving the leaves to a $2 \times 2 \text{ cm}^2$ field and verifying that the projected light field edge falls on the $2 \times 2 \text{ cm}^2$ printed box.

A second check was used to check the consistency of the output factor due to possible variations from secondary collimator calibration or other changes. This can be verified for all energies by taking the output ratio for $2 \times 2 \text{ cm}^2$ and $8 \times 8 \text{ cm}^2$ fields. This test can be administered using film or potentially any other detector suitable for small radiation field dosimetry. It is possible that the central axis diode of the MapCHECK could be used to check the output factors just prior to delivering the QA plan.

4.3.3 Creation of MERT plan

During the optimization process, it was found that limiting the energies to between 9 and 20 MeV produced superior DVH distributions to those including 6 MeV. For PTVs with distal edges located at deeper depths, and therefore requiring higher electron energies for complete coverage, it is expected that lower energies will contribute less to the overall quality of the plan. Also, it is plausible that increased complexity from including a greater number of energies in the solution space would degrade the final solution due to an increased possibility of the optimization algorithm becoming stuck in local minima. It is therefore concluded that the planner should manually limit the range of energies based upon the various depths of the distal edge of the PTV. One positive benefit of limiting the choice of energies used is the increase in speed of calculation and optimization, particularly by eliminating the 6 MeV beam quality, which represents approximately 40% of the total simulation time of all five energies. Planning time is widely based upon the experience of the planner. It is hypothesized that once the beamlet dose calculation was complete, an experienced planner would be able to produce acceptable plans in approximately one hour. This estimate includes time spent drawing planning structures on the CT and running the optimization script (1-2 minutes) in an iterative process and changing dose criteria and penalties at each step until the user is satisfied with the plan quality.

Figure 1(a) shows the calculated and optimized MERT plan on the planning CT with various visible contours including the PTV, heart, lung and planning

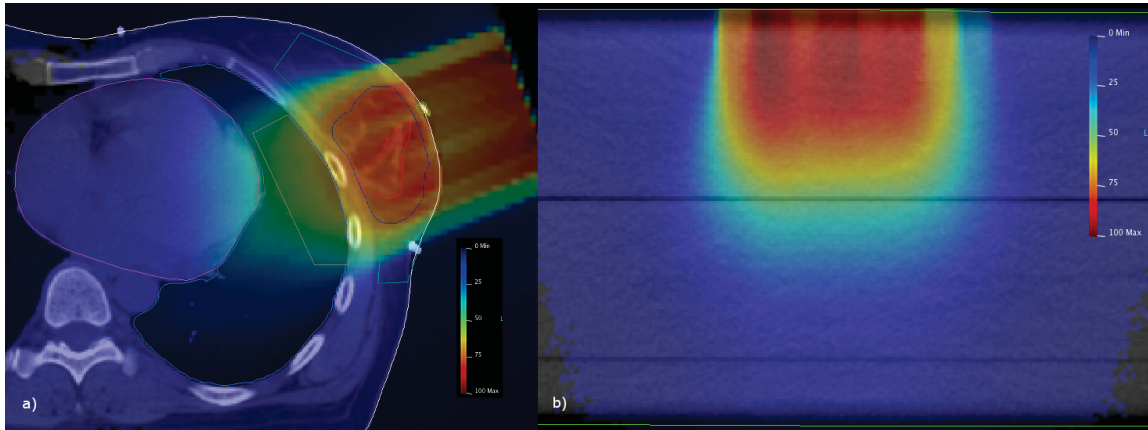


Figure 4–1: (a) The MERT plan as planned on the patient CT and b) the dose distribution calculated onto the Solid Water QA phantom.

structures. Figure. 1(b) shows the plan recalculated onto the Solid Water QA phantom.

4.3.4 Delivery of the MERT plan

A test MERT plan was delivered to identify possible issues in the workflow and to determine the time required to complete the delivery. The chosen plan, with a prescription dose of 2.78 Gy to 95% of the PTV, included four different energies (each with 49 subfields, or 196 total) and the delivery took approximately 25.8 minutes negating phantom setup. A summary of the delivery time breakdown is shown in Table II. The beam-on time represented roughly 6.2 minutes to deliver the 6183 total MU at the maximum dose rate of 1000 MU per minute. One possible way to reduce this component is to reduce or remove the scattering foil from the beamline as discussed by Connell *et al.* [20], however the amount of time reduction is a topic of future work. A summary of the MU settings broken

down by energy is included in Table 4-3. Also shown in the former table are the MU values weighted by the output factor. This weighted MU value gives an approximate representation of the total dose contributions of each energy relative to the others. A histogram of the MU distribution separated by energy is shown in Figure 4-2.

FLEC leaf travel time represented a moderate fraction of the total time taking 7.5 minutes. Possible optimizations to this phase of the delivery include performing leaf sequencing before importing the plan into the FLEC controller. Currently the fields were delivered one row at a time, with the leaves returning to the far side of the FLEC at the beginning of each row, similar to how a typewriter would write lines. By starting the next row on the near side, the leaves would only travel 1 cm (down to the next row) as opposed to 6 cm (to the far side of the FLEC), saving 5 cm worth of leaf travel time. It was calculated that this would reduce the time spent in leaf motion by a factor of 0.58. Another possible way to improve the time spent in the phase would be to increase the FLEC leaf speed. When projected to isocenter, the current stepper motors on the FLEC are limited to 0.74 cm/s due to torque limitations, while the linac jaws (as measured for this accelerator in service mode) operate at 1.9 +/- 0.2 cm/s and 1.5 +/- 0.1 cm/s for the X and Y jaws respectively. Since the FLEC leaves and linac jaws move at the same time, if the FLEC leaves could be driven as fast or faster than the Y linac jaws, the FLEC leaf travel time could be reduced by at least a factor of 0.50 before being bottlenecked by linac jaw travel time.

The remainder of the delivery time, which totals 12.1 minutes (or 3.7 seconds per beam) is spent by the automated software sending keystrokes to the accelerator in service mode and waiting for the accelerator to respond to those commands (set MU, set jaw setting and set energy when needed). There is also a small delay introduced by the operator who is required to press the enter key twice when the accelerator has finished delivering the last beam in order to start the automated setup and delivery of the next field. It is possible that through better interfacing with the accelerator, which might be possible using new technology such as the developer mode of the Varian TrueBeam linac, some of these delays could be reduced.

Other general optimizations might include more careful selection of energies. From Table 4-3, it can be seen that the 9 MeV beams contribute much less dose to the overall plan, leading to the possibility that comparable plans might be achieved using 12, 16 and 20 MeV alone. Removal of one energy would have the effect of reducing the delivery time by a factor of approximately 0.75, however, this is expected to be entirely case specific. One other possibility lies in eliminating beams with MU below a certain threshold. As seen from Figure 4-2, the distribution of fields is concentrated at lower MUs. Since low MU fields contribute little to the total plan dose, it is likely that up to a certain threshold, these fields could be removed and the plan reoptimized with only the remaining higher weighted fields. With one or more such iterations, the number of fields could be reduced, leading to lower delivery time while maintaining plan quality.

Table 4-2: A summary of the time required for each phase of the delivery in the current implementation and with possible optimizations to leaf sequence and FLEC leaf speed.

Stage of delivery	Current time (min)	Potential time with field sequencing and faster FLEC leaf speed (min)
Beam time	6.2	6.2
FLEC leaf travel time	7.5	2.2
Remainder	12.1	12.1
Total	25.8	20.5

Table 4-3: MU statistics for each beam quality tested. Also shown are the MU values weighted by the respective output factor giving an indication of the relative total dose contribution of each energy compared to the others.

Energy(MeV)	MU	Output Factor 2(3.0) cm/8(9.0) cm	MU*Output Factor	Number of fields with MU > 0
9	1208	0.241	291	46
12	1939	0.399	774	48
16	1595	0.542	865	46
20	1441	0.676	973	45
Total	6183	-	-	196

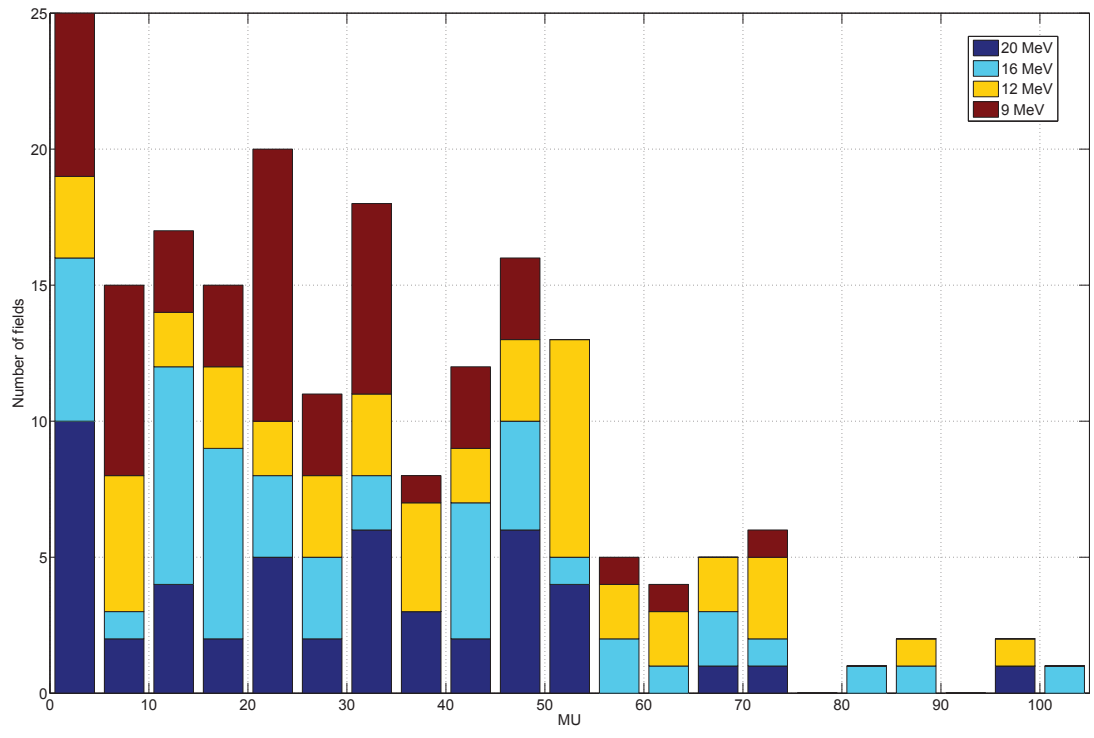


Figure 4-2: The MU distribution broken down by energy. MU bin width is 5 MU.

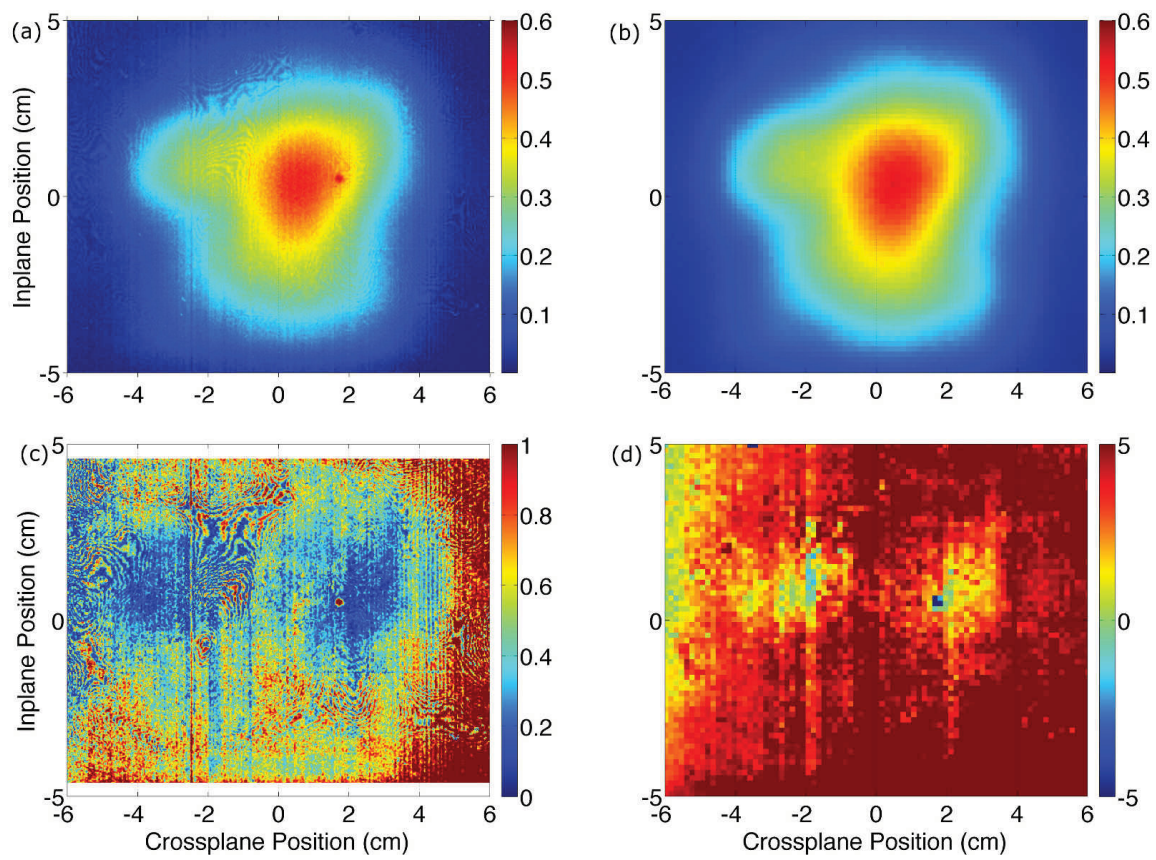


Figure 4-3: The 9 MeV film (a) and planned (b) dose distributions at a depth of 2 cm along with the 5%/5mm gamma map (c) and the plan minus film image subtraction as a percentage of the local planned dose (d).

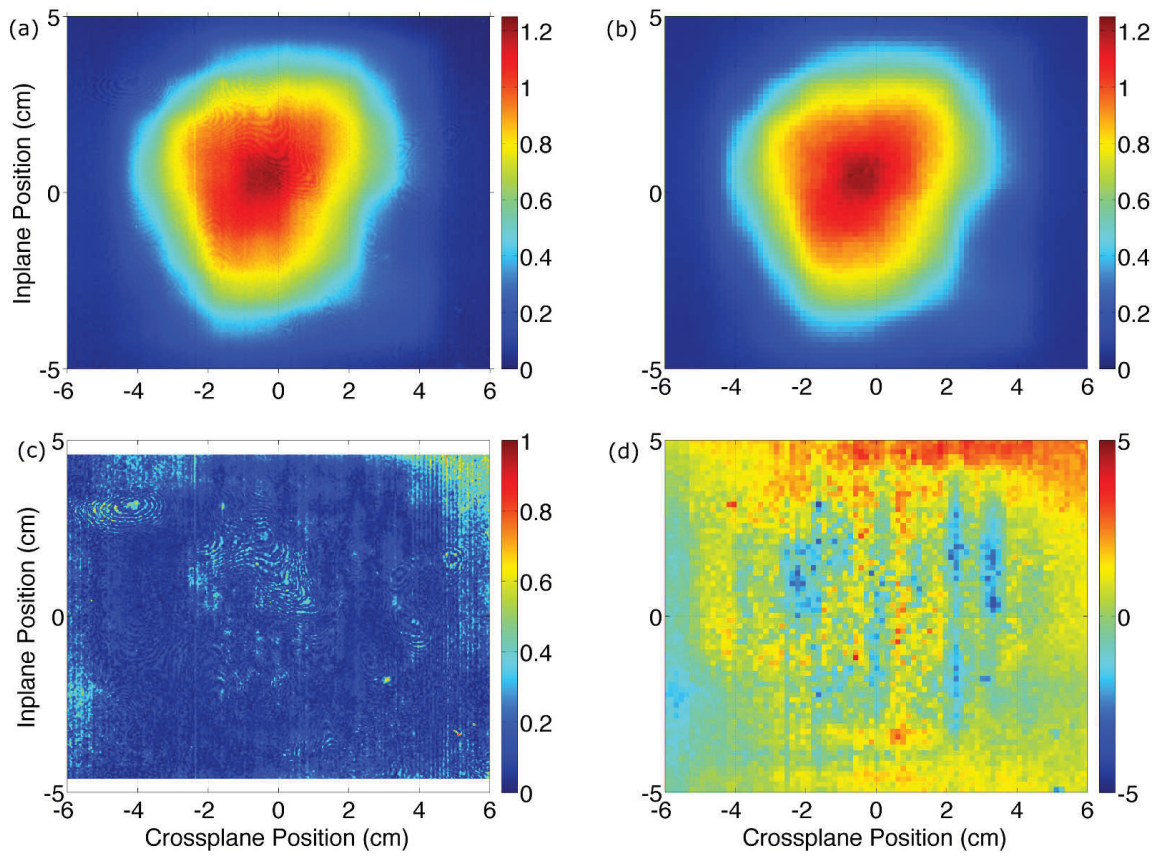


Figure 4-4: The 12 MeV film (a) and planned (b) dose distributions at a depth of 2 cm along with the 5%/5mm gamma map (c) and the plan minus film image subtraction as a percentage of the local planned dose (d).

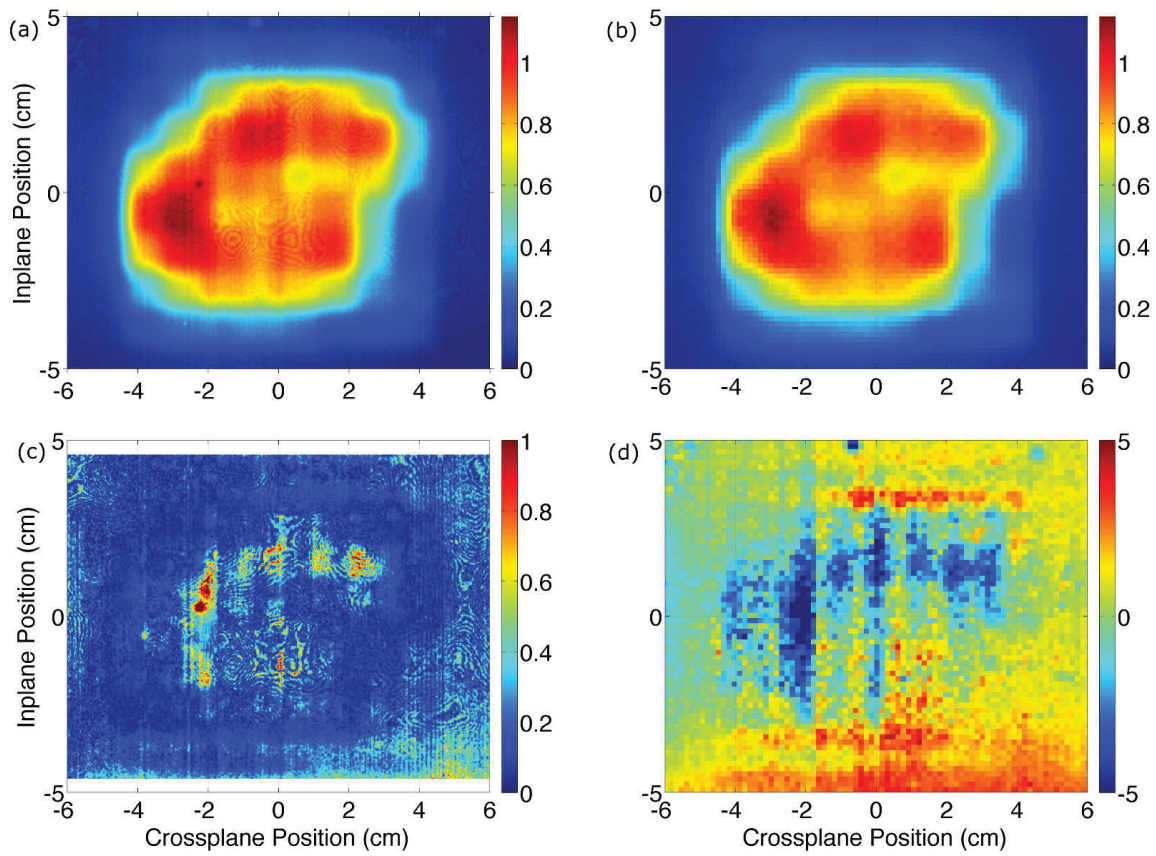


Figure 4-5: The 16 MeV film (a) and planned (b) dose distributions at a depth of 2 cm along with the 5%/5mm gamma map (c) and the plan minus film image subtraction as a percentage of the local planned dose (d).

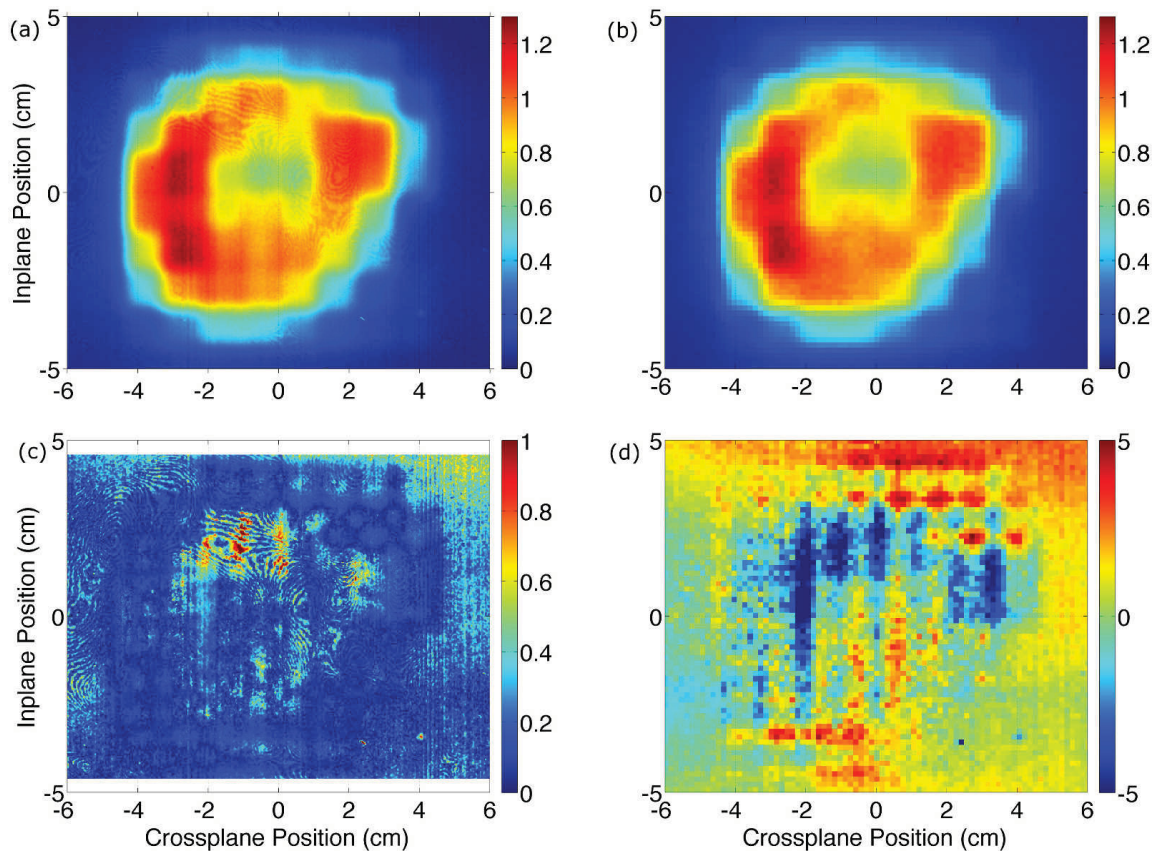


Figure 4-6: The 20 MeV film (a) and planned (b) dose distributions at a depth of 2 cm along with the 5%/5mm gamma map (c) and the plan minus film image subtraction as a percentage of the local planned dose (d).

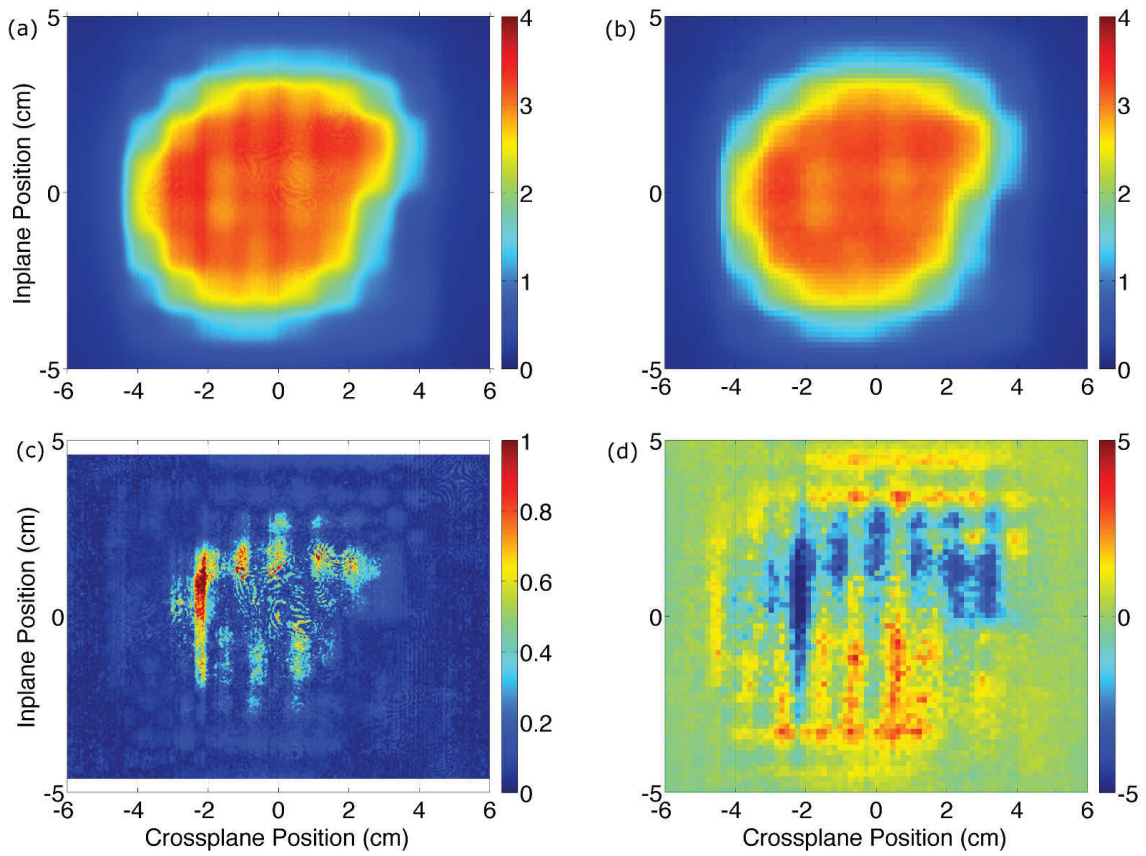


Figure 4-7: The combined-energy film (a) and planned (b) dose distributions at a depth of 2 cm along with the 5%/5mm gamma map (c) and the plan minus film image subtraction as a percentage of the local planned dose (d).

4.3.5 2D Verification of the plan delivery using EBT3 film

Figure 4–3 through Figure 4–7 show the results of the film-plan comparison for 9, 12, 16, 20 MeV and the combined-energy delivery respectively. Within each figure, panel (b) shows the planned dose distribution at a depth of 2 cm and the corresponding film distribution is seen in panel (a). The dose subtraction as a percentage of the planned dose minus the delivered dose divided by the planned dose is seen in panel (d) while panel (c) shows the gamma map. Gamma pass rates for the four energies plus the summed plan are summarized in Table 4–4. All gamma values are quite acceptable with the exception of 9 MeV, however, from the dose scale on the color bar to the right of panel (a) in Figure 4–3, it can be seen that the maximum 9 MeV dose is approximately half that of the other energies (0.55 Gy vs 1.15-1.3 Gy). The gamma map and image subtraction both show this systematic 5% relative difference between film and plan, however, the absolute dose difference is only approximately 2.75 cGy (5% of 0.55 Gy). A disagreement of this magnitude falls within the normal uncertainty expected from film dosimetry and should not be interpreted as a negative result on the part of the MERT planning or delivery process in either the dose subtraction or gamma analysis for 9 MeV. Energy response of the film was considered as a possible source of error, however, as reported by Arjomandy *et al.* [25], the energy response of EBT2 film (we used EBT3, but there is no reason to believe that there will be any significant differences) was found to be relatively small compared to their experimental uncertainty (1 sigma was 4.5%) and we determined that energy response would not have any major impact on the results.

Dose image subtraction after visually aligning the film-plan images is a convenient way to evaluate the dose output for various field positions and energies independent of positioning artifacts. Therefore, visual alignment of the plan and film images was done before subtraction and a summary of the shifts can be seen in Table 4-5. The subtraction results can be seen in panel (d) of Figure 4-3 through Figure 4-7 and again show good agreement for all deliveries except for 9 MeV (Figure 3), which is again attributed to small dose offsets present in the film dose results. Also visible in the 16 and 20 MeV dose subtraction images of Figure 4-5 and Figure 4-6 respectively, are small discrepancies along the field junctions. These are hypothesized to be due to deficiencies in the Monte Carlo beam model, which has difficulty reproducing the exact shape of the dose profile for these higher energies. The simulated profiles exhibited a slightly larger penumbra width compared to the measured profiles. It is expected that this will have minor impact on the plan quality as any dose over prediction of one field would be partially compensated for by an equivalent dose under prediction from the adjacent fields provided the beam was in a uniform dose region such as is found in the PTV.

In each of the film images in panel (a) of Figure 4-3 through Figure 4-7, newton ring artifacts can be seen. This is one potential film artifact which is usually relatively minor or non-existent. The appearance of this artifact was magnified by the use of the glass pane that was placed on top of the film to hold it flat against the scanner bed. Although visible in the images, it was of little consequence to the overall results and was acceptable given the superior reproducibility and accuracy observed when using the glass pane.

Table 4-4: Film gamma analysis values for all delivered energies for both 3%/3mm and 5%/5mm gamma criteria.

Energy(MeV)	3%/3 mm	5%/5 mm
9	62.1	92.3
12	99.8	100.0
16	97.8	99.9
20	98.3	99.9
Combined Plan	98.7	99.9

Table 4-5: A summary of the x and y shifts needed to produce the optimal dose subtraction image of panel (d) of Figs. 2-6. All shifts were determined visually.

Energy(MeV)	Crossplane shift (mm)	Inplane shift (mm)
9	-0.6	0.0
12	0.0	-0.5
16	0.4	-0.7
20	0.2	-0.5
Combined Plan	0.6	0.9

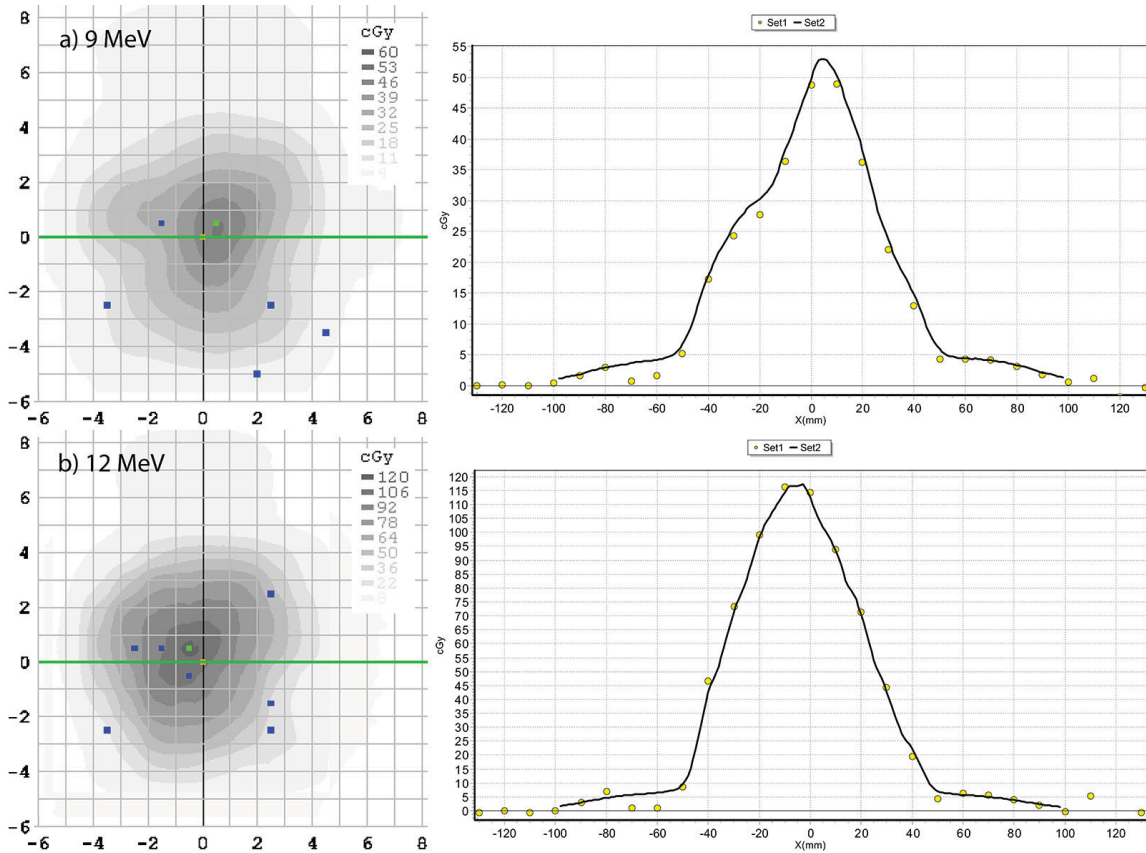


Figure 4–8: The (a) 9 MeV and (b) 12 MeV MapCHECK dose distributions shown on the left and the crossplane profile on the right.

4.3.6 2D Verification of the plan delivery using MapCHECK

Figure 4–8 shows the results of the MapCHECK report for (a) 9 MeV and (b) 12 MeV. For each energy, the left panel shows the dose distribution with pixels not satisfying the gamma criteria marked with blue squares for measured values below the planned values and red squares for measured values above. The right panel shows the crossplane profile across the central axis with the plan being represented by the solid black line (Set 2) and the MapCHECK dose points represented by

Table 4–6: Pass percentages from the MapCHECK gamma analysis

Energy(MeV)	3%/3 mm	5%/5 mm
9	88.8	98.0
12	86.1	95.2
16	89.4	95.7
20	94.8	96.7

yellow circles (Set 1). Similar figures are shown for (a) 16 MeV and (b) 20 MeV in Figure 4–9. The percentage of passing pixels for gamma criteria of 5%/5 mm and 3%/3 mm are summarized in Table 4–6. These results are consistent with the film results and are again generally quite good. Three detectors of the MapCHECK were identified as being defective and could not be fixed by recalibration or be excluded from the reported gamma results. These defective pixels would therefore cause the gamma values shown in Table 4–6 to be slightly worse than reality, although account for less than 2 percent of the total number of pixels that satisfied the 10% dose threshold. This test has the advantage of being faster than film as there is no need to wait for the radiochromic film to self-develop. Future work to improve the accuracy of MERT delivery dosimetry would involve calculating the planned distribution on a mathematical phantom of the MapCHECK that was based on the manufacturer's specifications.

4.4 Conclusions

In this work, we investigated the accuracy and efficiency of an end-to-end MERT delivery including planning, delivery, and dosimetric QA. A previously treated whole breast irradiation patient was chosen as a suitable test case and was put through the MERT planning process including Monte Carlo calculation

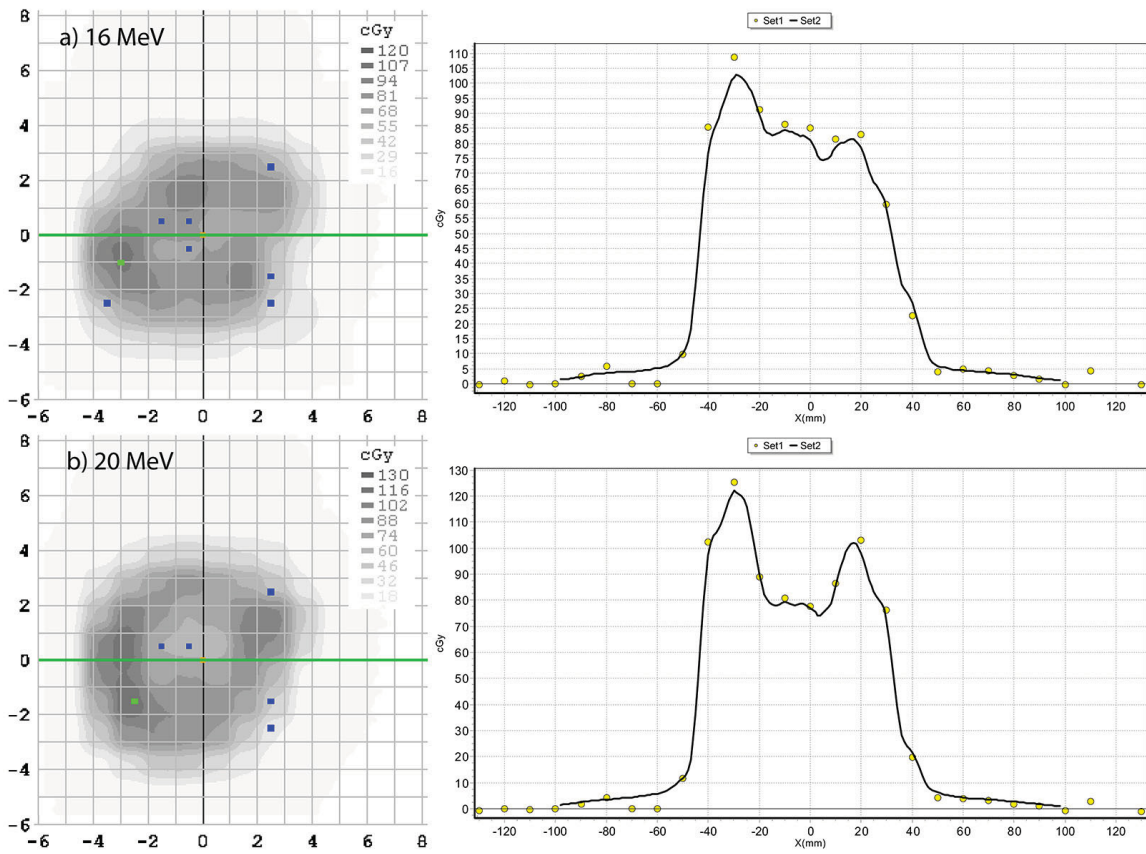


Figure 4-9: The (a) 16 MeV and (b) 20 MeV MapCHECK dose distributions shown on the left and the crossplane profile on the right.

of beamlets and inverse optimization of the beam weights within the MMCTP treatment planning system. Beam weights were then transferred to the FLEC collimation device software and a fully automated delivery of the plan was done covering four electron energies and 196 total subfields which took 25.8 minutes to deliver. The plan was delivered to both EBT3 film and to the MapCHECK QA device. Film analysis of the delivery showed good results with 3%/3 mm gamma values of 62.1, 99.8, 97.8, 98.3, and 98.7 percent for the 9, 12, 16, 20 MeV, and combined energy deliveries respectively. Delivery to the MapCHECK device also showed good agreement with 3%/3 mm gamma pass rates of 88.8, 86.1, 89.4, and 94.8 percent for the 9, 12, 16, and 20 MeV energies respectively. These results showed that accurate delivery utilizing an add-on tertiary electron collimator is possible using Monte Carlo calculated plans and inverse optimization. This brings MERT closer to becoming a viable option for physicians in treating superficial malignancies.

4.5 Acknowledgments

This work was partially supported by grants from the Canadian Institutes of Health Research, CIHR MOP 102550 and Natural Sciences and Engineering Research Council Discovery grants numbers 298191 and 386009. Also, this work was partially supported by the Medical Physics Research Training Network, Natural Sciences and Engineering Research Council/Collaborative Research and Training Experience initiative no #432290. Slobodan Devic is Senior Research Scientist supported by the Fonds de Recherche en Santé du Québec (FRSQ).

REFERENCES

- [1] K. Al-Yahya, F. Verhaegen, and J. Seuntjens. Design and dosimetry of a few leaf electron collimator for energy modulated electron therapy. *Med Phys*, 34(12):4782–91, 2007. Al-Yahya, Khalid Verhaegen, Frank Seuntjens, Jan Research Support, Non-U.S. Gov't United States Medical physics Med Phys. 2007 Dec;34(12):4782-91.
- [2] A. Alexander, F. Deblois, G. Stroian, K. Al-Yahya, E. Heath, and J. Seuntjens. Mmctp: a radiotherapy research environment for monte carlo and patient-specific treatment planning. *Phys Med Biol*, 52(13):N297–308, 2007. Alexander, A Deblois, F Stroian, G Al-Yahya, K Heath, E Seuntjens, J Research Support, Non-U.S. Gov't England Physics in medicine and biology Phys Med Biol. 2007 Jul 7;52(13):N297-308. Epub 2007 Jun 6.
- [3] F. C. du Plessis, A. Leal, S. Stathakis, W. Xiong, and C. M. Ma. Characterization of megavoltage electron beams delivered through a photon multi-leaf collimator (pmlc). *Physics in medicine and biology*, 51(8):2113–29, 2006. du Plessis, F C P Leal, A Stathakis, S Xiong, W Ma, C-M England Phys Med Biol. 2006 Apr 21;51(8):2113-29. Epub 2006 Apr 3.
- [4] Eric E Klein, Joseph Hanley, John Bayouth, Fang-Fang Yin, William Simon, Sean Dresser, Christopher Serago, Francisco Aguirre, Lijun Ma, and Bijan Arjomandy. Task group 142 report: quality assurance of medical accelerators. *Medical physics*, 36:4197, 2009.
- [5] L. Jin, C. M. Ma, J. Fan, A. Eldib, R. A. Price, L. Chen, L. Wang, Z. Chi, Q. Xu, M. Sherif, and J. S. Li. Dosimetric verification of modulated electron radiotherapy delivered using a photon multileaf collimator for intact breasts. *Physics in medicine and biology*, 53(21):6009–25, 2008. Jin, L Ma, C-M Fan, J Eldib, A Price, R A Chen, L Wang, L Chi, Z Xu, Q Sherif, M Li, J S England Phys Med Biol. 2008 Nov 7;53(21):6009-25. Epub 2008 Oct 3.
- [6] M. G. Karlsson, M. Karlsson, and C. M. Ma. Treatment head design for multileaf collimated high-energy electrons. *Medical physics*, 26(10):2161–7,

1999. Karlsson, M G Karlsson, M Ma, C M Med Phys. 1999 Oct;26(10):2161-7.
- [7] J. Mihaljevic, M. Soukup, O. Dohm, and M. Alber. Monte carlo simulation of small electron fields collimated by the integrated photon mlc. *Physics in medicine and biology*, 56(3):829–43, 2011. Mihaljevic, Josip Soukup, Martin Dohm, Oliver Alber, Markus England Phys Med Biol. 2011 Feb 7;56(3):829-43. Epub 2011 Jan 17.
- [8] C. M. Ma, T. Pawlicki, M. C. Lee, S. B. Jiang, J. S. Li, J. Deng, B. Yi, E. Mok, and A. L. Boyer. Energy- and intensity-modulated electron beams for radiotherapy. *Phys Med Biol*, 45(8):2293–311, 2000. Ma, C M Pawlicki, T Lee, M C Jiang, S B Li, J S Deng, J Yi, B Mok, E Boyer, A L CA78331/CA/NCI NIH HHS/United States Comparative Study Research Support, Non-U.S. Gov't Research Support, U.S. Gov't, Non-P.H.S. Research Support, U.S. Gov't, P.H.S. England Physics in medicine and biology Phys Med Biol. 2000 Aug;45(8):2293-311.
- [9] M. C. Lee, S. B. Jiang, and C. M. Ma. Monte carlo and experimental investigations of multileaf collimated electron beams for modulated electron radiation therapy. *Med Phys*, 27(12):2708–18, 2000. Lee, M C Jiang, S B Ma, C M 5T32GM08294-11/GM/NIGMS NIH HHS/United States CA 78331/CA/NCI NIH HHS/United States Research Support, U.S. Gov't, Non-P.H.S. Research Support, U.S. Gov't, P.H.S. United States Medical physics Med Phys. 2000 Dec;27(12):2708-18.
- [10] T. Gauer, D. Albers, F. Cremers, R. Harmansa, R. Pellegrini, and R. Schmidt. Design of a computer-controlled multileaf collimator for advanced electron radiotherapy. *Physics in medicine and biology*, 51(23):5987–6003, 2006. Gauer, T Albers, D Cremers, F Harmansa, R Pellegrini, R Schmidt, R England Phys Med Biol. 2006 Dec 7;51(23):5987-6003. Epub 2006 Oct 30.
- [11] K. R. Hogstrom, R. A. Boyd, J. A. Antolak, M. M. Svatos, B. A. Faddegon, and J. G. Rosenman. Dosimetry of a prototype retractable emlc for fixed-beam electron therapy. *Medical physics*, 31(3):443–62, 2004. Hogstrom, Kenneth R Boyd, Robert A Antolak, John A Svatos, Michelle M Faddegon, Bruce A Rosenman, Julian G Med Phys. 2004 Mar;31(3):443-62.
- [12] J. Deng, M. C. Lee, and C. M. Ma. A monte carlo investigation of fluence profiles collimated by an electron specific mlc during beam delivery for

- modulated electron radiation therapy. *Med Phys*, 29(11):2472–83, 2002. Deng, Jun Lee, Michael C Ma, C M CA78331/CA/NCI NIH HHS/United States Evaluation Studies Research Support, U.S. Gov't, Non-P.H.S. Research Support, U.S. Gov't, P.H.S. Validation Studies United States Medical physics Med Phys. 2002 Nov;29(11):2472-83.
- [13] T. Vatanen, E. Traneus, A. Vaananen, and T. Lahtinen. The effect of electron collimator leaf shape on the build-up dose in narrow electron mlc fields. *Phys Med Biol*, 54(23):7211–26, 2009. Vatanen, T Traneus, E Vaananen, A Lahtinen, T Research Support, Non-U.S. Gov't England Physics in medicine and biology Phys Med Biol. 2009 Dec 7;54(23):7211-26. Epub 2009 Nov 17.
- [14] A. A. Eldib, M. I. ElGohary, J. Fan, L. Jin, J. Li, C. Ma, and N. A. Elsherbini. Dosimetric characteristics of an electron multileaf collimator for modulated electron radiation therapy. *Journal of applied clinical medical physics / American College of Medical Physics*, 11(2):2913, 2010. Eldib, Ahmed Abdel Rahman ElGohary, Mohamed I Fan, Jiajin Jin, Lihui Li, Jinsheng Ma, Charlie Elsherbini, Nader A J Appl Clin Med Phys. 2010 Apr 12;11(2):2913.
- [15] E. E. Klein, M. Vicic, C. M. Ma, D. A. Low, and R. E. Drzymala. Validation of calculations for electrons modulated with conventional photon multileaf collimators. *Physics in medicine and biology*, 53(5):1183–208, 2008. Klein, Eric E Vicic, Milos Ma, Chang-Ming Low, Daniel A Drzymala, Robert E England Phys Med Biol. 2008 Mar 7;53(5):1183-208. Epub 2008 Feb 11.
- [16] C. M. Ma, M. Ding, J. S. Li, M. C. Lee, T. Pawlicki, and J. Deng. A comparative dosimetric study on tangential photon beams, intensity-modulated radiation therapy (imrt) and modulated electron radiotherapy (mert) for breast cancer treatment. *Phys Med Biol*, 48(7):909–24, 2003. Ma, C M Ding, M Li, J S Lee, M C Pawlicki, T Deng, J CA78331/CA/NCI NIH HHS/United States Comparative Study Evaluation Studies Research Support, U.S. Gov't, Non-P.H.S. Research Support, U.S. Gov't, P.H.S. Validation Studies England Physics in medicine and biology Phys Med Biol. 2003 Apr 7;48(7):909-24.
- [17] K. Al-Yahya, M. Schwartz, G. Shenouda, F. Verhaegen, C. Freeman, and J. Seuntjens. Energy modulated electron therapy using a few leaf electron collimator in combination with imrt and 3d-crt: Monte carlo-based planning and dosimetric evaluation. *Med Phys*, 32(9):2976–86, 2005. Al-Yahya, Khalid Schwartz, Matthew Shenouda, George Verhaegen, Frank Freeman, Carolyn

Seuntjens, Jan Research Support, Non-U.S. Gov't United States Medical physics Med Phys. 2005 Sep;32(9):2976-86.

- [18] T. Gauer, K. Engel, A. Kiesel, D. Albers, and D. Rades. Comparison of electron imrt to helical photon imrt and conventional photon irradiation for treatment of breast and chest wall tumours. *Radiotherapy and oncology : journal of the European Society for Therapeutic Radiology and Oncology*, 94(3):313–8, 2010. Gauer, Tobias Engel, Konrad Kiesel, Antje Albers, Dirk Rades, Dirk Ireland Radiother Oncol. 2010 Mar;94(3):313-8. Epub 2010 Jan 28.
- [19] F. J. Salguero, B. Palma, R. Arrans, J. Rosello, and A. Leal. Modulated electron radiotherapy treatment planning using a photon multileaf collimator for post-mastectomized chest walls. *Radiotherapy and oncology : journal of the European Society for Therapeutic Radiology and Oncology*, 93(3):625–32, 2009. Salguero, Francisco Javier Palma, Bianey Arrans, Rafael Rosello, Joan Leal, Antonio Ireland Radiother Oncol. 2009 Dec;93(3):625-32. Epub 2009 Sep 14.
- [20] T. Connell, A. Alexander, M Evans, and J Seuntjens. An experimental feasibility study on the use of scattering foil free beams for modulated electron radiotherapy. *Phys Med Biol*, 57(11):3259–3272, 2012.
- [21] H. Tolli, R. Sjogren, and M. Wendelsten. A two-dose-rate method for general recombination correction for liquid ionization chambers in pulsed beams. *Phys Med Biol*, 55(15):4247–60, 2010. Tolli, Heikki Sjogren, Rickard Wendelsten, Mikael eng Research Support, Non-U.S. Gov't England 2010/07/10 06:00 Phys Med Biol. 2010 Aug 7;55(15):4247-60. doi: 10.1088/0031-9155/55/15/004. Epub 2010 Jul 8.
- [22] D W O Rogers, B A Faddegon, G X Ding, C M Ma, J We, and T R Mackie. Beam: a monte carlo code to simulate radiotherapy treatment units. *Med. Phys.*, 22:503–24, 1995.
- [23] A. Alexander, F. DeBlois, and J. Seuntjens. Toward automatic field selection and planning using monte carlo-based direct aperture optimization in modulated electron radiotherapy. *Phys Med Biol*, 55(16):4563–76, 2010. Alexander, Andrew DeBlois, Francois Seuntjens, Jan England Physics in medicine and biology Phys Med Biol. 2010 Aug 21;55(16):4563-76. Epub 2010 Jul 29.

- [24] A. Micke, D. F. Lewis, and X. Yu. Multichannel film dosimetry with nonuniformity correction. *Med Phys*, 38(5):2523–34, 2011. Micke, Andre Lewis, David F Yu, Xiang eng 2011/07/23 06:00 Med Phys. 2011 May;38(5):2523-34.
- [25] B. Arjomandy, R. Tailor, A. Anand, N. Sahoo, M. Gillin, K. Prado, and M. Vivic. Energy dependence and dose response of gafchromic ebt2 film over a wide range of photon, electron, and proton beam energies. *Med Phys*, 37(5):1942–7, 2010. Arjomandy, Bijan Tailor, Ramesh Anand, Aman Sahoo, Narayan Gillin, Michael Prado, Karl Vivic, Milos eng 2010/06/10 06:00 Med Phys. 2010 May;37(5):1942-7.

CHAPTER 5

An experimental feasibility study on the use of scattering foil free beams for modulated electron radiotherapy

Tanner Connell, Andrew Alexander, Michael Evans and Jan Seuntjens

Phys. Med. Biol., 57(11):3259-3272, 2012

Contents

5.1	Introduction	107
5.2	Materials and Methods	109
5.2.1	Beamline Modification and Experimental Measure- ments	109
5.2.2	Monte Carlo Model Commissioning	111
5.2.3	Inverse Treatment Planning Study	114
5.3	Results and Discussion	116
5.3.1	Characterization of Scattering Foil-Free Beams	116
5.3.2	Monte Carlo Beam Matching	119
5.3.3	Inverse Treatment Planning Study	128
5.3.4	Dosimetric considerations from scattering foil removal	129
5.4	Conclusion	130

One main strength of MERT is its potential to spare healthy tissue from the relatively more significant low dose bath that is present in modulated photon

modalities. This advantage becomes particularly significant for patients who have relatively higher risks of developing secondary malignancies induced from the therapy, such as younger patient populations and females undergoing breast irradiation who are at risk of developing malignancies in the contralateral breast. It was hypothesized that the removal of the scattering foil from the beamline could further enhance this advantage for any possible MERT implementation. The following published manuscript describes the dosimetric advantages of such a modification.

Abstract The potential benefit of using scattering foil free beams for delivery of modulated electron radiotherapy is investigated in this work. Removal of the scattering foil from the beamline showed a measured bremsstrahlung tail dose reduction just beyond R_p by a factor of 12.2, 6.9, 7.4, 7.4 and 8.3 for 6, 9, 12, 16 and 20 MeV beams respectively for 2x2 cm² fields defined on-axis when compared to the clinical beamline. Monte Carlo simulations were matched to measured data through careful tuning of source parameters and the modification of certain accelerator components beyond the manufacturer's specifications. An accelerator model based on the clinical beamline and one with the scattering foil removed were imported into a Monte Carlo-based treatment planning system (McGill Monte Carlo Treatment Planning). A treatment planning study was conducted on a test phantom consisting of a PTV and two distal organs at risk (OAR) by comparing a plan using the clinical beamline to a plan using a scattering foil free beamline. A DVH comparison revealed that for quasi-identical target coverage, the volume of

each OAR receiving a given dose was reduced, thus reducing the dose deposited in healthy tissue.

5.1 Introduction

Electrons have been widely used in radiation therapy clinics for the treatment of malignancies confined to superficial regions due to their superior dose deposition properties as a function of depth when compared to photon treatments. Recently, modulated electron radiation therapy (MERT) continues to be of interest due to its potential to offer an alternative modality to physicians treating these malignancies. MERT relies on energy and intensity modulation of the electron beam to conform the prescription dose to the distal edge of the tumor volume while maintaining dose homogeneity within the target volume resulting in greater healthy tissue sparing when compared to static single-energy fields. Collimation of multiple MERT subfields using traditional cutouts is not feasible due to the time intensive nature of their construction and use. Various groups [1, 2, 3, 4, 5] have reported on the feasibility of using the photon MLC as a possible collimation device while others [6, 7, 8, 9, 10, 11, 12] have manufactured add-on electron MLCs that are positioned closer to the patient in an effort to minimize the penumbra width due to air scatter. One possible approach to minimizing in air scatter and penumbra from photon MLCs was investigated that used helium gas to replace the atmosphere in the head of the accelerator as well as adding a helium bag below the MLC [4]. Otherwise, acceptable penumbra can be obtained with photon MLCs by using SSDs in the 70 cm range [13]. Other groups have reported on the design and use of a computer-controlled few-leaf electron collimator (FLEC)

that is positioned in the electron applicator tray within a few cm from the patient surface [14].

There have been multiple dosimetric comparisons of MERT with other electron and photon modalities. MERT has been benchmarked against IMRT and conventional photon treatments for treatment of breast cancer with the MERT plans giving reduced maximum dose to the lung and heart compared to the photon modalities [15]. The efficacy of MERT in combination with 3D-CRT and IMRT with results showing reduced whole body dose over the photon modalities alone [16]. These studies show promise for MERT as a valid treatment option either on its own or in combination with other modalities that may prove to be clinically beneficial over photon based treatments alone.

The potential reduction of dose to healthy tissue and distal structures through the modification of the accelerator beamline using MERT is the primary focus of this study. Despite the rapid dose fall off of electron beams beyond a certain depth, there exists a photon component produced by bremsstrahlung interactions within the treatment head as well as the patient. This additional dose bath, referred to as the bremsstrahlung tail, typically represents less than 4% at 20 MeV with standard field sizes and dual scattering foils [17]. However, for increasingly smaller fields, the bremsstrahlung component of the accumulated delivery will become greater, especially at high energies, amounting to 5.7% at 20 MeV for a 2x2 cm² field. In this work, we investigate the potential reduction in the bremsstrahlung tail due to the removal of the scattering foil that is used to spread out the pencil beam. Any reduction in this dose would translate into a

reduced dose bath to healthy tissue leading to less risk of secondary malignancies, especially for younger cohorts of patients. In principle, any variations in the fluence due to the absence of the scattering foil can be accounted for in the treatment planning system while maintaining the dosimetric advantages of lower photon contamination. This study will also investigate the potential for increased dose rates possible with the scattering foil removed that may potentially lead to shorter treatment times.

5.2 Materials and Methods

5.2.1 Beamline Modification and Experimental Measurements

Measurements with and without the scattering foil were performed using a Varian 2100 EX linear accelerator (Varian Medical, Inc., Palo Alto, CA) currently in clinical operation. The accelerator was modified by removing the thin metal plate located over an unused port in the carousel and manually rotating the vacant port into the beamline using the controls on the bending magnet control board. The accelerator could then be operated in this experimental mode after overriding the appropriate dosimetry interlocks. Profiles and PDDs were acquired using a Wellhofer WP700 water tank (IBA Dosimetry, Bartlett, TN) and a Wellhofer unshielded p-type diode (model number F1421) for all available electron energies consisting of 6, 9, 12, 16, and 20 MeV. All scans were conducted at an SSD of 100 cm and profiles were acquired at a depth of d_{max} for the respective energy. The over-response of diodes in electron beams due to the presence of contamination x-rays has been well studied. For depths between the surface and near R_{50} the change in response per unit dose stays within 1% for 22 MeV electron beams (22

MeV representing the worst case due to having the highest photon contamination). However, between R_{50} and R_p , the diode response increases by about 4-5% and maintains this response just beyond R_p (Wang and Rogers, 2007). Another study reported the over-response in the bremsstrahlung tail to be 0.5-1.0% for a 21 MeV electron beam [18]. Despite this over-response, particularly in the tail, the magnitude is small enough that it does not detract from the conclusions drawn in this study.

Fields were defined using a custom built electron collimation device (designated the few-leaf electron collimator, or FLEC) that is held in place by the electron applicator [14]. The device consists of 4 independent computer controlled jaws that are capable of collimating any rectangular field size defined at SSD 100 cm of up to 8×8 cm². A schematic diagram of the FLEC is shown in Figure 5-1. Previous studies [19] have determined that 2×2 cm² beamlets were the best compromise between higher resolution and lower total MU when delivering MERT plans. The commissioning data was therefore acquired for 2×2 cm² fields centered on the central axis and 2×2 cm² fields at the crossplane lateral limit of the FLEC. To later aid in tuning of the beam model, 8×8 cm² FLEC defined fields were also acquired as well as 9×9 cm² secondary-collimator defined fields with no applicator or FLEC in place. For each FLEC defined field, the secondary collimator was set to include a 5 mm margin beyond each of the four leaves which was shown to be the best compromise between sharp penumbra and secondary dose peaks in the peripheral region of the profiles due to scatter around the backside of the 3 cm FLEC jaw [14].

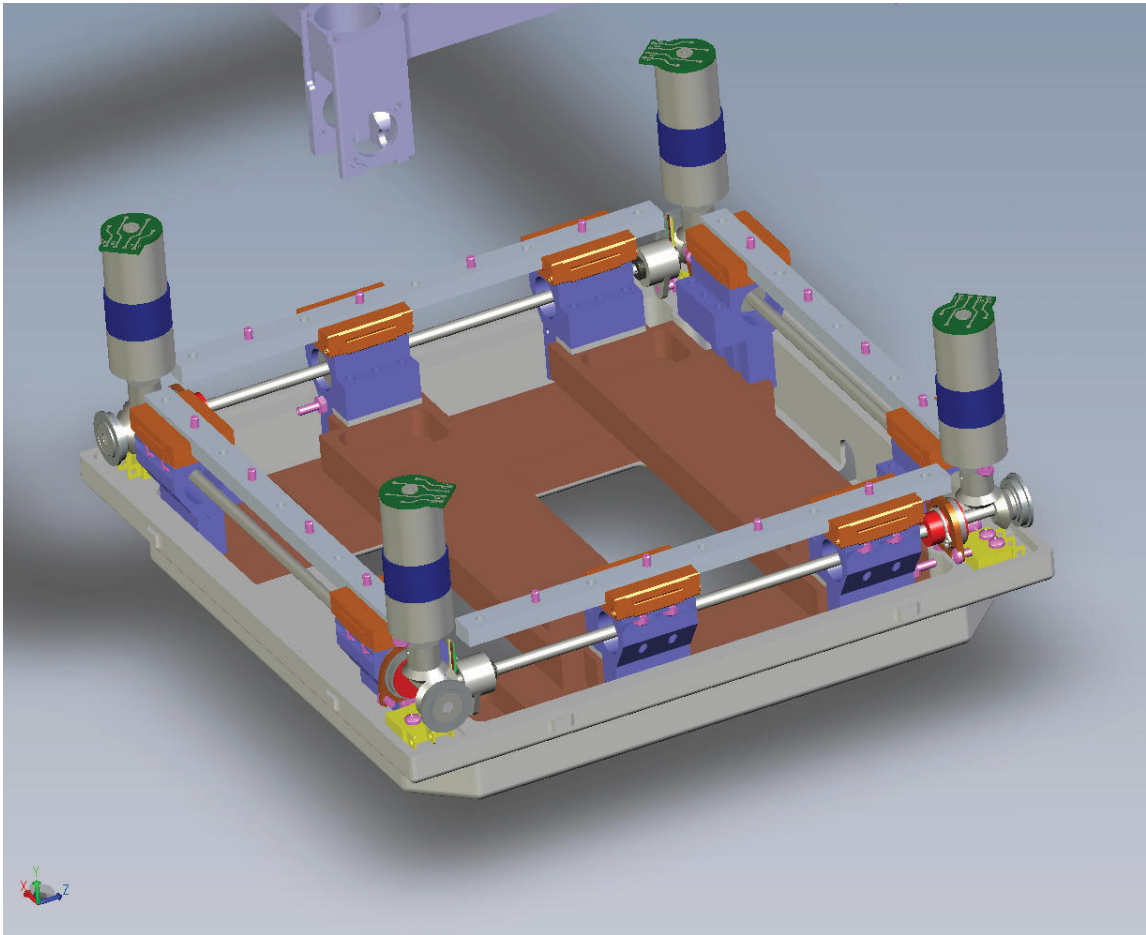


Figure 5–1: A schematic diagram of the Few Leaf Electron Collimator (FLEC) used in this study.

5.2.2 Monte Carlo Model Commissioning

A Monte Carlo model based on manufactures data was constructed within the BEAMnrc [20] user code. Each accelerator model was built as a shared library such that simulated particles could be passed directly as an input to

DOSXYZnrc [21] without the need to store particles in a phasespace. A rectangular water phantom was created with $4 \times 4 \times 3$ mm³ voxels in x, y and z respectively. A sufficient number of histories were simulated such that the uncertainty was less than 1% at the depth of maximum dose. ECUT (the energy cut-off for electron transport) was set to 700 keV and 521 keV for the BEAMnrc and DOSXYZnrc simulation respectively. PCUT (the energy cutoff for photon transport) was set at 10 keV for both simulations. Below these energy limits the kinetic energy of the particle is considered to be absorbed on the spot. The BCA (Boundary Crossing Algorithm) was set to EXACT (within 3 mean free paths of a boundary, multiple scattering is switched off and the transport across the boundary is performed using single elastic scattering) in the BEAMnrc simulation and PRESTA-1 (the electron is not allowed to take steps longer than the perpendicular distance to the closest boundary unless the perpendicular distance is less than a user defined min step length) in the DOSXYZnrc simulation. The simulated profiles and PDDs were extracted from the 3ddose files using MATLAB (Mathworks, Natick MA) and plotted against the clinical data using the same software.

Source Parameters and Upper Head Modeling

Commissioning of the beam model was conducted using an iterative approach that initially focused on as few components in the beamline as possible. This allowed for verification of the model with few degrees of freedom at any one time. Through removal of the scattering foil component module (CM), applicator CM and the FLEC CM, the electron pencil beam passes through the head of the accelerator with the only major scatter interactions taking place in the beryllium

exit window and the linac transmission ionization chamber. This allowed for verification and tuning of these CMs independent of the other components so that once confidence was obtained in their parameters, they could be later eliminated as possible sources of discrepancy between simulated and measured data as the additional CMs were added. A secondary collimator setting of $9 \times 9 \text{ cm}^2$ was chosen as it represented the maximum jaw setting that was used due to the limited field size of $8 \times 8 \text{ cm}^2$ of the FLEC. Profiles and PDDs were matched by varying source parameters such as the FWHM of the Gaussian source, mean angular spread (MAS), beam energy, the thickness of the beryllium exit window and the thickness of the ionization chamber. In this work, it was assumed that the beam angle was always normal relative to the exit window. Previous investigations undertook a sensitivity analysis of incident beam angle [22] and found that dose profiles were relatively sensitive to this parameter with a 0.9 degree change in incident beam angle resulting in between a 5.3 and 10.3 percent change in the slope of the electron dose region. However, upon acquiring beam data on the accelerator, profiles were seen to be quite symmetric, allowing the assumptions that that beam could be modeled as normally incident and with no lateral shift with respect to the secondary foil. The beam energy was chosen based upon agreement of the R_{50} value between measured and simulated data. Once satisfactory agreement was achieved, the scattering foil was included in the model and thicknesses were modified from the manufacturer's specifications as necessary.

Applicator and FLEC Modeling

Once the chosen model parameters of the upper section of the accelerator head produced good agreement with measured data, the applicator and FLEC components were added to the model. Performance of the model was qualified against $8 \times 8 \text{ cm}^2$ and $2 \times 2 \text{ cm}^2$ on-axis FLEC defined fields as well as $2 \times 2 \text{ cm}^2$ fields at the lateral crossplane limit (field centered at $\pm 3 \text{ cm}$ from axis) of the FLEC. Improvements to the FLEC model used in previous work [14] were made. These modifications consisted of adding additional components of the FLEC frame to the model in an effort to more accurately model the scatter contribution from the frame and the peripheral components. The FLEC defined fields were verified with both the scattering foil removed and in place as well as for all available electron energies in the accelerator used in the previous section.

5.2.3 Inverse Treatment Planning Study

Previous authors [23] have reported on the development of an in-house Monte Carlo based treatment planning system (McGill Monte Carlo Treatment Planning) with inverse treatment planning capabilities. This software was used to conduct a direct comparison between two MERT plans, one with the scattering foil present and one without. The finalized beam models described in section 5.2.2 were used in the planning system for dose calculation. The planning software automates the planning process by generating a large dataset of beamlets with variations in beamlet energy and position. Each plan utilized the same $30 \times 30 \times 24 \text{ cm}^3$ Solid Water $\text{\textcircled{R}}$ phantom that was imported into the system after being scanned with a CT scanner. One irregular shaped PTV as well as two organs at risk (OAR) of

different geometries and depths beyond the PTV were contoured. A central slice of the phantom showing the PTV and OAR regions can be seen in Figure 5–7(a). These contours were then used to set constraints in the inverse planning process built into the treatment planning system.

The planning optimizer generated a total of 245 possible fields of $2 \times 2 \text{ cm}^2$ for each plan. Seven beam positions in both x and y were sufficient to cover the maximum lateral limits of $\pm 4 \text{ cm}$ of the collimator. This allowed feathering (partial overlap) of each beam by 1 cm which contributed to better target coverage and OAR sparing compared to when no feathering is used. Each FLEC aperture position was also calculated for each of the 5 available energies. Precalculation of each dose distribution was conducted on a 66 core cluster and took approximately 4 days and 14 days for the plan without and with the scattering foil respectively. Simulations were run until the dose uncertainty in voxels with a dose greater than 50% of the maximum dose was less than 1.5%. The weight of each beam was then adjusted using an inverse planning algorithm that utilized a cost function based on constraints of tumor coverage and OAR sparing. Each of the two plans was independently optimized to produce the best OAR sparing for a given PTV homogeneity and coverage. The software was then used to generate full dose distributions and DVHs of the structures contoured in the phantom.

5.3 Results and Discussion

5.3.1 Characterization of Scattering Foil-Free Beams

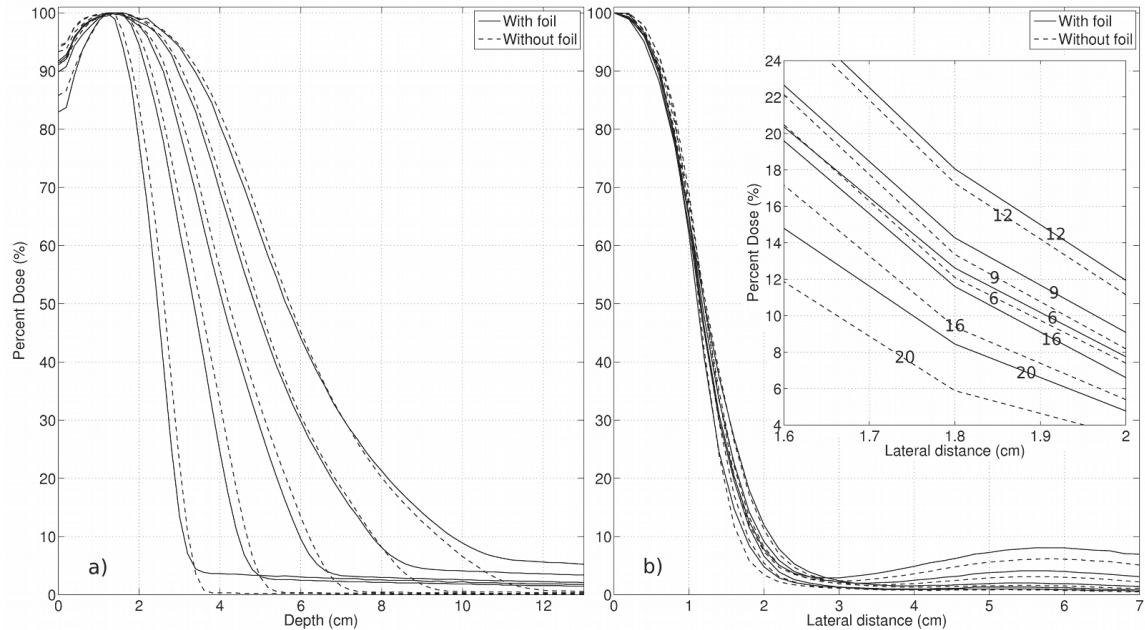


Figure 5–2: PDDs (a) and profiles (b) for 6, 9, 12, 16 and 20 MeV with (solid) and without (dashed) the scattering foil. In the profiles of (b), the secondary dose peak in the 4 to 7 cm region due to scatter of electrons over the back edge of the collimator jaw can be seen.

The measured percent depth dose curves and profiles for the various energies at field sizes of $2 \times 2 \text{ cm}^2$ can be seen in 5–2(a). Of note is the slight increase in the depth of penetration of the PDDs with the scattering foil removed. With the scattering foil absent, the beam will experience less energy degradation as it travels through the head of the accelerator and will have a higher mean energy upon reaching the surface of the phantom. Also of note is the relatively high dose in the bremsstrahlung tail region with scattering foil present. The dose in the tail

region typically represents less than 4% at 20 MeV with standard field sizes (10x10 cm²) and dual scattering foils [17], however, when the field sizes are reduced, the dose in the tail region is seen to increase (up to 5.7% in the case of a 2x2 cm² field at 20 MeV) as bremsstrahlung photons created in the head of the accelerator contribute more to the dose in water relative to the primary electron dose. This increase is attributed to the reduction in electron fluence at the isocenter per monitor unit (MU) due to the narrow secondary collimator aperture (3x3 cm² field size projected at isocenter) that blocks many of the primary electrons that otherwise would have contributed to the dose in water along the central axis. However, the bremsstrahlung component from the scattering foil and the other components in the head incur only a minimal field size dependence similar to the relative dose factor in photon beams. As expected, for relatively high-energy beams, the bremsstrahlung dose decreases as the energy is reduced, however, it is seen that the dose increases again for 6 MeV. This increase is attributed to the fact that the accelerator efficiency drops off for smaller field sizes and a low dose at isocenter per MU is observed. The underlying inefficiency is a result of the higher mass angular scattering power of the lower energy electrons that contributes to a large fraction of the primary electron fluence being scattered mainly into the up-stream surface of the secondary collimator. This in turn results in a reduction in the fluence of electrons reaching the isocenter per MU that is more pronounced for lower energies. The most important distinction is the great reduction of dose in the bremsstrahlung tail region of the PDDs with the scattering foil removed (dashed lines). Dose reductions in the tail region just beyond the practical range

were calculated to be 12.2, 6.9, 7.4, 7.4 and 8.3 times less with the foil removed from the beamline for 6, 9, 12, 16, and 20 MeV respectively for 2x2 cm² defined on-axis fields. As discussed in section 5.2.1, there exists a small over response of the dose in the tail region on the order of 0.5-1.0%, however, the magnitude is sufficiently small that it does not significantly affect the dose reductions reported. Crossplane profiles of the 2x2 cm² fields taken at d_{\max} for each energy can be seen in Figure 5-2(b). Within the central portion of the beam, all profiles show a similar shape with the higher energy beams giving a sharper penumbra due to less lateral scatter of the primary electrons. The penumbra is seen to be sharper with the scattering foil removed due to the absence of bremsstrahlung photons produced in the scattering foil and their subsequent transmission through the FLEC jaws. Due to design limitations, the FLEC jaws were chosen to be 3 cm wide; this results in a small fraction of scattered primary electrons spilling over the back edge of the jaw and contributing to dose outside the field. This electron spillage can be seen in the peripheral region of the profiles and is worse for lower energies due to their greater scattering potential. The effect is reduced when the scattering foil is removed as the beam takes on a more forward peaked Gaussian shape therefore reducing the electron fluence behind the jaws.

5.3.2 Monte Carlo Beam Matching

Modeling of the Upper Accelerator Head

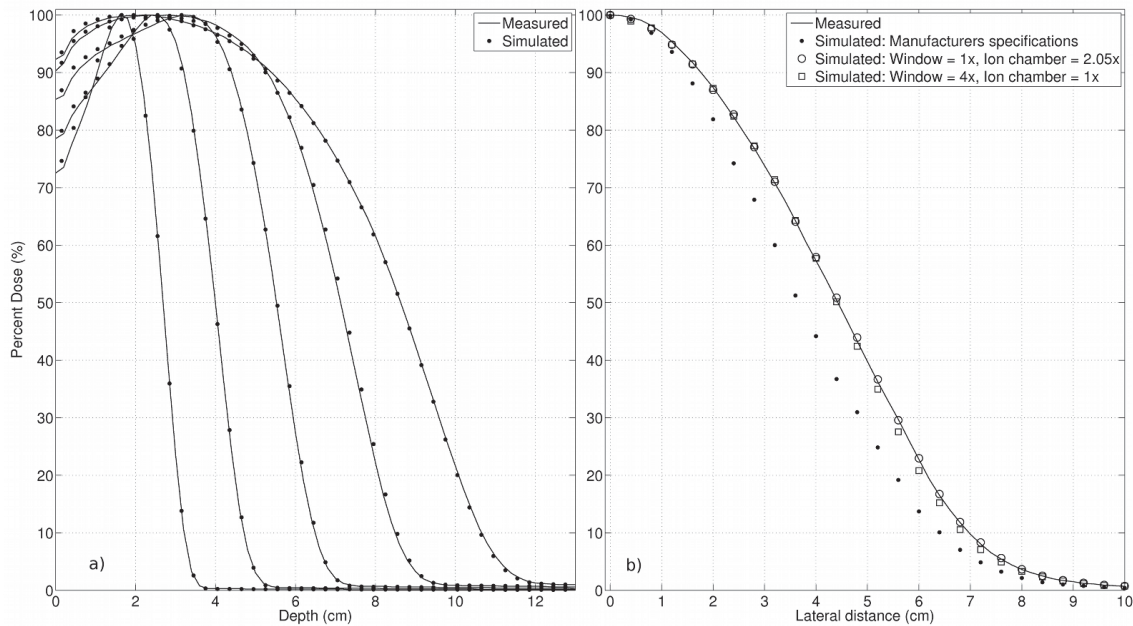


Figure 5-3: PDDs without the scattering foil, applicator or FLEC showing agreement between simulated and measured data for electron energies of 6, 9, 12, 16 and 20 MeV. (b) 9x9 cm² profiles in the crossplane direction for 16 MeV again without the scattering foil, applicator or FLEC. Simulated results are plotted against measured data (solid line) for different thickness of the beryllium exit window and ionization chamber.

Measured and simulated PDDs for the 9x9 cm² field with the scattering foil removed can be seen in Figure 5-3(a). Initially, modeled results produced poor agreement for both the profiles and PDDs. The initial mismatch in the profiles is illustrated in Figure 5-3(b) for the 16 MeV case where the ionization chamber

and the beryllium exit window were modeled as per the manufacturer's specifications. It was observed from the profiles that simulated results based on these specifications gave a smaller FWHM in the profile compared to the measured data indicating that the modeled beam was not sufficiently scattered by components in the head or the chosen source parameters were incorrect. A sensitivity analysis was carried out for the source FWHM, mean angular spread (MAS) and beam energy including monoenergetic and spectral energy distributions. It was found that the profile shape was relatively insensitive to source FWHM which is consistent with reported findings [22]. The FWHM was not varied in subsequent simulations and its value was chosen to be 0.2 cm based on previously reported values [24] on a similar accelerator. An increase of the MAS produced minor shift of the depth of maximum dose to shallower depths for 16 MeV and 20 MeV, however it had little effect at the lower energies due to the relatively high mass angular scattering power at lower energies. Higher MAS values showed a broadening of the 16 and 20 MeV profiles in the central region, but again had little effect on lower energy profiles. It was determined that a MAS of 0 degrees produced sufficient agreement for all energies. No combination of source parameters (including spectral distributions and point sources) was found to produce acceptable agreement with measured data and it was necessary to investigate changes in material thickness in the beryllium exit window and ionization chamber. As the thickness of any component was increased, a subsequent increase in the monoenergetic electron source energy was made to maintain the correct R_{50} value. Increases to the thickness of either the exit window or the ionization chamber produced the following observations: (i) an

increase in thickness of the exit window vs. the ionization chamber contributed to a relatively greater broadening of the central region of the profile relative to the peripheral regions and (ii) an increase in the thickness of the ionization chamber vs. the exit window contributed to a relatively greater broadening of the peripheral regions relative to the central regions. The effects of (i) and (ii) are attributed to the geometry and positions of the two CMs along the z axis relative to the secondary collimator which was set to $9 \times 9 \text{ cm}^2$ at isocenter. As the exit window is located 5.2 cm above the ionization chamber, a pencil beam scattered at the window will result in a narrower profile at isocenter after collimation relative to a pencil beam scattered at the lower location of the ionization chamber. Using this fact, it was possible to isolate which component required an increase in thickness by examining the match of the profiles in the central and peripheral regions. Final agreement of within 1.5 percent and 1.5 mm was obtained for depths shallower than 2 cm in the PDDs and 1 percent and 1 mm at greater depths. Agreement of 1 percent and 1 mm was achieved for all profiles except the 6 MeV profile which matched to within 1.5 percent and 1.5 mm.

This method of beam tuning allows accurate determination of component geometry and is preferred over removal of the ionization chamber (as performed in some studies [25] in a clinically operational accelerator due to the time consuming process involved in its removal, replacement and dosimetric checks. The result of varying the thickness of the two components is demonstrated in Figure 5-3(b). The thickness of both the exit window and the ionization chamber were individually increased until the best agreement with the measured profile was

obtained. An exit window thickness of four times what was specified by the manufacturer gave good agreement in the central region of the profile, however, a dose underestimate existed in the peripheral region. An increase in the thickness of the ionization chamber by a factor of 2.05 produced good agreement at all positions along the profile. It was determined from this result that no increase to the exit window in the final model was necessary while the increase in the thickness of the ionization chamber by a factor of 2.05 was used. This necessary increase can be attributed to the presence of the electrodes within the ionization chamber that are intentionally left out of the provided manufacturer’s Monte Carlo package. Further study into the exact structure of the ionization chamber for modeling purposes is a potential avenue for further research and should likely be undertaken for any clinical implementation of scattering foil free or minimal foil MERT. A summary of the final source parameters and changes to thickness of the CM in the upper head can be seen in Table 5–1.

Table 5–1: Accelerator head parameters determined through comparison to measured data.

Parameter	Nominal beam energy (MeV)				
	6	9	12	16	20
Monoenergetic source energy (MeV)	7.2	10.2	13.8	17.9	22.5
Change in upper scattering foil thickness	-15%	-15%	0%	-22.50%	-10%
Source FWHM	Set to 0.2 cm				
Source mean angular spread	Set to 0 degrees				
Change in Be window thickness	No change from manufactures specifications				
Ion Chamber	Increased in thickness by a factor of 2.05 from the manufacturers specifications				

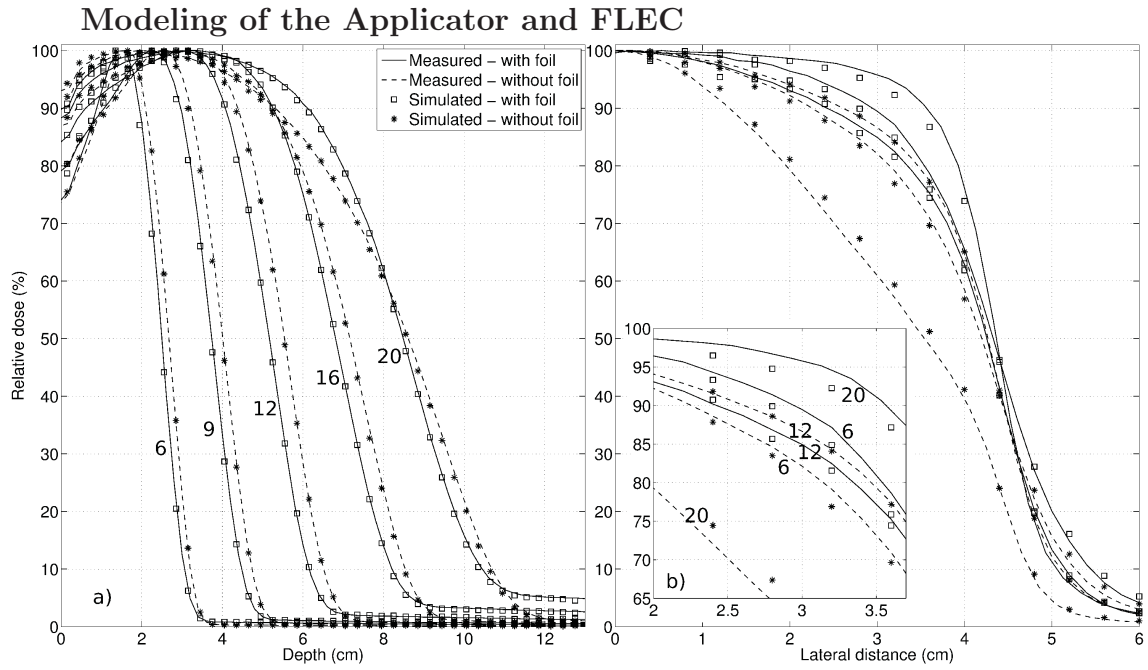


Figure 5-4: (a) PDDs of an 8x8 cm² FLEC defined field for 6, 9, 12, 16 and 20 MeV showing measured and simulated results for both the clinical beamline and the experimental beamline. (b) Profiles under the same conditions are shown for 6, 12 and 20 MeV.

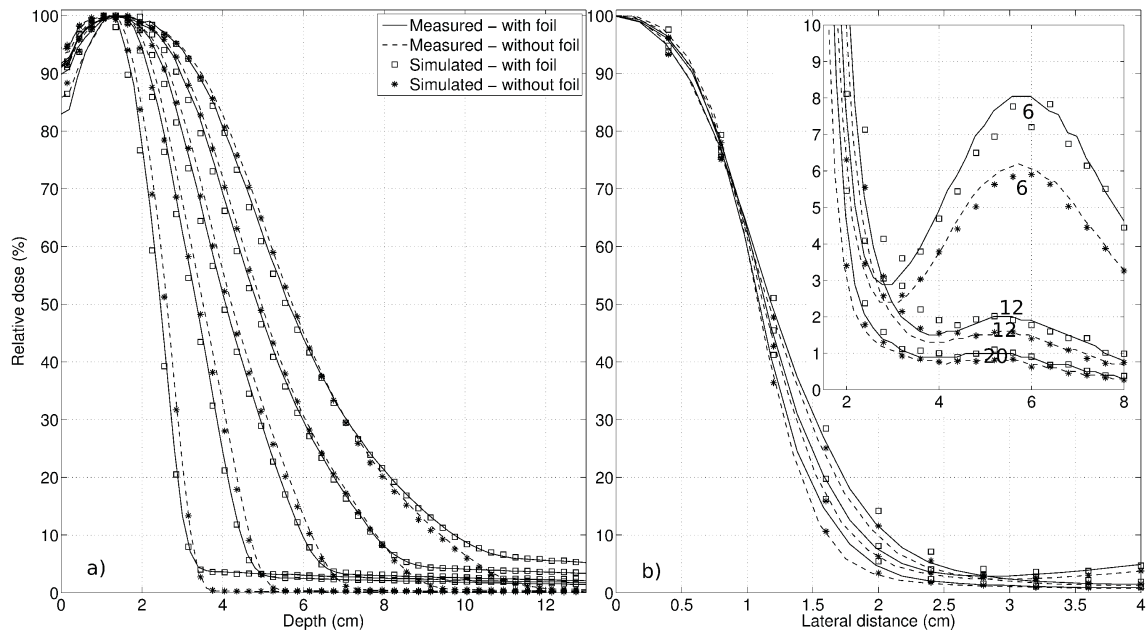


Figure 5-5: (a) PDDs of a 2x2 cm² on-axis FLEC defined field for 6, 9, 12, 16 and 20 MeV showing measured and simulated results for both the clinical beamline and the experimental beamline. (b) Profiles under the same conditions are shown for 6, 12 and 20 MeV.

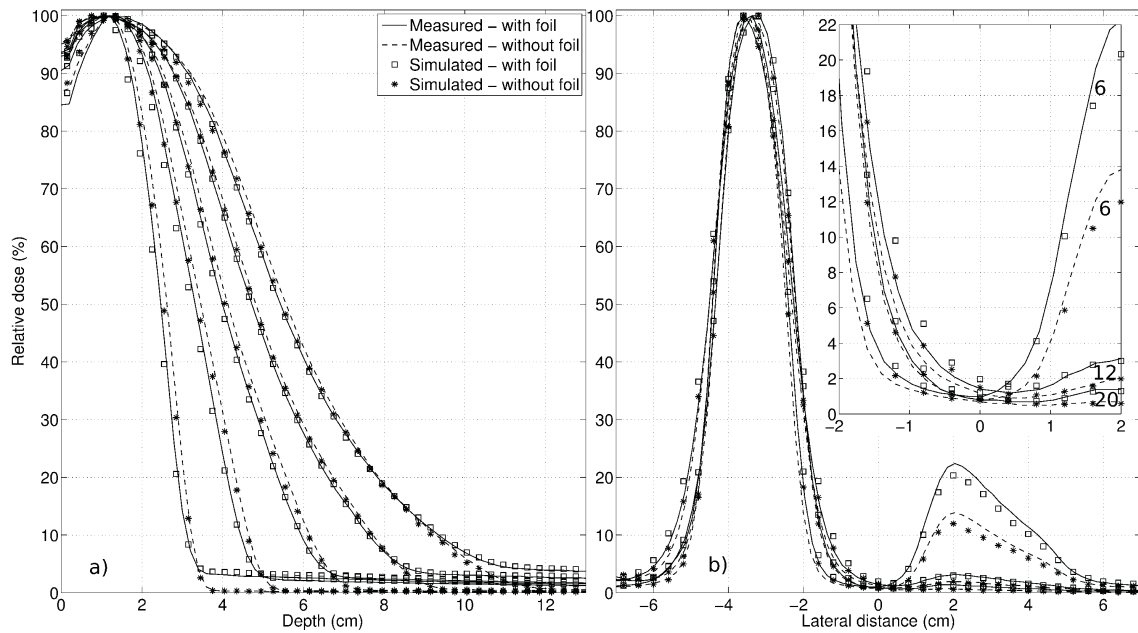


Figure 5-6: (a) PDDs of a 2x2 cm² off-axis FLEC defined field for 6, 9, 12, 16 and 20 MeV showing measured and simulated results for both the clinical beamline and the experimental beamline. (b) Profiles under the same conditions are shown for 6, 12 and 20 MeV.

Measured PDDs and profiles for different field sizes of 8x8 cm², 2x2 cm² on-axis, and 2x2 cm² off-axis at the crossplane lateral limit of the FLEC are shown in Figures 5-4 through Figures 5-6 respectively for both simulated and measured data. In Figure 5-4, the PDDs (a) and profiles (b) for the 8x8 cm² fields are shown. Good agreement of 1% and 1 mm between simulated and measured data was achieved in all cases except for the 20 and 16 MeV profiles where differences up to 2% and 2 mm in the +/- 2-4 cm region of the profile were seen. It is hypothesized that these discrepancies are caused by complex features (such as the drive screws, motors, encoders etc.) present in the frame of the FLEC that

were not sufficiently represented in the beam model therefore causing the scatter conditions to be slightly different between modeled and measured data for certain field sizes. The 2x2 cm² on-axis field PDDs (a) and profiles (b) are represented in Figure 5-4. PDDs matched to within 1.2% and 1 mm for all energies except 6 and 9 MeV which matched to within 2% and 1.5 mm and all profiles matched to within 1.5% and 1.6 mm. The increase in dose beyond 3 cm in the profiles is due to the limited width of the FLEC jaw that allows scattered electrons to pass behind the back edge of the 3 cm wide jaw and deposit dose in the phantom. This artifact is addressed in previous work [14] and will not be discussed in detail here, however, it is observed that the removal of the scattering foil has the effect of minimizing the dose contribution in this region by between 2 percent for the lowest energy and 1 percent for the highest energy. Tuning of the scattering foil thickness was done with the field size set to 2x2 cm² due to the greater sensitivity of the bremsstrahlung dose to foil thickness when compared to larger fields. This greater sensitivity can be explained by the fact that the bremsstrahlung dose is generally higher for smaller fields, as demonstrated in the PDDs of Figure 5-4 (a) and Figure 5-5 (a). Changes to the foil thickness were made for the upper foil only as the upper foil is approximately an order of magnitude thinner than the lower foil and due to machining tolerances, it is expected that the variability in the ratios of the actual thickness to the specified thickness will be greater. The changes to the upper foil thickness are summarized in 5-1. Figure 5-6 shows PDDs (a) and profiles (b) for the case where the 2x2 cm² field was shifted in the crossplane direction to the lateral limit of the FLEC. It can be seen in the profiles that there

is a large fraction of dose (up to 20 percent for 6 MeV) deposited behind the positive X-jaw. This fraction is reduced with the scattering foil removed, however, it still represents a large fraction of dose that may not be clinically acceptable. Possible solutions include modifications to the FLEC device to include out of field shielding, reconsidering the position of the secondary collimator for off-axis fields or by removing the 6 MeV beam, the energy for which the effect is greatest, from the set of energies used in the plan optimization. It can be noted that there is a small lateral shift of the high dose region of the profiles on the order of a couple mm due to the fact that the profiles were acquired at the depth of dose maximum which corresponded to 3.0, 3.0, 3.0, 2.1 and 1.4 cm, for 20, 16, 12, 9 and 6 MeV beams respectively. PDDs matched to within 1.5% and 2mm with the largest discrepancies appearing in the build-up region for low energies and in the high dose region beyond d_{\max} for the 20 MeV beam. The profiles had a 1.5% and 2 mm agreement in the main field, however, showed a 2.2% discrepancy in the region behind the positive x jaw.

5.3.3 Inverse Treatment Planning Study

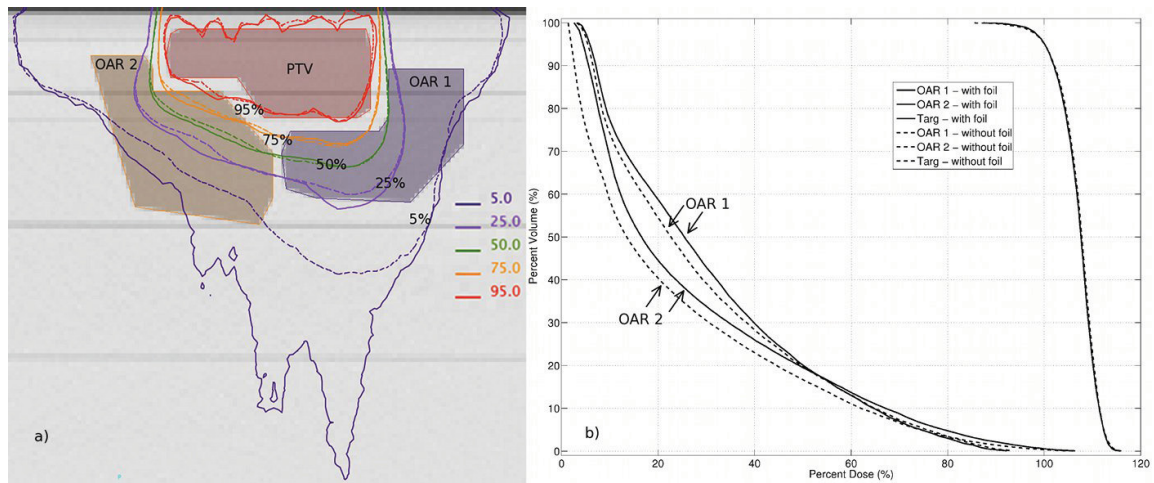


Figure 5-7: (a) Isodose lines from planned treatments using the clinical beamline (solid) and the experimental beamline (dashed). Also visible is the target (red) and the two organs at risk (orange and blue). (b) A DVH comparison of the same plan as in (a).

A central slice of the test phantom with contoured PTV and organs at risk can be seen in 5-7 (a) along with the optimized results of the MERT treatment plan with the foil present (solid lines) and removed (dashed lines). For plans with similar PTV coverage, the high dose isodose lines covering the organs at risk show a smaller area of coverage in the case where the scattering foil was removed. This reduction in dose to healthy tissue is particularly evident when comparing the areas enclosed by the 5 percent dose isodose lines. 5-7 (b) shows the cumulative DVH of the scattering foil free beamline (dashed lines) and the beamline with the foil (solid lines). It can be seen that for quasi-identical target coverage, the removal of the scattering foil was able to produce plans with improved OAR

sparing, particularly for lower doses. The moderate reduction in volume receiving a low-dose bath due to removal of the scattering foil confirms the hypothesis and shows potential for future adaptation in any commercial implementations of MERT.

5.3.4 Dosimetric considerations from scattering foil removal

It was observed that after removal of the scattering foil, the dose per MU was greatly increased. For 2x2 cm² fields on the central axis, the dose per MU was 16, 15, 18, 31 and 36 times higher for the 6, 9, 12, 16 and 20 MeV beams respectively with the scattering foil removed. This increase in dose rate would lead to less beam-on time which would result in shorter treatment times when compared to treatments using the clinical beamline. Due to the shape of the unscattered pencil beam, the fluence will decrease as a function of lateral distance off central axis. This decrease will serve to detract from the gains in fluence obtained by removal of the scattering foil, however, as seen in the profiles of 5-3(b) with no applicator or FLEC, the decrease in fluence for the 16 MeV beam at the jaw limit of the FLEC (± 4 cm) is only a factor of 2.3 less than the central axis value and a factor of 1.3 less for the 6 MeV beam (this despite the secondary collimator defining a field of 9x9 cm² at isocenter). It is concluded then that any reduction in dose per MU due to fields positioned at the exterior limits of the FLEC would be minimal compared to the great increase in dose per MU obtained by removing the scattering foil. However, should the currently used collimation device be modified to have greater limits on jaw position, or scattering foil free beamlines be used with other electron MLCs, care must be taken not to define fields at positions too far from the central

axis due to large reductions in particle fluence per MU. The dosimetric advantages of scattering foil free beams could potentially be preserved in electron MLCs with large maximum field sizes by designing a thin scattering foil with the intent of not flattening the beam, but scattering it sufficiently to produce the desired fluence at the limits of the collimation device.

Certain challenges may exist however in the dosimetry of unscattered beams due to a small lateral gap that exists between the two inner signal plate sections in the central region of the ionization chamber [26]. X-ray images of a similar ionization chamber from a decommissioned accelerator revealed a gap in the electrodes of approximately 1.5 mm. For comparison, simulations show the FWHM of the electron pencil beam at the upstream plane of the ionization chamber to be 2.4 and 4.3 mm for a 20 MeV and 6 MeV beam respectively. It is possible that small deflections of the beam due to variations in the bending magnet current or beam steering coils could produce problematic errors in the dosimetry of these beams. As the ionization chamber lies downstream of the scattering foil, it is possible that a new thin-foil design that achieves a compromise between scattering power and bremsstrahlung production may be required to overcome this issue and is a possible avenue for future work.

5.4 Conclusion

The potential benefit of using scattering foil free beams for delivery of modulated electron radiotherapy is investigated in this work. A beam model was tuned to match measured data with the scattering foil and applicator removed such that only the exit window, ionization chamber and secondary collimator were

in the beamline. Source parameters consistent with previously reported values were found to produce good agreement between measured and simulated data, however, an increase to the thickness of the accelerators ionization chamber away from the manufacturer's specifications to account for the internal electrodes was needed to produce this agreement. The applicator and FLEC were then added to the model and the parameters for these components were adjusted to match measured data. Scattering foil thickness were also modified beyond the specified manufacturer's data. Analysis of the PDDs showed a promising reduction of dose in the bremsstrahlung tail region by factors of 12.2, 6.9, 7.4, 7.4 and 8.3 times less with the foil removed from the beamline for 6, 9, 12, 16, and 20 MeV respectively for 2x2 cm² defined on-axis fields. The matched beam models were then imported into a Monte-Carlo-based inverse treatment planning system to allow comparison of a beamline with the scattering foil in place and one with the scattering foil removed. Analysis of the DVHs showed reductions to the volume of the OARs receiving a given dose in the plan with the experimental beamline compared to the clinical beamline. By removing the scattering foil, it was found that the component of bremsstrahlung photons produced within the head of the accelerator is significantly reduced thereby reducing the dose delivered to healthy tissue at the distal edge of the target while maintaining similar target coverage. By incorporating this methodology into future MERT deliveries, there exists the potential to further spare healthy tissue to reduce acute effects and long-term complications, thereby improving patient quality of life.

REFERENCES

- [1] F. C. du Plessis, A. Leal, S. Stathakis, W. Xiong, and C. M. Ma. Characterization of megavoltage electron beams delivered through a photon multi-leaf collimator (pmlc). *Physics in medicine and biology*, 51(8):2113–29, 2006. du Plessis, F C P Leal, A Stathakis, S Xiong, W Ma, C-M England Phys Med Biol. 2006 Apr 21;51(8):2113-29. Epub 2006 Apr 3.
- [2] Eric E Klein, Joseph Hanley, John Bayouth, Fang-Fang Yin, William Simon, Sean Dresser, Christopher Serago, Francisco Aguirre, Lijun Ma, and Bijan Arjomandy. Task group 142 report: quality assurance of medical accelerators. *Medical physics*, 36:4197, 2009.
- [3] L. Jin, C. M. Ma, J. Fan, A. Eldib, R. A. Price, L. Chen, L. Wang, Z. Chi, Q. Xu, M. Sherif, and J. S. Li. Dosimetric verification of modulated electron radiotherapy delivered using a photon multileaf collimator for intact breasts. *Physics in medicine and biology*, 53(21):6009–25, 2008. Jin, L Ma, C-M Fan, J Eldib, A Price, R A Chen, L Wang, L Chi, Z Xu, Q Sherif, M Li, J S England Phys Med Biol. 2008 Nov 7;53(21):6009-25. Epub 2008 Oct 3.
- [4] M. G. Karlsson, M. Karlsson, and C. M. Ma. Treatment head design for multileaf collimated high-energy electrons. *Medical physics*, 26(10):2161–7, 1999. Karlsson, M G Karlsson, M Ma, C M Med Phys. 1999 Oct;26(10):2161-7.
- [5] J. Mihaljevic, M. Soukup, O. Dohm, and M. Alber. Monte carlo simulation of small electron fields collimated by the integrated photon mlc. *Physics in medicine and biology*, 56(3):829–43, 2011. Mihaljevic, Josip Soukup, Martin Dohm, Oliver Alber, Markus England Phys Med Biol. 2011 Feb 7;56(3):829-43. Epub 2011 Jan 17.
- [6] C. M. Ma, T. Pawlicki, M. C. Lee, S. B. Jiang, J. S. Li, J. Deng, B. Yi, E. Mok, and A. L. Boyer. Energy- and intensity-modulated electron beams for radiotherapy. *Phys Med Biol*, 45(8):2293–311, 2000. Ma, C M Pawlicki, T Lee, M C Jiang, S B Li, J S Deng, J Yi, B Mok, E Boyer, A L CA78331/CA/NCI

NIH HHS/United States Comparative Study Research Support, Non-U.S. Gov't Research Support, U.S. Gov't, Non-P.H.S. Research Support, U.S. Gov't, P.H.S. England Physics in medicine and biology *Phys Med Biol*. 2000 Aug;45(8):2293-311.

- [7] M. C. Lee, S. B. Jiang, and C. M. Ma. Monte carlo and experimental investigations of multileaf collimated electron beams for modulated electron radiation therapy. *Med Phys*, 27(12):2708–18, 2000. Lee, M C Jiang, S B Ma, C M 5T32GM08294-11/GM/NIGMS NIH HHS/United States CA 78331/CA/NCI NIH HHS/United States Research Support, U.S. Gov't, Non-P.H.S. Research Support, U.S. Gov't, P.H.S. United States Medical physics *Med Phys*. 2000 Dec;27(12):2708-18.
- [8] T. Gauer, D. Albers, F. Cremers, R. Harmansa, R. Pellegrini, and R. Schmidt. Design of a computer-controlled multileaf collimator for advanced electron radiotherapy. *Physics in medicine and biology*, 51(23):5987–6003, 2006. Gauer, T Albers, D Cremers, F Harmansa, R Pellegrini, R Schmidt, R England *Phys Med Biol*. 2006 Dec 7;51(23):5987-6003. Epub 2006 Oct 30.
- [9] K. R. Hogstrom, R. A. Boyd, J. A. Antolak, M. M. Svatos, B. A. Faddegon, and J. G. Rosenman. Dosimetry of a prototype retractable emlc for fixed-beam electron therapy. *Medical physics*, 31(3):443–62, 2004. Hogstrom, Kenneth R Boyd, Robert A Antolak, John A Svatos, Michelle M Faddegon, Bruce A Rosenman, Julian G *Med Phys*. 2004 Mar;31(3):443-62.
- [10] J. Deng, M. C. Lee, and C. M. Ma. A monte carlo investigation of fluence profiles collimated by an electron specific mlc during beam delivery for modulated electron radiation therapy. *Med Phys*, 29(11):2472–83, 2002. Deng, Jun Lee, Michael C Ma, C M CA78331/CA/NCI NIH HHS/United States Evaluation Studies Research Support, U.S. Gov't, Non-P.H.S. Research Support, U.S. Gov't, P.H.S. Validation Studies United States Medical physics *Med Phys*. 2002 Nov;29(11):2472-83.
- [11] T. Vatanen, E. Traneus, A. Vaananen, and T. Lahtinen. The effect of electron collimator leaf shape on the build-up dose in narrow electron mlc fields. *Phys Med Biol*, 54(23):7211–26, 2009. Vatanen, T Traneus, E Vaananen, A Lahtinen, T Research Support, Non-U.S. Gov't England Physics in medicine and biology *Phys Med Biol*. 2009 Dec 7;54(23):7211-26. Epub 2009 Nov 17.

- [12] A. A. Eldib, M. I. ElGohary, J. Fan, L. Jin, J. Li, C. Ma, and N. A. Elsherbini. Dosimetric characteristics of an electron multileaf collimator for modulated electron radiation therapy. *Journal of applied clinical medical physics / American College of Medical Physics*, 11(2):2913, 2010. Eldib, Ahmed Abdel Rahman ElGohary, Mohamed I Fan, Jiajin Jin, Lihui Li, Jinsheng Ma, Charlie Elsherbini, Nader A J Appl Clin Med Phys. 2010 Apr 12;11(2):2913.
- [13] E. E. Klein, M. Vivic, C. M. Ma, D. A. Low, and R. E. Drzymala. Validation of calculations for electrons modulated with conventional photon multileaf collimators. *Physics in medicine and biology*, 53(5):1183–208, 2008. Klein, Eric E Vivic, Milos Ma, Chang-Ming Low, Daniel A Drzymala, Robert E England Phys Med Biol. 2008 Mar 7;53(5):1183-208. Epub 2008 Feb 11.
- [14] K. Al-Yahya, F. Verhaegen, and J. Seuntjens. Design and dosimetry of a few leaf electron collimator for energy modulated electron therapy. *Med Phys*, 34(12):4782–91, 2007. Al-Yahya, Khalid Verhaegen, Frank Seuntjens, Jan Research Support, Non-U.S. Gov't United States Medical physics Med Phys. 2007 Dec;34(12):4782-91.
- [15] C. M. Ma, M. Ding, J. S. Li, M. C. Lee, T. Pawlicki, and J. Deng. A comparative dosimetric study on tangential photon beams, intensity-modulated radiation therapy (imrt) and modulated electron radiotherapy (mert) for breast cancer treatment. *Phys Med Biol*, 48(7):909–24, 2003. Ma, C M Ding, M Li, J S Lee, M C Pawlicki, T Deng, J CA78331/CA/NCI NIH HHS/United States Comparative Study Evaluation Studies Research Support, U.S. Gov't, Non-P.H.S. Research Support, U.S. Gov't, P.H.S. Validation Studies England Physics in medicine and biology Phys Med Biol. 2003 Apr 7;48(7):909-24.
- [16] K. Al-Yahya, M. Schwartz, G. Shenouda, F. Verhaegen, C. Freeman, and J. Seuntjens. Energy modulated electron therapy using a few leaf electron collimator in combination with imrt and 3d-crt: Monte carlo-based planning and dosimetric evaluation. *Med Phys*, 32(9):2976–86, 2005. Al-Yahya, Khalid Schwartz, Matthew Shenouda, George Verhaegen, Frank Freeman, Carolyn Seuntjens, Jan Research Support, Non-U.S. Gov't United States Medical physics Med Phys. 2005 Sep;32(9):2976-86.
- [17] E. B. Podgorsak. *Radiation Oncology Physics: A Handbook for Teachers and Students*. IAEA, 2005.

- [18] B. A. Faddegon, J. Perl, and M. Asai. Monte carlo simulation of large electron fields. *Physics in medicine and biology*, 53(5):1497–510, 2008. Faddegon, Bruce A Perl, Joseph Asai, Makoto R01 CA104777-01A2/CA/NCI NIH HHS/ R01 CA104777-02/CA/NCI NIH HHS/ England Phys Med Biol. 2008 Mar 7;53(5):1497-510. Epub 2008 Feb 21.
- [19] A. Alexander, F. DeBlois, and J. Seuntjens. Toward automatic field selection and planning using monte carlo-based direct aperture optimization in modulated electron radiotherapy. *Phys Med Biol*, 55(16):4563–76, 2010. Alexander, Andrew DeBlois, Francois Seuntjens, Jan England Physics in medicine and biology Phys Med Biol. 2010 Aug 21;55(16):4563-76. Epub 2010 Jul 29.
- [20] D W O Rogers, B A Faddegon, G X Ding, C M Ma, J We, and T R Mackie. Beam: a monte carlo code to simulate radiotherapy treatment units. *Med. Phys.*, 22:503–24, 1995.
- [21] B Walters, I Kawrakow, and D W O Rogers. Dosxyz users manual. Report, National Research Council of Canada, 2009.
- [22] E. C. Schreiber and B. A. Faddegon. Sensitivity of large-field electron beams to variations in a monte carlo accelerator model. *Physics in medicine and biology*, 50(5):769–78, 2005. Schreiber, E C Faddegon, B A England Phys Med Biol. 2005 Mar 7;50(5):769-78. Epub 2005 Feb 17.
- [23] A. Alexander, F. DeBlois, G. Stroian, K. Al-Yahya, E. Heath, and J. Seuntjens. Mmctp: a radiotherapy research environment for monte carlo and patient-specific treatment planning. *Phys Med Biol*, 52(13):N297–308, 2007. Alexander, A Deblois, F Stroian, G Al-Yahya, K Heath, E Seuntjens, J Research Support, Non-U.S. Gov't England Physics in medicine and biology Phys Med Biol. 2007 Jul 7;52(13):N297-308. Epub 2007 Jun 6.
- [24] T. Connell and J. L. Robar. Low-z target optimization for spatial resolution improvement in megavoltage imaging. *Medical physics*, 37(1):124–31, 2010. Connell, Tanner Robar, James L Med Phys. 2010 Jan;37(1):124-31.
- [25] B. A. Faddegon, D. Sawkey, T. O’Shea, M. McEwen, and C. Ross. Treatment head disassembly to improve the accuracy of large electron field simulation. *Medical physics*, 36(10):4577–91, 2009. Faddegon, Bruce A Sawkey, Daren O’Shea, Tuathan McEwen, Malcolm Ross, Carl R01 CA104777/CA/NCI NIH HHS/ Med Phys. 2009 Oct;36(10):4577-91.

- [26] CJ Karzmark, CS Nunan, and E Tanabe. *Medical Electron Accelerators*. McGraw-Hill, 1992.

CHAPTER 6
**Design and validation of novel scattering foils for Modulated Electron
Radiation Therapy**

Tanner Connell and Jan Seuntjens

Phys. Med. Biol., Under review, 2012

Contents

6.1	Introduction	139
6.2	Materials and methods	141
6.2.1	Design of custom foils	141
6.2.2	Experimental validation of custom foils	141
6.3	Results and discussion	143
6.3.1	General design goals	143
6.3.2	Experimental validation of custom foils	148
6.4	Conclusion	151
6.5	Acknowledgments	154

Following the previous chapter on the feasibility of scattering foil free beam-lines for MERT applications was the question of the need for some minimal amount of scatter. The question arose from concern for the dosimetric stability of unscattered beams due to technical reasons surrounding the effectiveness of the transmission monitor chamber in narrow unscattered beams. Also, for higher

beam energies, the lack of scatter resulted in insufficient particle fluence beyond a certain distance from the central axis that would limit the maximum possible treatment area to an unacceptably small area. The following submitted manuscript introduces an investigation into the design and testing of custom scattering foils designed specifically for MERT applications with a generalized hypothetical electron collimator.

Abstract.

Modulated Electron Radiation Therapy continues to be an area of interest to various groups, however, the scattering foils used in beam flattening have not been optimized for this modality. In this work, the feasibility of novel scattering foils specifically designed for Modulated Electron Radiation Therapy is investigated using Monte Carlo methods. Different designs based on foil material, shape and thickness were analyzed. It was shown that low atomic number materials such as aluminum were optimal, while shaped foils such as those employed in current dual foil designs were not necessary. Aluminum foil thickness between 0.36 and 1.50 mm were capable of sufficiently broadening beams with energies between 12 and 20 MeV respectively, with beams of lower energies receiving sufficient scatter from the treatment head components and air scatter. Finally, custom foils were manufactured based upon previously simulated designs and were placed into the beamline of a Varian 2100 EX accelerator, and showed excellent agreement between the simulated and measured PDDs and profiles. Custom foils achieved higher dose rates on the central axis compared to the clinical foils by factors of 5.4, 4.9 and 4.5 for 12, 16 and 20 MeV respectively.

6.1 Introduction

Modulated Electron Radiation Therapy (MERT) remains an active area of interest for various groups, however, as of yet no commercial implementation has been attempted. MERT relies on energy and intensity modulation of the electron beam to conform the prescription dose to the distal edge of the tumor volume while maintaining dose homogeneity within the target volume resulting in greater healthy tissue sparing when compared to static single-energy fields.

Current scattering foil designs have changed very little in past decades. In order to achieve flat profiles, early designs of the 70s have relied on single foils that effectively broaden the multiple scattering distribution while at the same time incorporating box-type applicators of low-Z material to provide scatter off of the walls of these devices to fill in the dose off axis. However, these applicator types result in a very broad electron energy spectrum which leads to a higher surface dose, reduced depth of dose maximum and slower dose fall off [1]. In the late 70s, some investigators began experimenting with dual foil designs. Bjarngard *et al.* reported on the trial and error design of a secondary foil meant to shape the beam without the use of applicator scattering [1]. The same year, Kozlov and Shishov reported on a similar design and included a mathematical formulism to determine approximate parameters for the secondary foil [2]. Others showed the advantages of increasing the separation between the primary and secondary foils to at least a few cm, resulting in reduced bremsstrahlung and improved flatness characteristics [3]. Additionally, they used high-Z primary foils as a way of minimizing energy degradation of the primary beam. Grusell *et al.* presented a detailed theoretical

model to deduce the minimum total scatterer thickness as well as shape of the second scatterer for any given particle type, energy and field size [4].

Recently, the potential benefits of removing the scattering foil entirely from the beamline for MERT specific applications has been investigated [5]. It was shown that the main advantages of such a configuration is a much reduced bremsstrahlung dose due to the scattering foil being the main source of contamination photons in the head. Another advantage discussed was the greatly increased dose rate on the central axis, however, the dose rate would become unacceptably low at large distances off axis, in particular for higher energies.

It is clear that the current clinical foils, which were designed to produce flat beams for conventional electron therapy, are overdesigned for MERT applications as flat fields are not a requirement for this modality. As with flattening-filter free IMRT, non-uniformities in the dose profiles can easily be compensated for by adjustment of the beam weights within the inverse-optimization based treatment planning system, in any case, which is already an essential component of any MERT-based planning and delivery system. In this work, we investigate the feasibility of custom scattering foil designs that are optimized for MERT-specific applications that would incorporate a hypothetical electron MLC (eMLC) capable of defining a maximum field size of $20 \times 20 \text{ cm}^2$ at the isocenter. We then test these designs by manufacturing prototypes and comparing measured results with those expected from Monte Carlo simulation. Also discussed is possible stability and or beam steering issues arising from the use of the clinical transmission ionization chamber with minimally scattered beams.

6.2 Materials and methods

6.2.1 Design of custom foils

Various potential scattering foil designs were investigated using Monte Carlo methods. A previously commissioned accelerator model of a Varian (Varian Medical, Inc., Palo Alto, CA) 2100 EX series accelerator was used in all simulations without any variation to the simulation parameters [5]. Uncertainty in all voxels with a dose greater than 50% of the maximum dose was kept below 0.5%. The simulated water phantom consisted of $5 \times 5 \times 5 \text{ mm}^3$ voxels covering a volume of $30 \times 30 \times 20 \text{ cm}^3$ in x, y and z respectively. The simulated profiles and PDDs were extracted from the 3ddose files using MATLAB (Mathworks, Natick MA) and plotted against the clinical data using the same software.

Custom scattering foils were designed with three variables in mind, the (i) foil material, (ii) foil shape and (iii) foil thickness. Foil material was restricted to choices of aluminum and Tungsten which represent the low and high range of atomic numbers (Z). The foil shapes of interest included simple disk-shaped designs, and shaped foils (one or two stacked disks) similar to the shape of the clinical secondary scattering foils. Foil thickness for the different combinations was varied to achieve the best compromise between beam spread and minimal bremsstrahlung dose.

6.2.2 Experimental validation of custom foils

In order to hold the custom foils steady and at a known position in the beamline, a suitable holder was required. One fitting these criteria was borrowed from the Nova Scotia Cancer Center for the duration of this work. This holder

was previously used to hold low-Z targets in the beamline of a 2100 EX Varian accelerator [6] and was designed to get the target as close to the source as possible without risking collision as the carousel rotated. The Z position of the foils was therefore approximately at the level of the clinical primary scattering foil.

Manufacturing of three aluminum foils was done in-house by first machining multiple disks with a diameter of 50 mm and a thickness of 6.35 mm from 6061-T651 grade aluminum plate. To achieve the desired foil thickness, a manual milling machine was used to bore a hole in the central region of one side of the disk. As the electron pencil beam is still very narrow at the level of the primary foil, the diameter of this hole was only 15 mm. This allowed the surrounding area to provide mechanical stability to the relatively thin foil region and to allow mounting in the holder. The depth of the hole was calculated such that the remaining foil region was approximately 0.05 mm greater than the desired thickness and the remaining material was carefully removed from the upstream side (opposite of the bored side) of the disk through wet sanding with fine-grained sandpaper. Sanding continued until repeated measurements with a micrometer produced the desired thickness.

The holder and foil was placed into an empty port in the carousel and the carousel was then manually rotated to position the foil in the beamline. Water tank measurements were acquired with a Wellhofer WP700 water tank (IBA Dosimetry, Schwarzenbruck, Germany) and a Wellhofer unshielded p-type diode (model number F1421) as well as a PPC-40 parallel plate ion chamber (IBA Dosimetry, Schwarzenbruck, Germany). Diodes were used for both PDDs and

profiles, while the PPC-40 was used for PDDs only. Ionization signal from the PPC was converted to dose using Monte Carlo calculation of the stopping power ratios using the sprznrc user code [7]. All scans were conducted at an SSD of 100 cm and profiles were acquired at a depth of d_{\max} for the respective energy. No applicator was used to avoid interference of the scatter distribution produced in the accelerator head components, resulting in undisturbed profiles over a very large field size. For the three energies where custom foils were used (12, 16 and 20 MeV), the jaws were set to define a 22x22 cm² field at isocenter as this would represent a realistic jaw setting for an eMLC defining a 20x20 cm² field.

6.3 Results and discussion

6.3.1 General design goals

The choice of the minimum amount of beam broadening is somewhat of an arbitrary one. In this work, certain reasonable assumptions were made. Firstly, it has been reported that the clinical use of electron fields larger than 20x20 cm² is very rare [8], leading to the assumption that the foils need only be designed to sufficiently cover the area defined by this field size. Secondly, the choice of what constitutes sufficient electron fluence at the eMLC leaf ends (at the upstream edge) when fully retracted was chosen to be approximately 30% of the central axis fluence. This value was chosen for the following three reasons:

1. The fluence profile at the proximal surface of the eMLC, given this amount of beam scatter, is sufficiently flattened so that the optimizer should have little trouble in achieving a somewhat homogeneous dose distribution.

In a MERT planning study on scattering-foil-free beams, Connell *et al.*

showed that identical target coverage could be achieved when comparing a scattering-foil-free beamline to the conventional accelerator configuration for energies including 20 MeV, however, this study was done with a maximum collimator area of $8 \times 8 \text{ cm}^2$ (Connell et al., 2012). The ability to match the target coverage so closely was mostly due to the near identical shape of the $2 \times 2 \text{ cm}^2$ defined profiles with and without the scattering foil, despite the strong fluence gradients present at the proximal surface of the collimator with the foil removed.

2. An effort should be made to preserve a certain minimum dose rate for beamlets near the collimator limits as the total beam-on time could become highly concentrated in these beamlets, causing long treatment times for targets of large lateral extent. However, overall beam-on time is expected to be greatly reduced due to the large increases in dose rate along the central axis with the foil removed, which based on simulations, is expected to be approximately 6.2, 6.9, 9.9, 14.0 and 20.8 times greater for 6, 9, 12, 16 and 20 MeV when using the $10 \times 10 \text{ cm}^2$ standard applicator. Dose rate increases using the custom foils are discussed in section 6.3.1 Choice of foil thickness.
3. The chosen minimum amount of beam scatter coincided with the distribution of the 9 MeV beam with the scattering foil removed. Due to this inherent beam scatter from the exit window, monitor chamber and air scatter, custom foils would only be required for energies higher than 9 MeV and energies of 9 MeV and lower energies (if included as part of the MERT solution space) would be adequately served by a scattering foil free beamline.

Choice of foil material

The ideal scattering foil material for this application was evaluated for different materials of varying atomic number (Z). It has been discussed that the ideal primary scattering foil would consist of a high- Z material due to the fact that for a given amount of scatter, high- Z materials will result in less energy degradation of the electron beam [3]. This is indeed an important parameter in conventional foil design, where larger thicknesses of material are required to achieve flat beams, particularly for higher energies. For our case however, given the relaxed criteria in the desired amount of beam scattering, the small thickness of material required resulted in negligible primary electron energy loss, regardless of the material used. The choice of material was therefore dictated by other factors. Given the thin nature of the foils used (as thin as 0.36 mm of Al), machining tolerances (errors become a relatively large fraction of the foil thickness for very thin foils), ease of machining and mechanical stability became the reasons for choosing Al over higher- Z alternatives.

Choice of foil shape

As previously shown, shaped foils (one or more stacked disks mounted on a relatively thin base plate) are highly advantageous when trying to achieve flat electron profiles [2]. The lower amount of material placed into the path of the electron beam when using a shaped foil results in a much lower bremsstrahlung dose as well as less primary-particle energy loss when compared to a foil alone. Various combinations of 1 or 2 stacked aluminum disks of varying thickness and diameters were investigated, however, as with the choice of foil material

Table 6–1: The aluminum foil thicknesses required to achieve the desired amount of beam broadening given as a percentage of the CSDA range in that material and the thickness. Beam energies are stated, with the nominal accelerating potential shown in brackets.

CSDA (%)	20(22.5) MeV		16(17.9) MeV		12(13.8) MeV	
	g/cm ²	mm	g/cm ²	mm	g/cm ²	mm
100	11.605	42.983	9.650	35.739	7.759	28.737
1.25	-	-	-	-	0.097	0.359
2.25	-	-	0.217	0.804	-	-
3.50	0.406	1.504	-	-	-	-

in designing custom MERT specific foils, the very thin nature of these custom foils relative to standard clinical designs showed very little advantage of shaped foils over simple foils. It was observed that the bremsstrahlung production and primary-particle energy degradation of the shaped foils differed very little from the regular foils under investigation which means that the main advantage of using these shaped foils was not present for minimally scattered beams. Due to the fact that machining tolerances would again cause great difficulty in manufacturing such thin foils of non-trivial geometry, shaped foils were therefore eliminated as viable choices and simple foils were used for the remainder of this investigation.

Choice of foil thickness

The proper foil thickness required to achieve the desired amount of beam spread, as discussed in section 6.3.1, was determined by iteratively changing the thickness of a simple aluminum foil placed in close proximity to the location of the clinical primary foil and observing the resulting fluence profile. A summary of the thickness found to satisfy these criteria for the three beam energies are shown in Table 6–1.

Figure 6–1 shows the results of the simulated fluence profiles at the upper surface (92 cm SCD) of a hypothetical collimator (the edge of which, for a fully retracted state, is marked by the grey shaded region) for the three custom foils used in the 12, 16 and 20 MeV beamline. The three profiles for these custom foils are marked with lines accented with asterisks. Also included in the figure are the fluence profiles from the clinical beamline for all five energies in clinical use, as well as fluence profiles of each beamline with the foils removed. In Figure 6–2, the percent depth dose curves for all of the above beamline configurations are shown. From the main figure, it can be seen that the custom foils avoid much of the energy degradation present in the clinical foils. The custom foils had the effect of increasing the R_{80} value when compared to both the clinical and no-foil beamlines, except for the 12 MeV PDDs where the R_{80} value of the custom foil is nearly identical to the scattering-foil-free case. Looking at the figure insert, the relative fractions of bremsstrahlung dose can be compared for the various configurations. It is seen that the dose in the tails from the custom foils is only marginally worse when compared to the no-foil beamline. It was also estimated from the simulations that the increase in dose rate along the central axis would be increased by factors of 5.47, 4.91 and 4.54 for 12, 16 and 20 MeV respectively using custom foils. These parameters are summarized quantitatively in Table 6–2 for the various foil configurations. It is therefore concluded from the previously mentioned results that the proposed custom foils are able to sufficiently broaden the beam for the three higher energies, while simultaneously improving the shape

of the PDDs in the falloff region as well as keeping the amount of contamination photons produced in the foils to a level much lower than the clinical foils.

The performance of the transmission ionization chamber is also a concern when using minimally scattered beams. Typical ion chamber design involves two sets of collecting plates where each set contains 4 independent sectors. Two of these sectors lie away from the central axis and are responsible for displacement steering. If the incident electron beam was insufficiently scattered, it is possible that the signal at these peripheral plates could become low enough to impact the ability of the accelerator to actively correct for displacement errors in the beam. However, from previously reported experimental work with scattering foil beamlines no stability issues were encountered for any energy [5]. In Table 6–2, FWHM planar fluence values at the level of the ion chamber are shown for the custom foils as well as for the clinical foils and the foil-free beamline. It is therefore hypothesized that by using minimal scattering foils for the higher energies, the risk of encountering ionization chamber issues would be minimal, however, this remains a topic of future work.

6.3.2 Experimental validation of custom foils

Custom foils were manufactured based on the proposed thickness of aluminum shown in Table 6–1. With careful preparation of the foils, the measured thickness of the foils could be brought to within one thousandth of an inch (approximately 0.03 mm, which represented the finest gradation on our micrometer) of the desired value that was used in the simulations. The measured thickness are summarized in Table 6–3.

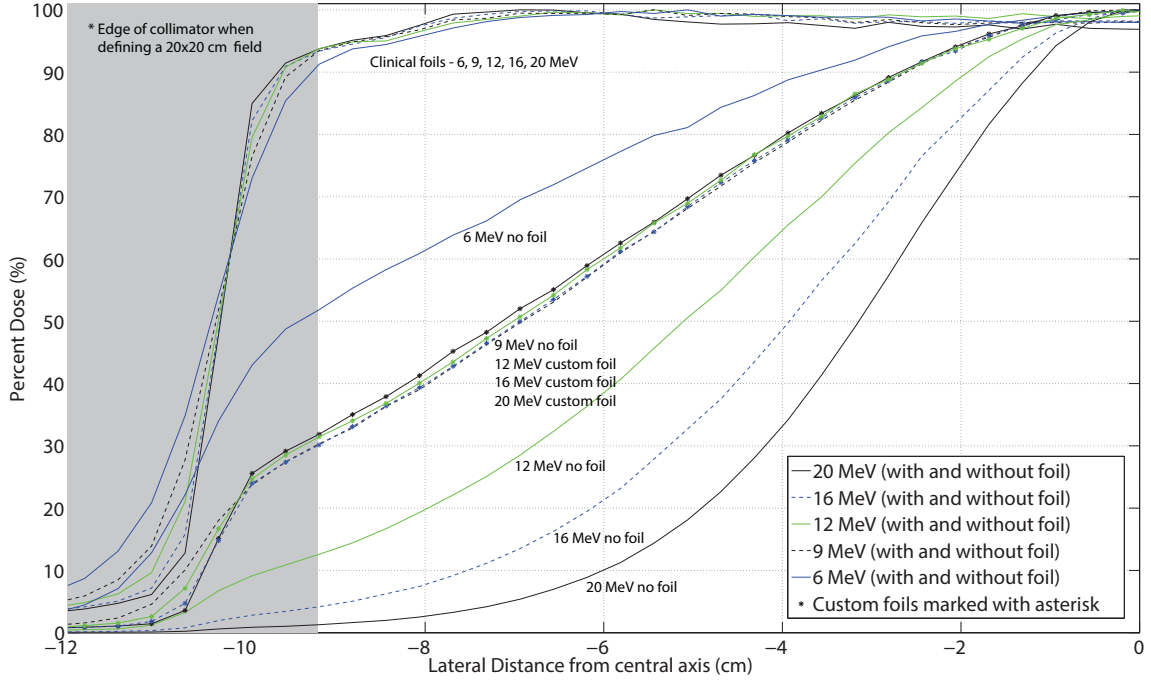


Figure 6–1: Electron fluence profiles taken at a SCD of 92 cm for 6, 9, 12, 16 and 20 MeV. Included in the figure are fluence profiles from the clinical scattering foils as well as profiles from a beamline with the foils removed (all shown as lines). The profiles simulated using custom designed foils for 12, 16 and 20 MeV are shown as lines marked with an asterisk. The grey shaded are represents the leaf edge of a hypothetical eMLC defining a 20x20 cm² field.

Table 6–2: A comparison of different parameters between the clinical, no scattering foil and custom foil beamlines.

Energy MeV	Factor of bremsstrahlung reduction under the clinical foil		Factor of dose rate increase on central axis over the clinical foil		Fluence FWHM at level of monitor chamber (cm)			R ₈₀ value		
	No foil	Custom foil	No foil	Custom foil	Clinical foil	No foil	Custom foil	Clinical foil	No foil	Custom foil
20	5.28	2.84	21.03	4.54	2.11	0.27	0.88	7.03	6.53	7.32
16	4.10	2.71	13.93	4.91	2.20	0.30	0.80	5.78	5.94	6.09
12	3.20	2.65	9.69	5.47	2.19	0.35	0.71	4.40	4.77	4.73
9	2.68	-	7.02	-	2.40	0.43	-	3.14	3.42	-
6	2.52	-	6.49	-	3.24	0.56	-	2.11	2.31	-

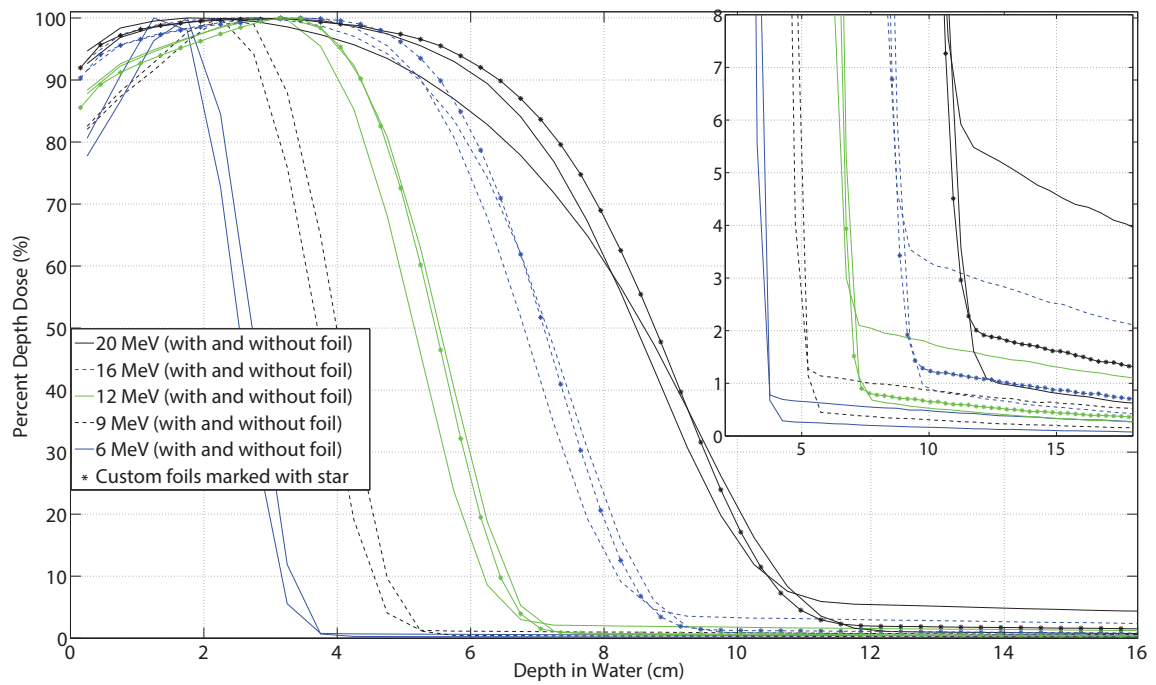


Figure 6–2: PDD curves for the all energies are shown with the clinical foils and without foils (plain lines). The custom foils are labeled as lines marked with an asterisk. The insert shows a zoomed in portion of the bremsstrahlung tail.

Table 6–3: A summary of the simulated and manufactured (as determined by measurements) foil thickness for 12, 16 and 20 MeV.

Beam energy (MeV)	Percent of CSDA range (%)	Simulated thickness (mm)	Measured thickness (mm)
20	3.50	1.504	1.50 ± 0.03
16	2.25	0.804	0.80 ± 0.03
12	1.25	0.359	0.36 ± 0.03

The comparisons between the simulated custom foils and their manufactured equivalents are shown in Figure 6–3 through Figure 6–5 for 20, 16 and 12 MeV respectively. The left panel of each figure shows the PDDs as measured by both the diode and the corrected parallel plate ionization chamber while the right panel shows the simulated and measured dose profiles at a depth of d_{\max} for that energy. From the excellent agreement seen for all cases, it can be concluded that production of custom thin scattering foils for MERT applications is entirely feasible. In addition to this being able to accurately match simulations to measurements is an important factor as having an accurate and robust beam model is critical in achieving accurate MERT plans due to the complexity involved when using many irregular and small shaped fields.

6.4 Conclusion

In this work we investigated the feasibility of creating custom scattering foils for modulated electron radiation therapy. Possible foil designs were evaluated on criteria such as foil material, shape and thickness. Based on assumptions of the maximum necessary field sizes required for possible future MERT implementations, recommendations on MERT-specific foil designs were made so that moderate beam broadening could be achieved without the need to produce a flat dose

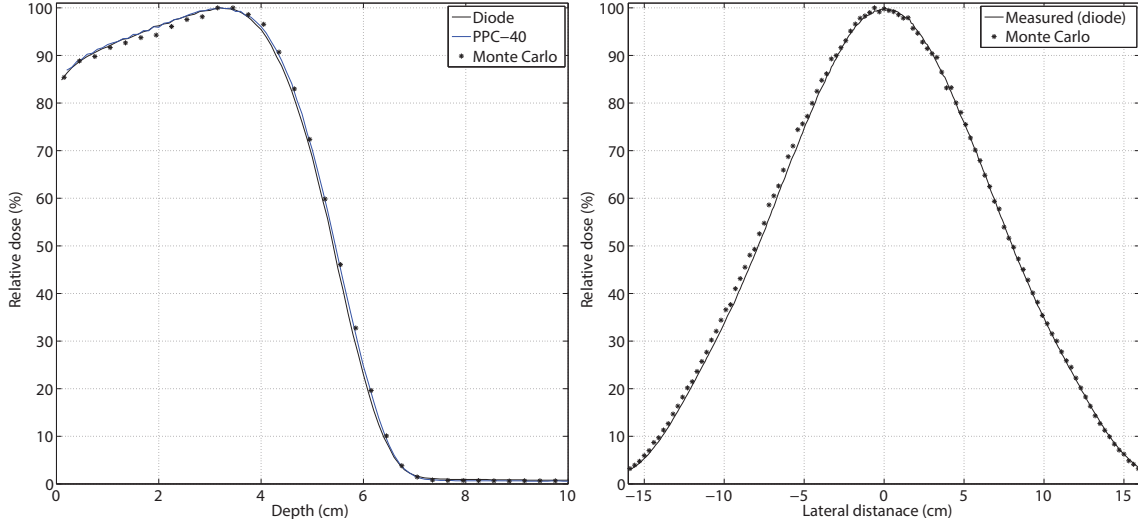


Figure 6-3: 12 MeV measured and simulated PDDs and profiles. On the left, the measured diode (black line) and PPC-40 (blue line) PDDs compared to the simulated values (asterisk). Shown right is the diode profile measurement (black line) compared to the simulated values (asterisk).

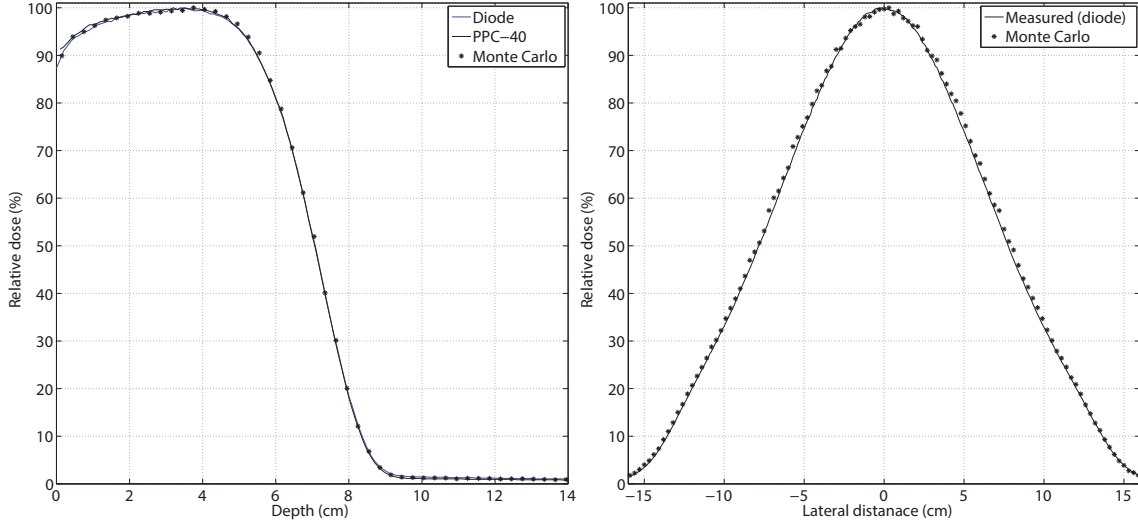


Figure 6-4: 16 MeV measured and simulated PDDs and profiles. On the left, the measured diode (black line) and PPC-40 (blue line) PDDs compared to the simulated values (asterisk). Shown right is the diode profile measurement (black line) compared to the simulated values (asterisk).

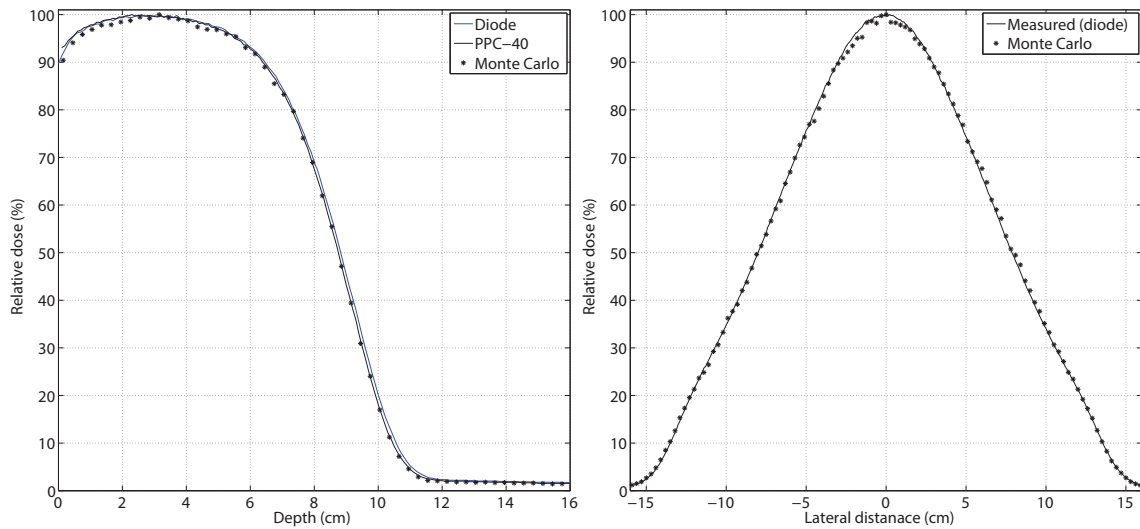


Figure 6–5: 20 MeV measured and simulated PDDs and profiles. On the left, the measured diode (black line) and PPC-40 (blue line) PDDs compared to the simulated values (asterisk). Shown right is the diode profile measurement (black line) compared to the simulated values (asterisk).

profile like those currently employed in traditional clinical electron therapy.

The determination of the optimal foil parameters included a simple, flat foil of lower atomic number material such as Al. Foil thickness would vary depending upon the energy used, however, foils were only determined to be necessary for energies greater or equal to 12 MeV with lower energies achieving sufficient scatter naturally through their propagation through the various components in the treatment head as well as air. Finally, custom foils were manufactured based upon previously simulated designs and were placed into the beamline of a 2100 EX accelerator. Measured and simulated PDDs and profiles showed excellent agreement and it was concluded that MERT specific custom foils were feasible for use in any future MERT implementations. This work showed that the clinical

foils in their current state are overdesigned in terms of their suitability for MERT applications. Custom foils for this purpose offer much reduced bremsstrahlung dose, less energy degradation and higher dose rates when compared to clinical foils. These advantages add to the potential benefits of MERT alone or in conjunction with other modalities, making it an ever more attractive option for physicians treating certain malignancies should it ever be offered as a commercial product.

6.5 Acknowledgments

We would like to thank the Nova Scotia Cancer Center for allowing the use of their target/scattering foil holder. This work was partially supported by grants from the Canadian Institutes of Health Research, CIHR MOP 102550 and Natural Sciences and Engineering Research Council Discovery grant # RGPIN 298191. Also, this work was partially supported by the Medical Physics Research Training Network, Natural Sciences and Engineering Research Council/Collaborative Research and Training Experience initiative no #432290.

REFERENCES

- [1] B. E. Bjarngard, R. W. Piontek, and G. K. Svensson. Electron scattering and collimation system for a 12-mev linear accelerator. *Med Phys*, 3(3):153–8, 1976. Bjarngard, B E Piontek, R W Svensson, G K eng Research Support, U.S. Gov't, P.H.S. 1976/05/01 *Med Phys*. 1976 May-Jun;3(3):153-8.
- [2] A. P. Kozlov and V. A. Shishov. Forming of electron beams from a betatron by foil scatterers. *Acta Radiol Ther Phys Biol*, 15(6):493–512, 1976. Kozlov, A P Shishov, V A eng SWEDEN 1976/12/01 *Acta Radiol Ther Phys Biol*. 1976 Dec;15(6):493-512.
- [3] L. Taumann. The treatment head design for medical linear accelerators. *Ieee Transactions on Nuclear Science*, 28(2):1893–1898, 1981. Lm277 Times Cited:2 Cited References Count:4.
- [4] E. Grusell, A. Montelius, A. Brahme, G. Rikner, and K. Russell. A general solution to charged particle beam flattening using an optimized dual-scattering-foil technique, with application to proton therapy beams. *Physics in medicine and biology*, 39(12):2201–16, 1994. Grusell, E Montelius, A Brahme, A Rikner, G Russell, K England *Phys Med Biol*. 1994 Dec;39(12):2201-16.
- [5] T. Connell, A. Alexander, M Evans, and J Seuntjens. An experimental feasibility study on the use of scattering foil free beams for modulated electron radiotherapy. *Phys Med Biol*, 57(11):3259–3272, 2012.
- [6] T. Connell and J. L. Robar. Low-z target optimization for spatial resolution improvement in megavoltage imaging. *Medical physics*, 37(1):124–31, 2010. Connell, Tanner Robar, James L *Med Phys*. 2010 Jan;37(1):124-31.
- [7] DWO Rogers, I Kawrakow, JP Seuntjens, BRB Walters, and E Mainegra-Hing. Nrc user codes for egsnrc. *NRC Report No. PIRS-702*, 2003.
- [8] T. Gauer, D. Albers, F. Cremers, R. Harmansa, R. Pellegrini, and R. Schmidt. Design of a computer-controlled multileaf collimator for advanced electron radiotherapy. *Physics in medicine and biology*, 51(23):5987–6003, 2006. Gauer,

T Albers, D Cremers, F Harmansa, R Pellegrini, R Schmidt, R England Phys
Med Biol. 2006 Dec 7;51(23):5987-6003. Epub 2006 Oct 30.

CHAPTER 7
Conclusions

Contents

7.1	Delivery of a modulated electron radiotherapy plan .	158
7.2	Design of custom scattering foils	159
7.3	Future Work	159

This work serves to further advance development of an experimental MERT program at McGill University. This technique offers certain advantages over non-modulated electron and modulated photon deliveries such as greater dose sparing of critical structures for superficial targets. This technique could be beneficial to multiple patient groups such as breast cases, paranasal or any superficial malignancy, particularly in younger patients who are at greater risk of developing secondary cancers. We investigated the feasibility and accuracy of this technique by combining the previously developed treatment planning aspects of the program with the automated collimation hardware to produce a complete MERT plan and later perform a delivery to assess its accuracy.

We also investigated the modification of the accelerator beamline by removal of the clinical scattering foil as a means to reduce the bremsstrahlung dose to the patient. Additionally we proposed the development of a new minimal thickness scattering foil optimized for MERT applications.

7.1 Delivery of a modulated electron radiotherapy plan

The McGill Monte Carlo treatment planning system, a research platform capable of optimization and planning of MERT deliveries, and the FLEC electron collimation device were two forks of past work on aspects of modulated electron therapy. Current work focused on integrating each of these two forks into one unified workflow for the creation and delivery of a MERT plan. A hypothetical breast case was planned within the treatment planning system using Monte Carlo dose calculation and inverse optimization methods. Modifications to the planning system were made to allow export of the final beam arrangements, energies and MU settings into a FLEC control file. Using the automated FLEC control software, a previously planned MERT case was delivered to a Solid Water® phantom containing a sheet of radiochromic film to evaluate the accuracy of the delivery against the planned dose. The measured dose agreed well with expected values, with 3%/3 mm gamma pass rates of 62.1, 99.8, 97.8, 98.3, and 98.7 percent for the 9, 12, 16, 20 MeV, and combined energy deliveries respectively. Delivery was also performed with a MapCHECK 2 device and resulted in 3%/3 mm gamma pass rates of 88.8, 86.1, 89.4, and 94.8 percent for the 9, 12, 16, and 20 MeV energies respectively.

Additionally, feasibility was evaluated resulting in the delivery time taking just under 26 minutes. This time is clinically feasible and potential future optimizations could reduce this time significantly. We conclude that MERT remains a feasible technique in which highly accurate deliveries can be achieved. This

modality offers physicians an additional option in treating superficial malignancies where sparing of organs at risk represents a high priority.

7.2 Design of custom scattering foils

We investigated the removal and modification current clinical scattering foils to improve the quality of the beam for MERT. It was found that the complete removal of the scattering foil produced a large reduction in the bremsstrahlung dose received by the patient by a factor of 12.2, 6.9, 7.4, 7.4 and 8.3 for 6, 9, 12, 16 and 20 MeV beams respectively. This translates into a great potential reduction in the dose received to healthy tissue, however, the lack of scattering also limited the higher energies to small treatment areas due to insufficient particle fluence beyond a few cm from the central axis. Custom designed foils were proposed that achieved the optimal compromise between minimal beam scattering and bremsstrahlung reduction. The optimal foils were found to be aluminum disks with thickness that varied for 12, 16 and 20 MeV. The 6 and 9 MeV energies were found to have received sufficient scatter from the remaining beamline components that no foil was recommended. It was concluded that the use of no, or minimal thickness scattering foils are highly recommended in any future commercial MERT implementation due to the benefits of reduced dose to healthy tissue as well as the increased dose rate achievable.

7.3 Future Work

Additional work remains to be done on the topic of increasing the speed and efficiency of the MERT delivery. Possible avenues of research include modifying the collimation device to operate at faster speeds to reduce the time lost waiting

for jaw repositioning. Additional speed improvements could be made to the planning stage through modification to the field creation and selection process. By adding additional fields of larger and possibly variable sizes to the solution space while simultaneously adding a penalty to the cost function that discourages large numbers of fields could increase the speed of the delivery. Dose calculation speed in it's current form is not suitable for widespread clinical implementation. Though the process of incorporating faster algorithms, either analytical or fast Monte Carlo methods, this could be brought down to more acceptable limits.

List of Abbreviations

CM:	Component Module
CRT:	Conformal Radiation Therapy
CT:	Computed Tomography
DVH:	Dose Volume Histogram
EBRT:	External Beam Radiation Therapy
FLEC:	Few Leaf Electron Collimator
FWHM:	Full Width at Half Maximum
GPU:	Graphical Processing Unit
Gy:	Gray (SI unit: J/kg)
ICRU:	International Commission on Radiation Units
IMRT:	Intensity Modulated Radiation Therapy
KERMA:	Kinetic Energy Released per Unit Mass
Linac:	Linear Accelerator
MAS:	Mean Angular Spread
MC:	Monte Carlo
MERT:	Modulated Electron Radiation Therapy
MMCTP:	McGill Monte Carlo Treatment Planning System
MRI:	Magnetic Resonance Imaging
MU:	Monitor Unit

NTCP: Normal Tissue Complication Probability

OAR: Organ at Risk

PDD: Percent Depth Dose

PET: Positron Emission Tomography

PTV: Planning Target Volume

QA: Quality Assurance

RT: Radiation Therapy

SCD: Source to Collimator Distance

SSD: Source to Surface Distance

TCP: Tumor Control Probability

TPS: Treatment Planning System